Hydromechanical Stress in Aerated Stirred Tanks

Von der Fakultät für Maschinenwesen der Rheinisch-Westfälischen Technischen Hochschule Aachen zur Erlangung des akademischen Grades eines Doktors der Ingenieurwissenschaften genehmigte Dissertation

vorgelegt von

Andreas Daub

Berichter: Universitätsprofessor Dr.-Ing. Jochen Büchs
Universitätsprofessor Dipl.-Ing. Dr. techn. Christoph Herwig

Tag der mündlichen Prüfung: 28. Mai 2015

Preface

I would like to thank Professor Büchs for the opportunity to conduct my research project under his supervision at AVT-Biochemical Engineering, RWTH Aachen University. I greatly appreciated his guidance and advice and the fruitful discussions with him that proved to be key for the success of this project. I would like to express my gratitude for his patience with me and for the continuing support he offered me to finalize this thesis.

I would like to thank Professor Herwig for his commitment to take over the role of the co-examiner for my doctoral examination.

I want to thank the fermentation development team at Sandoz, Kundl for the excellent collaboration and their support and openness for my experimental work. Having Gerhard Schneider as a guide who helped me with his knowledge and experience was an invaluable support for me.

My special thanks go to the students who significantly contributed to this work or conducted complementing projects: M. Böhm, S. Delueg, D. Guttmann, M. Jordan, C. Leicht, A. Meierjohann, M. Mühlmann, V. Oberhofer, S. Salcher and M. Schmidt.

I want to thank my former colleagues at AVT-Biochemical Engineering for the good atmosphere at the department.

Finally, I want to express my deepest gratitude for the enduring and patient support I experienced from my family and my friends that was of invaluable importance for the success of this challenging project.

Parts of this thesis have already been published:

Daub A, Böhm M, Delueg S, Büchs J: Measurement of maximum stable drop size in aerated dilute liquid-liquid dispersions in stirred tanks. Chemical Engineering Science 2013, 104:147-155.

Daub A, Böhm M, Delueg S, Mühlmann M, Schneider G, Büchs J: Maximum stable drop size measurements indicate turbulence attenuation by aeration in a 3 m^3 aerated stirred tank. Biochemical Engineering Journal 2014, 86:24-32.

Daub A, Böhm M, Delueg S, Mühlmann M, Schneider G, Büchs J: Characterization of hydromechanical stress in aerated stirred tanks up to 40 m^3 scale by measurement of maximum stable drop size. Journal of Biological Engineering 2014, 8:17.

Abstract

Turbulence intensity, or hydromechanical stress, is a controlling parameter in many industrially relevant processes that are operated in aerated stirred tanks. These processes are often characterized by intense aeration and agitation, particularly in the fermentation industries. Measurement of hydromechanical stress under conditions of intense aeration and agitation is extremely difficult. Very few data on turbulence characteristics exist due to a lack of measurement techniques. Therefore, this thesis focused on three main topics: (1) the development of a measurement technique for hydromechanical stress in aerated stirred tanks, (2) the investigation of the influence of aeration on hydromechanical stress and (3) the characterization of the influence of geometry and scale on hydromechanical stress in aerated stirred tanks.

A new measurement method was developed that is based on the well established correlation of maximum stable drop size of a break-up controlled dispersion with hydromechanical stress. The continuous and dispersed phase properties were selected to be able for the first time to apply this principle to aerated operating conditions. This was achieved mainly by applying a dilute dispersion, a low ionic strength and by incorporating a dispersed phase, paraffin oil, with a negative spreading coefficient. The negative spreading coefficient prevents coalescence due to drop-bubble interactions for aerated operating conditions.

This new method was applied to investigate the influence of aeration on hydromechanical stress for a broad range of aerated and unaerated operating conditions in a 3 m^3 reactor. Results from drop dispersion experiments with two different setups of 6-bladed Rushton turbine impellers with diameters of d = 0.41 m (d/D_R = 0.34, setup B-1) and d = 0.51 m (d/D_R = 0.43, setup B-3) in a 3 impeller configuration were presented. The results from experiments without aeration were well in agreement with the existing literature on drop dispersion. The results from experiments with aeration indicated a strong attenuation of turbulence intensity in stirred tank reactors by the presence of air. The ratio between maximum and volume-averaged energy dissipation rate, ϕ, was reduced by aeration by 64 % for the d/D_R = 0.34 impeller setup (B-1) and by 52 % for the d/D_R = 0.43 impeller setup (B-3) when compared with unaerated operating conditions on the basis of equal volumetric power input. The value of the aeration rate had no measurable effect in the range of aeration rates applied, which was between 0.1 vvm and 1 vvm.

The method was then applied in a broad range of reactor scales (50 L, 3 m^3 and 40 m^3 volume), impeller geometries (Rushton turbines and an Ekato Phasejet/Combijet combination) and operating conditions to investigate the influence of geometry and scale on hydromechanical stress. Comparison of data between the different scales showed that there is a scale effect that results in higher values for ϕ in larger reactors. This behaviour is not covered by the classic theory of turbulent drop dispersion but is in good agreement with the theory of turbulence intermittency. The data for all impeller configurations and all aeration rates for the three scales correlated very well when calculated values for ϕ based on the measured values for d_{max} were used to calculate the maximum local energy dissipation rate. Most of the data was within 20 % around the theoretical prediction from the classic theory of drop dispersion when these values for ϕ were used. A correlation of the data for all scales and all impeller configurations in the form $\phi = 2.3 \cdot (\phi_{unaerated})^{0.34} \cdot (D_R)^{0.543}$ was suggested that successfully models the influence of scale and impeller geometry on ϕ for aerated operating conditions. Results for an Ekato Phasejet/Combijet impeller setup showed that this correlation can also be applied successfully to estimate hydromechanical stress for impeller geometries other than Rushton impellers.

The measurement method and the data presented in this thesis represent an important step forward in the characterization of hydromechanical stress in stirred tanks under aerated operating conditions. The newly developed measurement method can be applied in the future to characterize further agitator and reactor designs under process relevant operating conditions which was frequently not possible in the past due to a lack of measurement techniques. The correlation for ϕ developed in this work can be beneficially used for approximate calculations of hydromechanical stress for geometries for which experimental data is not available. In combination with further important process parameters like mass transfer characteristics and mixing characteristics of impeller setups, characteristics of hydromechanical stress can be incorporated in reactor and process optimization in a more relevant manner than possible before.

Contents

Notation

a	constant	[-]
A	linear scaling factor	[-]
A_{jacket}	surface area of reactor jacket	[m^2]
C	bottom clearance of first impeller	[m]
ΔC	impeller spacing	[m]
c_D	constant in Eq. 1.3	[-]
$c_{p,air}$	specific heat capacity of air	[kJ/kg/K]
$c_{p,vapor}$	specific heat capacity of vapour	[kJ/kg/K]
$c_{pV,steel}$	specific heat capacity of steel	[kg/m^3/K]
$c_{p,water}$	specific heat capacity of water	[kJ/kg/K]
d	impeller diameter	[m]
d_b	bubble diameter	[m]
d_i	average drop diameter in class i of Gaussian drop size distribution	[m]
d_{max}	maximum stable drop dimeter	[m]
$d_{max,0}$	maximum stable drop diameter for inviscid dispersed phase	[m] [m]
d_{mod}	modal value of Gaussian drop size distribution	[m]
D_R	reactor diameter	[m]
d_{steel}	wall thickness of reactor	[m]
d_{32}	Sauter mean diameter	[m]
EDCF	energy dissipation to circulation function	[Ws/m^3]
F	correction factor	[-]
Fl	impeller flow number	[-]
Fr	impeller Froude number	[-]
g	gravitational acceleration	[m/s^2]
Gr	Grashof number	[-]
h	impeller blade height	[m]
H	unaerated liquid height	[m]
H_{jacket}	height of the reactor jacket	[m]
Δh_v	heat of evaporation for water	[kJ/mol]
k_La	volumetric mass transfer coefficient	[1/s]
K_1	constant in Eq. 5.1	[-]

K_2	constant in Eq. 5.1	[-]
L	distance between inner and outer wall of reactor jacket	[m]
$\dot{m}$	mass flow	[kg/s]
$\dot{m}_{air}$	mass flow of air	[kg/s]
$\dot{m}_{vapour,in}$	mass flow of vapour at reactor inlet	[kg/s]
MW	molecular weight	[g/mol]
m_{water}	total mass of water inside reactor	[kg]
MW_{N2}	molecular weight of nitrogen	[g/mol]
MW_{O2}	molecular weight of oxygen	[g/mol]
MW_{water}	molecular weight of water	[g/mol]
n	agitation rate	[1/s]
n_{bl}	number of impeller blades	[-]
$\dot{n}_{tot,in}$	total molar flow at reactor inlet	[mol/s]
$\dot{n}_{tot,out}$	total molar flow at reactor outlet	[mol/s]
Nu	Nusselt number	[-]
Nu_{plate}	Nusselt number of a vertical plate	[-]
$\dot{n}_{vapour}$	molar flow of vapour	[mol/s]
P	(aerated) power input	[W]
p_{abs}	absolute pressure in reactor headspace	[bar]
$P_{agitation}$	power input from agitation	[W]
P_{gas}	pneumatic power input from aeration	[W]
$p^s_{H_2O}$	saturation vapour pressure	[bar]
$p^s_{H_2O,in}$	saturation vapour pressure at reactor inlet	[bar]
$p^s_{H_2O,out}$	saturation vapour pressure at reactor outlet	[bar]
p_{in}	absolute pressure of inlet air	[bar]
P_L	power loss	[W]
Po	power number	[-]
P_{loss}	power loss	[W]
Pr	Prandtl number	[-]
p_{vapour}	partial pressure of vapour	[bar]
P_0	unaerated power input	[W]
$\dot{Q}_{air+vapour}$	heat flow for tempering the inlet air	[W]
$\dot{Q}_{evaporation}$	heat flow from evaporation	[W]
q_g	(specific) aeration rate, volume of gas/volume liquid/min	[vvm]
Q_g	air flow rate	[m^3/s]

$\dot{Q}_{jacket}$	heat flow over reactor jacket	[W]
q_3^m	volumetric probability density distribution	[1/m]
Re	Reynolds number	[-]
S	standard deviation of drop size distribution	[µm]
Sp	spreading coefficient	[N/m]
t	time	[s]
T	temperature	[K]
T_{avg}	average temperature	[K]
t_c	circulation time	[s]
T_d	dew point	[K]
$T_{environment}$	environmental temperature	[K]
T_{in}	temperature of gas flow at reactor inlet	[K]
T_{out}	temperature of gas flow at reactor outlet	[K]
$T_{reactor}$	reactor temperature	[K]
u_b	bubble rise velocity	[m/s]
u_{tip}	impeller tip speed	[m/s]
$\dot{V}_{air}^N$	normal volume flow of air	[Nm^3/s]
V_L	total liquid volume	[m^3]
V_{mo}	molar volume of gas	[mol/m^3]
$\dot{V}^N$	normal volume flow	[Nm^3/s]
V_{steel}	total volume of steel	[m^3]
$\dot{V}_{tot,\,in}^N$	total normal volume flow at reactor inlet	[Nm^3/s]
$\dot{V}_{vapour,\,in}^N$	normal volume flow of vapour at reactor inlet	[Nm^3/s]
w	impeller blade width	[m]
y_{vapour}	molar fraction of vapour	[mol/mol]
$y_{vapour,in}$	molar fraction of vapour at reactor inlet	[mol/mol]
$y_{vapour,out}$	molar fraction of vapour at reactor outlet	[mol/mol]

Greek letters

α	constant in Eq. 5.1	[-]
α	heat transfer coefficient	[$W/m^2/K$]
ε	local energy dissipation rate	[W/kg]
ε_{max}	maximum local energy dissipation rate	[W/kg]
$\varepsilon_{Ø}$	volume averaged energy dissipation rate	[W/kg]

ϕ	$\varepsilon_{max}/\varepsilon_{Ø}$	[-]
$\phi_{aerated}$	ϕ for aerated operating conditions	[-]
$\phi_{unaerated}$	ϕ for unaerated operating conditions	[-]
η_c	dynamic viscosity of continuous phase	[Pa·s]
η_d	dynamic viscosity of dispersed phase	[Pa·s]
φ	relative humidity	[-]
φ_{in}	relative humidity of inlet air	[-]
λ	microscale of turbulence	[m]
λ_{air}	heat conductivity of air	[W/m/K]
Λ	macroscale of turbulence	[m]
ν	kinematic viscosity	[m^2/s]
ν_{air}	kinematic viscosity of air	[m^2/s]
ρ_c	density of continuous phase	[kg/m^3]
ρ_{air}	density of air	[kg/m^3]
σ_{BA}	surface tension buffer-air	[N/m]
σ, σ_{BO}	interfacial tension buffer-oil	[N/m]
σ_{OA}	surface tension oil-air	[N/m]
τ	torque	[Nm]

Figures

Tables

1 Introduction

1.1 Hydromechanical stress in stirred tanks

In aerobic fermentation processes, dissolved oxygen is consumed by microorganisms to supply energy for product formation and growth. The high turnover rate of oxygen combined with its low solubility in water results in a demand for efficient mass transfer. Reactor design for aerobic fermentation processes is frequently governed by this mass transfer operation. The aerated stirred tank reactor is the standard reactor type applied in the fermentation industries to solve this problem. It is used from development scale of a few hundred millilitres to large-scale production of up to several hundred m^3. Intense agitiation and aeration are typical in aerobic fermentation processes. Volumetric power input by agitation is typically in the range of 1 – 5 kW/m^3 and the aeration rate is in the order of 1 vvm (volume of gas/volume liquid/minute). The intense agitation applied to realize efficient mass transfer induces high levels of turbulence intensity.

Turbulence intensity, or hydromechanical stress, can be characterized by the maximum local energy dissipation rate ε_{max}. The energy dissipation rate ε is the rate at which kinetic energy introduced by agitation dissipates into heat. Energy dissipation is distributed inhomogeneously in the reactor volume. A maximum value exists in the vicinity of the impeller blades [1]. This maximum local energy dissipation rate defines the most severe effects of the flow field on gas bubbles and dispersed particles like mycelial pellets and oil drops.

The maximum local energy dissipation rate is a parameter with an important impact on a broad range of processes. Since it governs the break-up of bubbles and drops in a turbulent flow field [2, 3] it is generally very important in processes where interfacial area for mass transfer can become rate limiting [4]. A process of this type with wide application is solvent extraction [5]. Another example for a process that depends on turbulence intensity is suspension polymerisation where the quality characteristics of the produced polymer beads were shown to be widely dependent on the type of impeller used and the stirring speed, hence on the intensity of turbulence induced by stirring [6]. Furthermore, turbulence intensity has been discussed for a long time to have a large influence on biotechnological processes not only by its impact on mass transfer but by a direct action of turbulence on the biological phase [7]. It is well known, e.g., that even at comparable levels of volumetric power input pellets grow much larger in shake flask culture where turbulence levels are low compared to cultures in stirred tank reactors [8-10]. There is a close interaction between morphology, broth rheology and agitation intensity in submerged fungal fermentations in stirred tank reactors that can impact process performance [11-13]. Jüsten et al. showed in a series of publications that growth and productivity of submerged fungal cultures of *Penicillium chrysogenum* in stirred fermenters can be correlated with turbulence intensity [14-16]. Other reports preceded the work of Jüsten et al. that identified hydromechanical forces to influence submerged fungal cultures [e.g. 17, 18, 19]. Gregoriades et al. [20] showed that Chinese hamster ovary cells immobilised on microcarriers are damaged by hydromechanical forces of magnitudes that can be expected in stirred tank processes.

The development of large scale processes is conducted in lab or pilot scale. This poses the question how to scale down the conditions prevalent in large production scale to the development scale and vice versa. Typical parameters of interest may be mass transfer coefficient k_La, volumetric power input P/V_L, impeller tip speed u_{tip}, turbulence intensity in the form of maximum local energy dissipation rate ε_{max}, circulation frequency t_c, or a combination of these parameters like the energy dissipation to circulation function EDCF (first introduced by [14]) that is basically the ratio of ε_{max}/t_c. Based on an estimation of the values of these parameters in large scale, small scale operating conditions (agitation and aeration rates) can be estimated that resemble the respective values of these different parameters in large scale. Testing these operating conditions in small scale may reveal which of these parameters (if at all) is a suitable proxy for scaling up or scaling down a particular process. The work of Jüsten [14-16], e.g., showed that scale up of mycelial flocs can be correlated with hydromechanical stress and circulation frequency in the form of the energy dissipation to circulation function EDCF. The morphology of the fungus in this case

depends on the break up in the impeller region that is governed by hydromechanical stress and the aggregation of mycelial flocs in regions where turbulence intensity is low. Circulation frequency is decisive for the time for aggregation and for the frequency the mycelial flocs pass the high intensity region close to the impeller where they break up. The whole procedure of testing different parameter candidates strongly depends on the validity of the correlations used to calculate these parameters.

The development of an experimentally validated correlation for hydromechanical stress under conditions of intense aeration and agitation typical for aerobic fermentations is hard to achieve due to two distinct circumstances: First, in industrial practice, geometrical similarity throughout the scales is hardly found [21, 22]. Therefore, the influence of geometry on turbulence intensity must be accounted for. Second, the working medium is a multiphase gas-liquid dispersion which is characterized by a volumetric gas hold-up of up to 20 % in production scale reactors [22, 23]. Of course, this is accompanied by much higher gas hold-ups in the vicinity of the turbulence inducing agitators. High spatial and temporal resolution is necessary to directly measure the velocity fluctuations that define turbulence. This is even more difficult under conditions where volumetric gas hold-up is high and the medium turns opaque [24, 25]. In fact, there is only very few data available in literature on the effect of high gas hold-up on the continuous phase turbulence in stirred tanks, possibly because of the major challenges that are associated with the exercise of measuring under these conditions. [24, 25]. The application of computational fluid dynamics to predict energy dissipation in multiphase stirred tanks is a promising tool that can give a first principals access to the processes involved [26, 27]. But the simulations need experimental validation which is hardly available [28]. Montante et al. [29], e.g., conducted a study where bubble and flow characteristics in a turbulent stirred tank were measured and simulated. However, their aeration rate was below 0.07 vvm.

For single-phase operation, a substantial amount of data exists on the maximum energy dissipation rate, especially for the 6-bladed Rushton turbine. It is instructive to review the available data to emphasize the challenge of measuring an absolute value for ε_{max} even for unaerated operating conditions:

The typical geometry used for these studies is a single impeller in a reactor with an aspect ratio of unity ($H/D_R = 1$), an impeller bottom clearance of 1/3 or 1/2 the tank diameter ($C/D_R = 1/3$ or 1/2) and an impeller to tank diameter ratio of 1/3 ($d/D_R = 1/3$). The standard

impeller blade height is 0.2 times and its width 0.25 times the impeller diameter (h/d = 0.2, w/d = 0.25). Table 1.1 summarizes results for this geometry from different working groups:

Table 1.1: Comparison of literature values for $\phi = \varepsilon_{max}/\varepsilon_{\emptyset}$ for single-phase operation of stirred reactors with a single Rushton impeller in a $H/D_R = 1$ reactor.

Source	Reactor diameter D_R [m]	Experimental method	Volumetric power input P/V_L [kW/m^3]	ϕ [-]
Assirelli et al.[30]	0.29	Micromixing, fixed feed relative to tank	0.18 - 1.14	47 - 201
Assirelli et al. [30]	0.29	Micromixing, feed rotating with impeller	0.18 - 1.14	141 - 371
Baldi and Yianneskis [1]	0.1	PIV	0.6-11.7[a]	30 - 48[b]
Cutter [31]	0.29	Photographic	0.03 – 1.0[a]	70
Costes and Couderc [32]	0.45	LDV	0.01 – 0.11[a]	5 - 10
Ducci and Yianneskis [33]	0.29	LDA	0.02[a]	48[b]
Escudie and Line [34]	0.45	PIV	0.11	~55[b]
Micheletti et al. [35]	0.1	LDA / PIV	1.26	~42[b]
Sharp and Adrian [36]	0.15	PIV	0.0028[a]	10 – 25
Wu and Patterson [37]	0.27	LDV	0.01 – 0.28[a]	22
Zhou and Kresta [38]	0.24	LDA	0.086 - 1.0	48

[a] Volumetric power input estimated with Po = 5; [b] ϕ estimated with Po = 5 from ε_{max}/n^3d^5

The data is reported as the normalized energy dissipation rate ϕ which is the maximum local energy dissipation rate ε_{max} normalized with the volume averaged energy dissipation rate $\varepsilon_{\emptyset} = P/(\rho_c V_L)$. ϕ is independent of the agitation rate for unaerated operating conditions [38-40]. It is, therefore, a characteristic value for a given impeller. Widely used methods for the direct measurement of turbulent velocity fluctuations and maximum local energy dissipation rate are laser Doppler anemometry (LDA) and particle image velocimetry (PIV), especially in the newer publications. The major part of the data falls within a range of $\phi = 20 – 50$. The differences in the results from different working groups might partly be due to the different measurement techniques applied and partly due to uncontrolled differences in geometry like impeller blade thickness. The results from Micheletti et al. [35] cancel out the influence of geometry since they compare results with different methods in the same equipment. They find a difference for the measured ε_{max}-values of approximately a factor of 2 for ensemble-averaged methods compared to approximation methods. Their analysis of angle-resolved

LDA in comparison with angle-averaged LDA shows that considering the periodic fluctuation of turbulence intensity with the blade passage also accounts for approximately a factor of 2 difference in the measured value of ϕ, with the angle-resolved measurements resulting in higher values. Very high values for ϕ were reported by Assirelli et al. [30] who used a chemical method to determine local energy dissipation indirectly based on a micromixing model. Besides their very high absolute values it is interesting to note that they also report a much higher value of ϕ (2.7 times) when the reactants are fed at a position 20° behind an impeller blade, i.e. at a constant position relative to an impeller blade, compared to a constant position relative to the vessel. This reflects again the importance of the angle-dependent variation of energy dissipation between impeller blades. Ducci and Yianneskis [33] report a similar result based on LDA measurements and found a ratio of 3 for angle-resolved versus angle-averaged values. Although part of the differences in the results collected in Table 1.1 might be explained by small geometric differences, it is evident from this comparison that the method employed for measurement and post-treatment of the raw data has a large impact on the resulting absolute values for ϕ. This emphasizes the difficulty in determining the maximum local energy dissipation rate even for single-phase operation. It is also interesting to note that agitation was typically gentle with volumetric power inputs of 0.0028 kW/m^3 to slightly above 1 kW/m^3 except for the study of Baldi and Yianneskis [1] who reached nearly 12 kW/m^3.

For practical applications, it is of great interest to be able to estimate the influence of geometrical changes on ϕ. A few authors tried to correlate the maximum local energy dissipation rate with impeller geometry. Okamoto et al. [41] used a hot film anemometer to measure the turbulent velocity fluctuations in the impeller stream of 6-bladed Rushton turbines and deduced the local energy dissipation rate from these measurements. They correlated their data by

$$\phi = 0.85 \cdot \left(\frac{h}{D_R}\right)^{-1.38} \cdot e^{-2.46 \cdot d/D_R} \qquad (1.1)$$
$$\left(0.05 < h/D_R < 0.30;\ 0.25 < d/D_R < 0.70\right)$$

McManamey [42] introduced the idea to use the power related to the impeller swept volume as an estimate for the maximum energy dissipation rate which yields for Rushton impellers:

$$\phi = \frac{4}{\pi} \cdot \frac{V_L}{d^2 \cdot h} \qquad (1.2)$$

Davies [43] adapted McManamey's approach but found a better correlation when comparing literature data for stirred tanks, homogenizers and other mixing devices when using half the impeller swept volume to correlate ε_{max} for stirred tanks.

Liepe et al. [40] published two correlations that are based on the equation

$$\varepsilon_{max} = c_D \cdot \frac{u_{tip}^3}{h} \tag{1.3}$$

where c_D is a constant, $u_{tip} = \pi \cdot n \cdot d$ is the impeller tip speed and h is the height of the impeller blade. In contrast to the purely empirical character of Okamoto's equation, this relationship can be derived on the basis of scaling arguments with the impeller tip speed as the characteristic velocity and the impeller blade height as the characteristic length scale for the stirred tank [44]. It can also be applied to other mixing devices with turbulent flows like nozzles and valves if the characteristic velocity and length is chosen appropriately [40]. ϕ can be expressed with $\varepsilon_{Ø} = (P/\rho_c V_L) = Po \cdot n^3 \cdot d^5 / V_L$ based on Eq. 1.3 as

$$\phi = \frac{c_D \cdot \pi^3}{Po} \cdot \frac{V_L}{d^2 \cdot h} \tag{1.4}$$

As a first estimate $c_D = 0.1$ is given by Liepe et al. [40] for Rushton impellers which results in:

$$\phi = \frac{0.1 \cdot \pi^3}{Po} \cdot \frac{V_L}{d^2 \cdot h} \tag{1.5}$$

A second approach is $c_D = 0.11 \cdot Po \cdot h/d$ [40] leading to:

$$\phi = 0.11 \cdot \pi^3 \cdot \frac{V_L}{d^3} \tag{1.6}$$

The results for ϕ from these correlations for the standard geometrical setup as described above are given in Table 1.2. The values show a similar spread as observed in the collection of measured values in Table 1.1 and fit well into the range of values shown there.

Table 1.2: Comparison of $\phi = \varepsilon_{max}/\varepsilon_{\varnothing}$ calculated from literature correlations for single-phase operation of stirred reactors with a single Rushton impeller in a $H/D_R = 1$ reactor.

Equation	Source	ϕ [-]
1.1	Okamoto [41]	16
1.2	McManamey [42]	135
1.5	Liepe et al. [40]	66
1.6	Liepe et al. [40]	72

The above comparison shows that a large uncertainty exists in the determination of an absolute value for the maximum local energy dissipation rate even for lab scale equipment and single-phase operation. However, for practical applications, the absolute value of the maximum local energy dissipation rate is not necessarily the most important question. More importantly, it would be desirable to compare process equipment relative to each other, i.e. to assess the influence of geometry and scale on maximum energy dissipation under process relevant operating conditions. This includes large reactors, process relevant power inputs and intense aeration. This experimental range is not covered by the available literature. Particularly the influence of the dispersed gas phase on the continuous phase turbulence for aeration rates and gas hold-ups that are typical for fermentation processes has not been thoroughly investigated. The reason for this is a lack of measurement techniques which can be applied in such cases [45, 46].

1.2 Objectives

Since industry scale processes are influenced by the maximum local energy dissipation rate, three important questions arise that demand for experimental access to this parameter:

(1) What is the influence of the type of equipment used? In the fermentation industries, process development often starts in shake flasks. A transfer of results from shake flasks to the typical stirred tank reactor in the next development step is only possible if the characteristics and restrictions of these different types of processing equipment can be anticipated [23, 47]. Peter et al. [9] and Büchs and Zoels [10] described a method how to characterize hydromechanical stress in shake flasks. Mollet et al. [48] give an overview on hydromechanical stress in different process equipment used during the propagation of cell

cultures. However, there is a particular lack of available methods and data for the characterization of aerated stirred tanks under conditions that are close to process conditions. The first objective of this thesis is, therefore, to establish a method that can be applied to investigate the influence of geometry on hydromechanical stress in aerated stirred tanks.

(2) What is the influence of operating conditions? The major part of publicly available experimental data related to the maximum local energy dissipation rate is restricted to operating conditions with low agitation intensity in the range below 1 kW/m^3 and single phase operation [e.g. 38]. However, many processes are conducted under very different operating conditions. E.g. in most bioprocesses intense aeration is necessary to support the oxidative metabolism of microorganisms. Aeration is accompanied by strong agitation with volumetric power inputs typically in the range of 1 – 5 kW/m^3. Volume averaged gas hold-ups of 10-20 % (v/v) are typical in process equipment [22]. The influence of aeration on turbulence under such intense operating conditions has not been investigated experimentally up to now. Thus, the second objective of this thesis is to apply this newly established method to experimentally investigate the influence of aeration on hydromechanical stress in aerated stirred tanks.

(3) What is the influence of scale and geometry? Exact geometric similarity is typically not conserved throughout scale-up from lab to pilot to production scale [21, 22]. Therefore, it is important to be able to experimentally assess the influence of geometrical differences and scale on maximum local energy dissipation rate for a more rational approach to process scale-up and scale-down and for systematic experiments during process development in small scale. The third major objective of this thesis is, therefore, to apply the new experimental method to study the influence of geometry and scale on hydromechanical stress.

An indirect way to quantify the magnitude of hydromechanical stress is to measure its impact on an immiscible liquid phase. It is well established that the maximum stable drop diameter of a dilute, non-coalescing dispersed phase correlates directly with turbulence intensity [49]. This principle has been used to compare the levels of maximum energy dissipation rate in different mixing devices [43, 50] and to correlate hydromechanical stress for equipment and operating conditions that restrict the use of other methods, e.g. for characterizing hydromechanical stress in shake flasks [9, 10]. The application of this measurement principle has up to now been restricted to operating conditions without

aeration. The first main part of this work (Chapter 3) covers the establishment of a drop dispersion based experimental method for measuring hydromechanical stress that can be applied under intense operating conditions with aeration in "real life equipment". Since impeller power input plays a major role for the analysis of the experimental results a reliable estimation of impeller power input is an important basis for the interpretation of the drop-dispersion experiments. Therefore, a detailed investigation of the accuracy of the electrical power measurement in a 3 m^3 reactor that is used for drop dispersion experiments is provided in Chapter 4. The analysis of the power input measurement is a basis for the work in the subsequent chapters. The drop-dispersion method will then be applied in a 3 m^3 pilot scale reactor with 1.2 m inner diameter in a broad range of operating conditions with two different Rushton type impeller setups to investigate the influence of aeration on turbulence intensity (Chapter 5). In the next chapter (Chapter 6) the method will be applied with 8 different reactor configurations with Rushton type impellers in reactors of scales 50 L, 3 m^3 and 40 m^3 and an Ekato Phasejet/Combijet impeller setup in the 3 m^3 reactor. It is the goal of Chapter 6 to provide a broad data basis to demonstrate the applicability of the drop-based measurement method to real life equipment of different scales, to characterize different reactor configurations with respect to hydromechanical stress as a basis for successful scale-up or scale-down under aerated operating conditions and to test whether established literature correlations for the estimation of hydromechanical stress for different impellers can be applied with acceptable accuracy. The individual chapters in this thesis are organized as independent studies. To avoid redundancy in the materials and methods sections and to establish a consistent naming for the reactor configurations throughout the work the reactor geometries and impeller configurations will be introduced first in Chapter 2.

2 Reactors and impeller configurations

Experiments were conducted in 50 L, 3 m^3 and 40 m^3 scale. The reactors were stainless steel vessels with dished bottoms. A schematic drawing of the reactors is depicted in Figure 2.1:

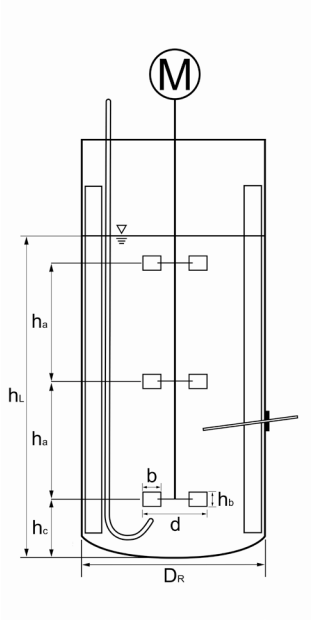

Figure 2.1: Schematic configuration of the reactors used. Impellers shown are 3 6-bladed Rushton type impellers.

Four equally spaced baffles of width $D_R/10$ were installed in the 50 L and in the 3 m^3 tanks. The 40 m^3 reactor had cooling pipes installed that act as baffles. Due to the size of the cooling pipes it can be assumed that the influence of the pipes on the flow field is comparable to conventional baffles [40, 51]. Geometrical details of the tanks are given in Table 2.1:

Table 2.1: Geometrical details of the reactors used. Values for impeller bottom clearance (C) and impeller distance (ΔC) are valid for Rushton impeller setups. Impeller bottom clearances for the Ekato setups are given in Table 2.3.

	Nominal reactor size		
	50 L	3 m^3	40 m^3
D_R [m]	0.293	1.2	2.8
V_L [m^3]	0.035	2.4 (2.6, 2.8)	30
H [m]	0.52	2.2	5.0
Number of impellers [-]	3	3	3
C [m]	0.095	0.51	0.92
ΔC [m]	0.19	0.69	1.8

Aeration rate was controlled by thermal mass flow controllers in all reactors. In the 50 L reactor, aeration was supplied by a single pipe of $5 \cdot 10^{-3}$ m inner diameter placed under the lowest impeller facing upwards at an angle of 60° to the horizontal. Ring-spargers were installed in the 3m^3 and in the 40 m^3 reactors.

Rushton type 6-bladed impellers with different geometries and Ekato Phasejet and Combijet impellers were used in the experiments. The geometrical details of the Rushton impellers are given in Table 2.2. The Rushton impellers were installed in a three impeller configuration which is typical for high aspect ratio reactors used, e.g., in the fermentation industries.

Table 2.2: Geometrical details of the Rushton impellers used in the different reactor configurations. The impellers are 6-bladed Rushton type impellers installed in a three impeller configuration. Power numbers were estimated with Eq. 6.9 (Section 6.3.3), except for setup B-1 and B-3 for which power numbers were measured.

Nominal reactor size	50 L				3 m^3			40 m^3
D_R [m]	0.293				1.2			2.8
Reactor configuration	A-1	A-2	A-3	A-4	B-1	B-2	B-3	C-1
d [m]	0.104	0.15	0.17	0.19	0.41	0.45	0.51	1.19
h [m]	0.023	0.05	0.05	0.05	0.09	0.09	0.12	0.22
w [m]	0.029	0.05	0.05	0.05	0.12	0.12	0.18	0.29
d/D_R [-]	0.35	0.51	0.58	0.65	0.34	0.38	0.43	0.42
h/d [-]	0.22	0.33	0.29	0.26	0.22	0.20	0.24	0.19
w/d [-]	0.28	0.33	0.29	0.26	0.28	0.26	0.34	0.24
Po [-]	5.5	8.0	7.1	6.4	4.9	5.0	5.9	4.7
Number of impellers [-]	3	3	3	3	3	3	3	3
C [m]	0.095	0.095	0.095	0.095	0.51	0.51	0.51	0.92
ΔC [m]	0.19	0.19	0.19	0.19	0.69	0.69	0.69	1.8

The power input measurements that will be presented in Chapter 4 were conducted with two different setups of Ekato Phasejet and Combijet impellers. The Ekato impellers are depicted in Figure 2.2. The Phasejet impeller is a hollow-blade radial-type impeller that is used as the lowest impeller stage for primary gas dispersion. The Phasejet impeller is complemented by either 2 (setup B-4) or 4 (setup B-5) Combijet impellers as the further impeller stages. The Combijet impellers are axial-type impellers.

Figure 2.2: Ekato Phasejet (left) and Combijet (right) impellers (from www.ekato.de).

The geometrical details of impeller configurations B-4 and B-5 are given in Table 2.3:

Table 2.3: Geometrical details of the Ekato Phasejet and Combijet impellers used in the 3 m^3 reactor. A picture of the impellers is shown in Figure 2.2. Power numbers were provided by the manufacturer.

Nominal reactor size	3 m^3	
D_R [m]	1.2	
Reactor configuration	**B-4**	**B-5**
Geometry of Phasejet impeller		
Impeller diameter d [m]	0.5	0.5
d/D_R [-]	0.42	0.42
Power number Po [-]	1.6	1.6
Geometry of Combijet impeller		
Impeller diameter d [m]	0.55	0.55
d/D_R [-]	0.46	0.46
Power number Po [-]	0.8	0.8
Off-bottom clearance:		
Phasejet [m]	0.43	0.43
Combijet 1 [m]	1.16	0.86
Combijet 2 [m]	1.89	1.29
Combijet 3 [m]	-	1.70
Combijet 4 [m]	-	2.11

Setup B-4 was only applied for power input measurements and was not used for drop dispersion experiments.

After introducing the reactors and impellers used in the experimental work of this thesis, the development of the drop dispersion based method for the investigation of hydromechanical stress will be presented in the next chapter.

3 Measurement of maximum stable drop size in aerated stirred tanks

It was highlighted in the introduction (Chapter 1) that there is a need for a measurement method that enables the comparison of different agitators in different scales with respect to hydromechanical stress in "real life equipment" under operating conditions that are comparable to process conditions. This chapter focuses on the establishment of such a measurement technique that is the foundation of the subsequent work. The method is based on the measurement of drop size distributions and maximum stable drop sizes in aerated dilute liquid-liquid dispersions in stirred tanks. The theoretical background for this approach will be introduced next in Section 3.1. Then, in Section 3.2 the methodological constraints for application in large scale experimentation will be discussed. After the definition of these constraints, the method and the experimental work will be described in Section 3.3. Finally, in Section 3.4 results for the verification of the sampling and measurement technique and first results for the maximum stable drop size under aerated operating conditions in a 50 L reactor will be presented.

3.1 Relevance of the maximum stable drop size

Drop sizes in dispersions evolve by the impact of the turbulent flow field of the continuous phase on the non-soluble dispersed phase. Turbulence causes the break-up of larger drops into smaller fragments, resulting in a drop size distribution that depends on geometry, operating conditions, physico-chemical properties of the continuous and dispersed phases and the age of the dispersion. Coalescence of drops may be superimposed which then further complicates the process. Chemical engineering aspects of such complex systems

have been investigated for many years. Hinze [2] and Kolmogorov [52] were amongst the first to model the break-up process of drops in a turbulent flow field. Their pioneering work was later extended by Arai [53] and by Calabrese [54] to viscous dispersed phases. Their break-up model is based on the concept that a drop exposed to a turbulent flow field experiences hydromechanical forces that cause a deformation. The deformation is counteracted by interfacial tension and viscosity of the drop. The drop breaks up if the deforming stress exceeds the cohesive forces from interfacial tension and viscosity. Drop break-up will persist until a drop size is reached for which the hydromechanical stresses are too weak to overcome the cohesive forces. The size of these largest drops that can resist break-up is called the "maximum stable drop size" (d_{max}). If coalescence can be neglected, the maximum stable drop size is directly related to the maximum local energy dissipation rate for low dispersed phase viscosity by the well known correlation of Hinze [2]:

$$d_{max,0} \sim \left(\frac{\sigma}{\rho_c}\right)^{0.6} \cdot \varepsilon_{max}^{-0.4} \tag{3.1}$$

With the maximum stable drop diameter of an inviscid dispersion $d_{max,0}$. Viscosity can be accounted for by a correction factor introduced by Arai [53]. A slightly modified version from Liepe et al. [40] is used in the present work:

$$d_{max} = d_{max,0} \cdot \left(1 + 2.5 \cdot \frac{\eta_d}{\sigma}\left(\varepsilon_{max} \cdot d_{max}\right)^{\frac{1}{3}}\right)^{0.6} \tag{3.2}$$

The classical concept of maximum stable drop size was extended by Baldyga et al. [55] to account for the observation that even for very long agitation times the maximum stable drop size keeps drifting slowly towards smaller values. This was explained by the intermittent character of turbulence which results in rare but strong bursts of turbulence. For practical applications the effect of turbulence intermittency must be judged in comparison to measurement accuracy and relevant time scales. During typical dispersion times of 1 – 3 h, the effect might be below the reproducibility of consecutive measurements.

The theory of turbulent drop dispersion is applicable if the flow field is fully turbulent and the drop size is in the size range of the turbulent eddies. Based on Kolmogorov's theory of isotropic turbulence, the size range of turbulent eddies can be estimated to fall within the macroscale of turbulence Λ and the microscale of turbulence λ. The macroscale of turbulence is a measure for the largest eddies that can be estimated to scale proportionally with the impeller blade height h [40]:

$$\Lambda = 0.4 \cdot h \tag{3.3}$$

By decaying, these large eddies pass on their energy to smaller eddies in an energy cascade until an eddy size is reached for which viscous forces become predominant. This smallest scale of eddies is the microscale of turbulence λ which can be estimated as:

$$\lambda = \sqrt[4]{\frac{\nu^3}{\varepsilon}} \tag{3.4}$$

Where ν is the kinematic viscosity and ε is the local energy dissipation rate per unit mass. Whereas the macroscale of turbulence only depends on impeller geometry, the microscale of turbulence depends on the physical properties of the liquid (ν) and the operating conditions (ε). The flow field can be considered fully turbulent when the Reynolds number $Re > 5 \cdot 10^3$ and $\Lambda/\lambda > 150$ [40]. Typical values for the macroscale of turbulence can be calculated as approx. 10^{-2} m for a 0.1 m^3 stirred tank and 10^{-1} m for a 100 m^3 stirred tank. The microscale of turbulence is typically of an order of 10^{-5} m [56]. The relationship between maximum local energy dissipation rate and maximum stable drop size can be applied to compare the turbulence intensity for different geometries and operating conditions by measuring d_{max}. From the theory explained above it can be concluded that the prerequisites for the validity of this method are a fully turbulent flow-field, a break-up controlled dispersion and a maximum stable drop size between the microscale and the macroscale of turbulence. Davies [43] demonstrated this approach for a wide range of energy dissipation rates in a selection of completely different homogenizers like colloid mills, valve homogenizers, static mixers and stirred tanks as shown in Figure 3.1:

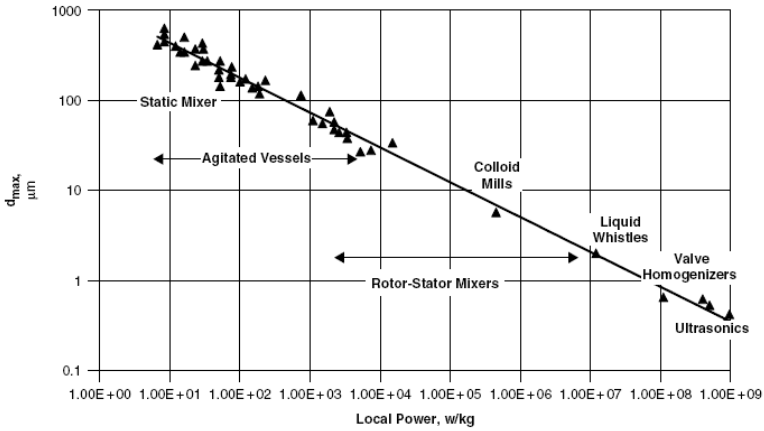

Figure 3.1: Maximum stable drop size (d_{max}) vs. maximum local energy dissipation rate (local power) in different mixing devices (from Atiemo-Obeng and Calabrese [57] after Davies [43])

Bauer [50] independently found the same correlation and his data also support this approach. This indirect method of determining turbulence intensity is very valuable in cases where other methods of direct determination of the maximum local energy dissipation rate are not applicable. E.g. Büchs and Zoels [10] and Peter et al. [9] used this method to compare energy dissipation rates in shake flasks with energy dissipation rates in stirred tanks. One major goal of this thesis is to characterize process equipment of different scales and geometry under aerated operating conditions. Under these conditions other methods can hardly be applied. The constraints that follow from this approach will be discussed in the next section.

3.2 Constraints for large scale experiments and high volumetric gas hold-up

Experimental data on scale-up of hydromechanical stress to large-scale equipment is extremely scarce. However, this data would be very valuable to test small-scale models for their validity.

Virtually inevitably, large scale facilities in the range of few to many m^3 in volume that are used for experimental purposes are production equipment provided by industries. This equipment has different characteristics than lab equipment that was built for the purpose of

experimentation. It is typically made from steel. Hence, visual observation of the process is very limited. This poses special challenges for techniques that need optical access to the process volume. Moreover, modifications of the equipment are generally not possible if they are not reversible. That means measurement methods have to make use of standard ports which also helps to minimize installation and removal times of measurement equipment. This is important because experimental time may be limited to short time slots between production batches. Further considerations like safety become essential as volume increases that may not be an issue in small scale. E.g. handling of organic solvents like toluene, that are frequently used in liquid-liquid experimentation in the lab environment [e.g. 58, 59] can be critical in m^3-scale due to their toxicity and fire hazard. Environmental safety is also important and has to be considered when continuous and dispersed phases are selected.

The measurement method presented in this study will be applied under conditions of high volumetric gas hold-up. A direct optical access from the tank wall to the impeller region cannot generally be realized and this restricts the application of many existing methods. Although laser-based methods for direct measurement of flow characteristics with very high spatial and temporal resolution have proven to be of great value for a more detailed understanding of impeller discharge flow in single-phase applications [33], they are limited to very low gas hold-ups in gas-liquid flows. E.g. Laakkonen et al. [60] used particle image velocimetry in an 18 L stirred tank to measure bubble and flow characteristics in a bubbly flow. The highest local gas hold-up measured in their work was 0.89 %. Khopkar et al. [46] reported that in a 0.19 m vessel accuracy of particle image velocimetry measurements was very limited at average gas hold-ups of 4 %. These methods cannot be applied under the operating conditions typical for high intensity gas-liquid processes because of their inherent methodological limitation to low values of gas hold-up.

Given the facts above, the indirect characterization of turbulence intensity by the measurement of maximum stable drop sizes in break-up controlled dispersions is a feasible and promising way to overcome the problems related with large scale experimentation and intense operating conditions with high volumetric gas hold-up. The prerequisite for the successful application of such a method is the careful choice of the continuous and dispersed phase properties and a reliable sampling and measurement procedure.

3.3 Materials and methods

3.3.1 Reactor

Experiments were conducted in a 50 L reactor as depicted in Figure 2.1. Geometrical details of the reactor are given in Table 2.1. The reactor was filled with 0.035 m^3 liquid volume, leading to an unaerated liquid height of H = 0.52 m. Impeller setup A-1 was used as described in Table 2.2. Temperature was controlled at 25°C in all experiments.

3.3.2 Continuous aqueous phase and organic phase physical properties

1 mM phosphate buffer at pH 7.3 was used as the continuous phase. 100 mM stock-solution was prepared by dissolution of 112 mmol NaH_2PO_4 x 2 H_2O (Merck, Darmstadt, Germany, >99% purity) and 388 mmol Na_2HPO_4 x 12 H_2O (Merck, Darmstadt, Germany, >99% purity) in 4 L of deionised water. The solution was then filled up to the final volume of 5 L. 350 mL of the stock-solution were diluted in deionised water inside the tank to give a total volume of the final buffer of 0.035 m^3. The buffer was used to ensure a constant pH during aeration when carbon dioxide from the air may be dissolved in the liquid. This is important because an influence of pH on coalescence behaviour in liquid-liquid dispersions has been reported [61]. A higher buffer concentration was not used because increasing ionic strength may promote drop coalescence as shown by Tobin and Ramkrishna [62]. The low concentration was sufficient to keep the pH constant. An experiment where aeration was switched from air to pure nitrogen showed no effect on measured drop sizes (see Section 5.4.3 and Figure 5.6). A powerful means of preventing coalescence in liquid-liquid dispersions is the addition of surface active agents. Under aerated conditions, however, preliminary experiments showed strong foam formation when surfactants were present. The addition of a surfactant to generate coalescence-inhibition in the reactor was, therefore, impossible. A second possibility to ensure break-up controlled dispersion is a low dispersed phase concentration. Leng and Calabrese [49] assume insignificant coalescence for dispersed phase concentrations below 0.05 L/L. Concentrations applied in experiments with break-up controlled dispersions are typically lower than this value [53: 0.003 L/L, 54: 0.0015 L/L, 63: 0.0058 L/L, 64: 0.003 L/L]. 0.003 L/L dispersed phase concentration was used in this work. Paraffin oil (Weissöl, Brenntag, Germany) was used as the dispersed phase. Paraffin oil has some traits that are important for experiments in larger scale. It is available as a relatively cheap bulk chemical in large amounts; it is not poisonous and does

not exhibit any particular risks during usage or for disposal. The oil had a density of 880 kg/m^3 (measured with a pyknometer) and a viscosity of 0.107 Pa·s (measured with a PaarPhysica MC1 plate-cone viscosimeter with cone MK91/2, Anton Paar, Germany) at 25°C. The interfacial and surface tensions of the buffer/air/oil system are given in Table 3.1. Interfacial properties were measured with a drop volume tensiometer (TVT2, Lauda, Germany).

Table 3.1: Interfacial properties of buffer/air/paraffin oil-system at 25°C (measured with drop volume tensiometer TVT2, Lauda, Germany)

Surface tension buffer-air σ_{BA}	72.5	mN/m
Surface tension oil-air σ_{OA}	33.5	mN/m
Interfacial tension buffer-oil σ_{BO}	47.3	mN/m
Spreading coefficient Sp	-8.3	mN/m

3.3.3 Sampling procedure

The sampling setup is illustrated in Figure 3.2. A steel pipe (1) of inner diameter of 3.5x10^{-3} m was installed in the tank through a standard Ingold port. The Ingold port ensures maximum flexibility in terms of the applicability of the method to pilot plant and large scale equipment. The diameter of the pipe was chosen to be in the range of at least 5 times the largest drop diameter to be expected. The port was located between the bottom and the middle agitator at 0.24 m from the tank bottom at 45° between two baffles. The pipe length inside the reactor was 0.1 m.

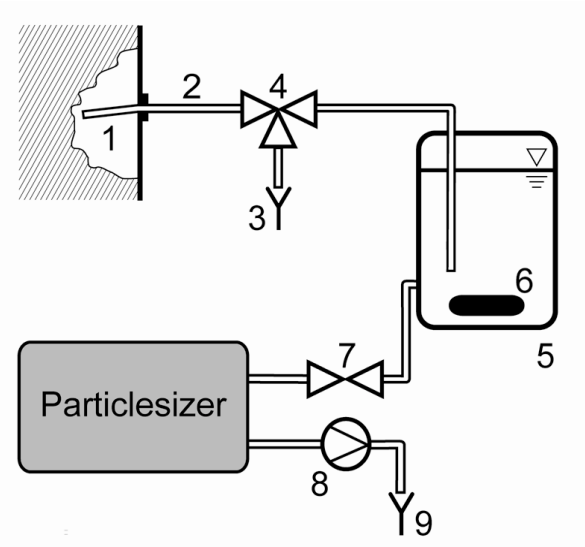

Figure 3.2: Schematic drawing of the measurement setup: 1: steel pipe; 2: silicone tubing; 3: discharge to provide steady flow before sampling; 4: three-$_{way}$ valve; 5: sample beaker; 6: magnetic stir bar, 7: valve to particlesizer; 8: peristaltic pump; 9: discharge for sample after measurement.

The pipe was connected with 4.0×10^{-3} m inner diameter silicone tubes (2). The sample stream was first directed to the discharge (3) to establish a steady flow and exchange the liquid hold-up in the piping by fresh sample. The flow rate of the sample was pressure driven. A three-way valve (4) allowed for fast switching to a sample beaker (5) without interruption of the flow. The valve between the sample beaker and the particlesizer (7) was closed during the whole sampling procedure. No pump was used to withdraw the sample to avoid alteration of the drop size distribution inside the pump. Normally, the head-space pressure was at ambient pressure. For experiments where the sample flow rate was manipulated, the head-space pressure was increased for the time of sample withdrawal and set back to ambient pressure directly after sampling. The pressure increase depended on the desired flow but did not exceed 0.5 bar overpressure which yielded the highest sampling velocity of 2.1 m/s. A cylindrical glass beaker with 0.4 L total volume and an inner diameter of 0.08 m was used as the sample beaker. For sampling, the beaker was filled beforehand with 7.5 mL of a 0.5 M sodium dodecyl sulphate solution (SDS, Texapon K 12 P, Cognis, Germany) in deionised water. SDS is a fast anionic surfactant that was used to stabilize the drop dispersion from the tank for the subsequent steps of the measurement. The final SDS-

concentration after sample injection was 0.012 M which is about 1.5 times the critical micelle concentration of the surfactant (manufacturer data).

The sample was gently stirred at a rate of ~2-3 1/s by a magnetic lab stirrer (6) during the whole time of sample withdrawal to ensure a good availability of the surfactant during the sample addition. A cylindrical stir bar of length 40 mm and diameter 8 mm with rounded edges was used for stirring. Continuous phase was dosed to the beaker with the SDS-solution prior to the addition of the sample from the tank to dilute the sample. The amount of continuous phase was varied to adjust the sample concentration to an optimal "measuring concentration" for the subsequent measurement of the drop size distribution in a Coulter LS-100Q (Beckman Coulter, Krefeld, Germany) laser diffraction particlesizer. The "measuring concentration" is not the volumetric concentration of the organic phase in the sample but an output parameter of the measurement device that is related to the drop density in the measuring cell (a higher dilution was necessary for samples with small drops than for samples with large drops to reach the optimal "measuring concentration"). The total sample volume in the beaker after dilution was 0.3 L in any case including the SDS-solution, the continuous phase for dilution and the sample withdrawn from the tank. The optimal amount of continuous phase for dilution had to be determined iteratively. If the first try did not yield a "measuring concentration" in the optimal range, the measurement was repeated with a different amount of continuous phase until the correct "measurement concentration" was reached which was typically the case with the second sample. The optimal "measuring concentration" was given by the manufacturer as a range of 8-12%. However, no influence of the measuring concentration on the drop size distribution was observed in our experiments up to values of 25%. This finding was consistent with results of Peter et al. [9] for a different organic phase. The sample volume taken from the tank was typically 0.2 L. The sampled volume was replaced in the aerated tank by continuous phase if more than 10 samples were withdrawn from the tank during one experiment. The magnetic lab stirrer in the sample beaker was turned off about 5 s after the final sample volume of 0.3 L was reached.

3.3.4 Measurement procedure

The three main functions of the sample beaker were (I) stabilization of the dispersion by the addition of the surfactant, (II) dilution of the sample by the addition of continuous phase and (III) separation of air bubbles that were entrained in the sample flow. The separation of the air bubbles was necessary because the measurement principle of the laser diffraction

particlesizer does not allow for an automatic separate recognition of air bubbles and oil drops. Hence, the presence of air bubbles in the sample would alter the measured drop size distribution. Part of the air bubbles already separated from the liquid during the sampling. After the complete sample volume was transferred to the sample beaker and the magnetic lab stirrer was turned off, the air separated quickly. The settling time was defined as the time between turning off the magnetic lab stirrer after sample addition and turning on the magnetic lab stirrer for resuspension of the oil drops prior to the measurement. The settling time necessary to allow all bubbles that could interfere with the drop size measurement to separate can be estimated from the rise velocity of single air bubbles in still water. The bubble rise velocity can be calculated from a balance of lift and drag forces using Stokes' law for the drag coefficient as $u_b = \rho_c \cdot g \cdot d_b^2/(18 \cdot \eta_c)$ with the bubble rise velocity u_b, the density of the continuous phase ρ_c, the gravitational acceleration g, the bubble diameter d_b and the viscosity of the continuous phase η_c (taken as 10^{-3} Pa·s). The liquid level in the sample beaker at 0.3 L sample volume was 0.06 m. Therefore, bubbles down to a size of 30 µm would rise to the surface within 2 min. With this result, the typical settling time was fixed to 3 min. Some foam was observed on the surface during settling due to the presence of the surfactant. Most of this foam disappeared within the first two minutes of the separation and did not disturb the subsequent measurement. Due to the lower density of the organic phase, also oil drops separated on the liquid surface, which was the main reason for the application of the surfactant. After the settling time the oil drops were resuspended into the continuous phase by stirring with a magnetic lab stirrer (same type as described above). Resuspension took approximately 15 s at a stirring rate up to 8 1/s to resuspend all drops from the surface. Drop size distributions were subsequently measured by the laser diffraction particlesizer that was equipped with a flow-through chamber (SC100/200, Beckman Coulter, Krefeld, Germany). The valve between sample beaker and particlesizer (7 in Figure 3.2) was opened after resuspension of the oil drops and the sample was pumped through the chamber by a peristaltic pump (8; Watson Marlow 505DU, Watson Marlow GmbH, Rommerskirchen, Germany) downstream of the measurement device with a volumetric flow rate of 0.3 L/min. The measurement time was set to 15 s. The measurement range of the particlesizer is specified as 0.4 µm to 900 µm. The Fraunhofer approximation was used for the analysis of the size distribution. The Fraunhofer theory is accurate in the range of drop sizes larger than ~ 50 µm. Drop size measurements below ~ 50 µm might be flawed when analyzed with the Fraunhofer approximation [ISO 13320-1:199965] but this does not restrict the results in this study since the drop sizes of interest were larger than 50 µm for all samples (see next paragraph). A background measurement with continuous phase

was performed before each measurement to account for possible effects of any impurities. The flow-through chamber was rinsed thoroughly with continuous phase directly after each measurement to ensure a complete wash-out of the sample.

3.3.5 Calculation of the maximum stable drop diameter

The maximum stable drop diameter was derived from a measured drop size distribution incorporating the approach described in detail in Peter et al. [9]. Briefly, a Gaussian distribution was fitted to the main peak of a measured drop size distribution as illustrated in Figure 3.3. The integral of the measured and the fitted Gaussian volume density distribution is unity by definition. However, only the main peak of the measured drop size distribution was considered for the calculation of d_{max} and the fraction of small drops was neglected. The main peak of the distribution always fell into the range of drop sizes larger than 50 µm, showing that the application of the Fraunhofer approximation is justified. Disregarding the small drops caused a reduction of the integral for the measured values that has to be accounted for during the fitting of the Gaussian distribution. This was realized by the introduction of a linear scaling parameter A to scale the Gaussian distribution [9]:

$$q_3^m(d_i) = A \cdot \frac{1}{S \cdot \sqrt{2\pi}} \cdot \exp\left[-\frac{1}{2} \cdot \left(\frac{d_i - d_{mod}}{S} \right)^2 \right] \tag{3.5}$$

The Gaussian distribution was fitted to the measured values by fitting the scaling parameter A, the modal value d_{mod} and the standard deviation S simultaneously. The maximum stable drop diameter was calculated from these parameters as

$$d_{max} = d_{mod} + 2.58 \cdot S \tag{3.6}$$

as indicated in Figure 3.3. I.e. all drops smaller than d_{max} account for 99.5% of the total drop volume.

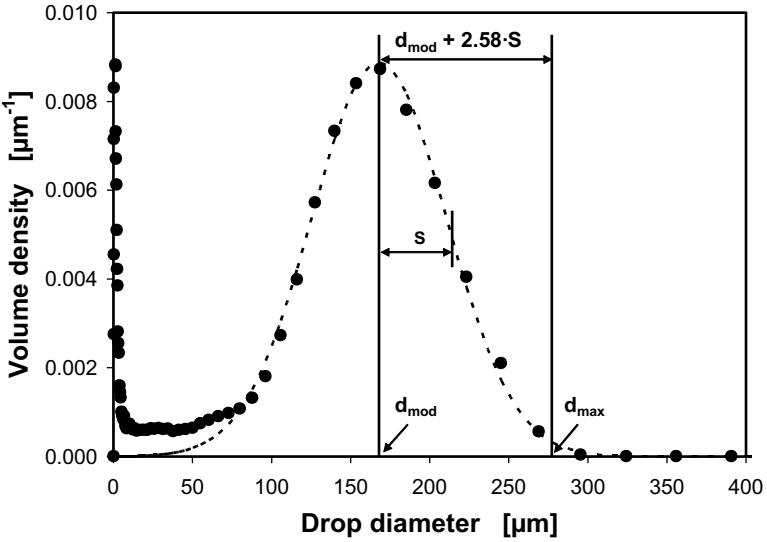

Figure 3.3: Determination of the maximum stable drop size. ● - measurement; dashed line – fitted Gaussian distribution. Experimental conditions: 0.05 m^3 stirred tank with 3 Rushton type impellers, filling volume 0.035 m^3, dispersed phase concentration 0.003 L/L, agitation rate 9.2 1/s, aeration rate 0.7 vvm, measurement was performed 170 min after oil addition.

3.4 Results and discussion

3.4.1 Selection of the dispersed phase

A careful choice of the dispersed phase is crucial to ensure that measured maximum stable drop sizes are solely defined by turbulent drop break-up. Preliminary results with different organic phases under aerated conditions showed that the introduction of air can lead to effects that massively influence drop sizes, even with low dispersed phase concentrations. A dispersion of soybean oil turned from translucent under unaerated conditions to opaque within few minutes after starting the aeration. Oil drops were not visible anymore with the naked eye in samples from the aerated dispersion; hence the drops must have become very small. Since it was apparent from these preliminary experiments that the soybean oil was not a suitable candidate for the dispersed phase, a more detailed investigation of the effect was not conducted and an explanation of the phenomenon cannot be given. A similar effect

was described by Dalmau et al. [66] who measured drop size distributions for aerated oleic acid dispersions (oleic acid is a major constituent of soybean oil) in a mineral medium for *Candida rugosa* fermentation in 1 L and 5 L reactors. The drop sizes reported by Dalmau et al. [66] are below 10 µm for all operating conditions. It was already pointed out by Galindo et al. [3] that these drop sizes were too small to be explained on the basis of the existing literature on liquid-liquid dispersion.

The opposite effect of an increase in drop sizes in the presence of air was also reported in literature [67]. The effect was explained by drop-bubble interactions that may lead to coalescence of drops in the presence of air. When a hydrophilic drop gets into contact with an air bubble it can either spread and form a liquid film around the bubble or it can form discrete lense-like drops on the surface of the bubble. If a second drop gets in contact with the rising drop-bubble complex, it can fuse with the organic phase layer leading to coalesced oil drops when the air bubble separates [67]. The tendency of an organic phase to spread on an air-water interface can be described by the spreading coefficient Sp that is defined as:

$$Sp = \sigma_{BA} - (\sigma_{OA} + \sigma_{BO}) \tag{3.7}$$

An organic phase will spread on the water-gas interphase if $Sp > 0$ and it will form lense-like drops, if $Sp < 0$. Therefore, $Sp > 0$ may lead to increased coalescence of the dispersed phase in the presence of air bubbles and $Sp < 0$ may inhibit coalescence caused by drop-bubble interaction.

Experiments with a silicone oil (Baysilone M 100, Bayer, Leverkusen, Germany) with a spreading coefficient of $+16 \times 10^{-3}$ N/m (calculated from manufacturer data) yielded a fast increase in drop sizes from a Gaussian like distribution with maximum stable drop diameter of 160 µm under unaerated conditions to a more log-normal distribution with a fraction of drops larger than the measurement range of 900 µm with aeration at the same agitation rate. An increase in drop sizes appeared already in the first sample only 1 min after starting the aeration. Hence, strong coalescence was present although the oil fraction was only 0.003 L/L. This coalescence effect can most probably be attributed to the drop-bubble interaction under aerated conditions.

The spreading coefficient of paraffin oil calculated from the measured values in Table 3.1 is negative with -8.3×10^{-3} N/m which is well in agreement with the value of -6.6×10^{-3} N/m measured by Yoshida [68] at 30°C. Consequently, paraffin drops will not spread out on the

gas-water interface when they get into contact with an air bubble. Coalescence behaviour of paraffin oil was tested in experiments with aeration with different dispersed phase concentrations from 0.0005 L/L to 0.01 L/L. No influence of the dispersed phase concentration on the maximum stable drop size was detectable although the dispersed phase concentration was increased 20 fold (see Section 5.4.3, Figure 5.5). Hence, the dispersion can be regarded as coalescence inhibited under the tested aerated conditions. Since coalescence depends on drop size and flow characteristics a generalisation of this result must be treated with some care. Negligence of coalescence should be tested especially when changing scales. Effects like described above for soybean oil and silicone oil were not observed with paraffin oil. The difference to the behaviour of the silicone oil is in agreement with the different spreading coefficients of the two oils. The results strongly indicate that coalescence is negligible for the development of the drop size distribution with paraffin oil as the dispersed phase. Therefore, paraffin oil was chosen as the model dispersed phase to establish the sampling and measurement procedure for measuring maximum stable drop sizes in aerated liquid-liquid dispersions. With the maximum stable drop size being break-up controlled the most important prerequisite for the correlation of results with maximum local energy dissipation rate is satisfied. In combination with a reliable sampling and measurement procedure this choice of dispersed and continuous phase with the properties described above allows an experimental access to the comparison of turbulence intensity under operating conditions and in equipment that are not accessible by most other methods.

3.4.2 Verification of the sampling and measurement procedure

The two major concerns with any technique involving sample removal and subsequent measurement is to ensure that the sample handling between sample withdrawal and measurement does not alter the drop size distribution and that the sample withdrawn from the bulk volume is representative for the drop size distribution at the point of sampling. The main step in sample handling was the separation of the air bubbles from the sample during the settling time. As described above, oil drops rise to the liquid surface during the settling time where the local oil concentration becomes high and the drops are in direct contact with each other. This might promote drop coalescence in the sample beaker during the settling time, which was in fact observed in preliminary experiments without surfactant. To assess the influence of settling time on the drop size distribution, measurements were conducted for settling times of 1 min to 20 min. The samples for the measurements were withdrawn between the second and the third hour after starting the dispersion process. A constant size

distribution was already established at that time (as discussed below). Figure 3.4A shows results for an agitation rate of the Rushton impellers of 7.5 1/s and an aeration rate of 0.7 vvm. The experiment with 2 min settling time was repeated twice (Index II in the legend). The cumulative volume frequency distributions exhibit only minor deviations from each other for a time range of one third to nearly seven fold the typical value of 3 min. The drop size distributions for drops in the range above ~ 150 µm (which appears as the main peak in a frequency distribution plot) is essentially linear in the probability plot shown in Figure 3.4A. The Gaussian distribution is therefore a suitable approximation for the measured drop size distributions. The results show that the drop size distribution is not influenced by the settling time in the investigated range. The insert in Figure 3.4A shows the maximum stable drop diameters calculated for these measurements. The average value was 408 µm in this experiment. No dependence on settling time was observed. Thus, it can be concluded, that an alteration of the drop size distribution after sample withdrawal by coalescence is effectively inhibited by the addition of the surfactant and the applied sampling procedure. Pereira and Ni [69] successfully applied a similar approach of sampling and direct stabilization of the sample by addition of a surfactant to a liquid-liquid dispersion of silicone oil in water, supporting the results found here.

The next step before the actual measurement was the resuspension of the oil drops. Since the surface tension was reduced by the surfactant, stirring for resuspension might induce drop break-up. This was tested by increasing the time for resuspending the oil drops after the settling time from the typical 15 s up to 2 min (results not shown). Consecutive samples showed no effect of the increased stirring time with the magnetic lab stirrer. That means the stirring is either too gentle to alter the drop size distribution or the time for resuspension is too short to have an impact on the measured drop sizes.

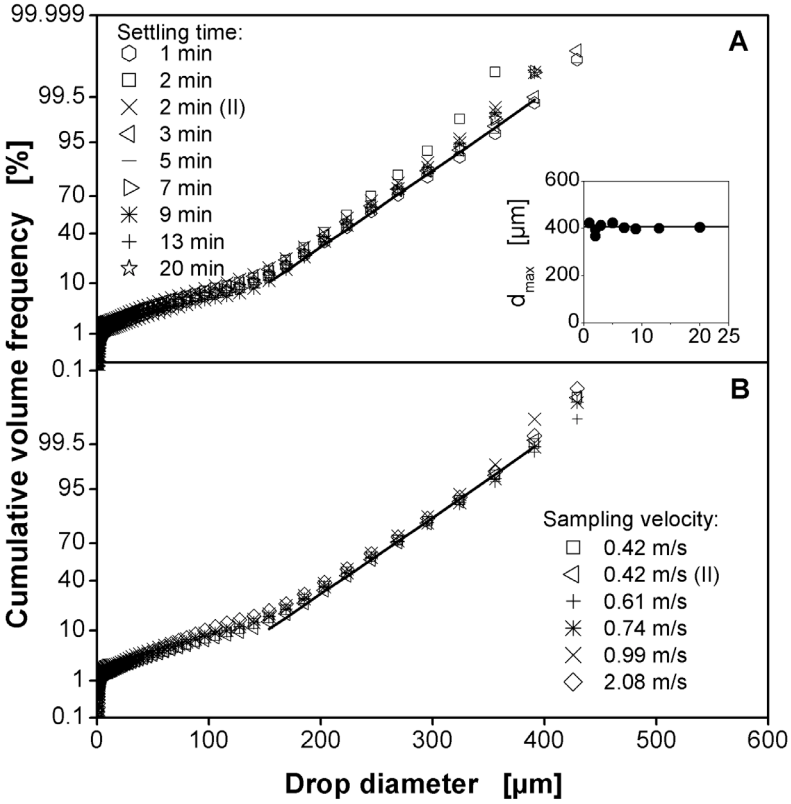

Figure 3.4: Influence of sample handling: A: influence of settling time on drop size distribution and maximum stable drop size (insert); settling time of 2 min was repeated twice. B: influence of sampling velocity on drop size distribution. Standard value of 0.42 m/s was conducted as first and last condition (Index II) to show reproducibility throughout the experiment. Solid lines show fitted normal distribution with parameters optimized for data in Figure 4B. Experimental conditions: reactor configuration A-1 (see Table 2.2), filling volume 0.035 m^3, dispersed phase concentration 0.003 L/L, agitation rate 7.5 1/s, aeration rate 0.7 vvm, measured between 120 min and 180 min after oil addition.

The integrity of the sample during the withdrawal from the reactor and the representativeness of the sample were tested by sampling with different sampling velocities. If the measured drop size distribution was dependent on the sample flow rate this could be an indication that the sample withdrawn from the reactor is not representative because of classification of drops due to the sampling process. This effect was described for probing solids suspensions where isokinetic sampling is suggested to avoid classification effects

[70]. It can be assumed that an alteration of the sample between the inlet of the sampling pipe inside the reactor and the suspension in the sample beaker would be dependent on the flow conditions and the residence time in the tube. The relevance of these effects was tested by sampling with different flow rates of 0.42 m/s to 2.1 m/s that were taken from a stationary dispersion at an agitation rate of the Rushton impellers of 7.5 1/s and an aeration rate of 0.7 vvm. The lowest sampling velocity of 0.42 m/s results for the standard case of ambient head-space pressure in the reactor. The drop size distribution for this sampling velocity was measured twice. The second sample at 0.42 m/s was measured after the samples with increased head-space pressure to test if the pressure manipulation for the time of sampling influenced the drop size distribution. Figure 3.4B depicts the results from these measurements.

All drop size distributions fall within a narrow range. Sampling velocity showed no effect on the measured drop size distribution in the investigated range. This is in agreement with the findings of Bae and Tavlarides [71] who reported the independence of drop size distribution and Sauter mean diameter for sampling velocities above 0.2 m/s for toluene drops dispersed in a mixing vessel. It can thus be concluded that the samples are representative for the drop size distributions inside the tank, that the drop size distributions are not distorted between the inlet of the pipe and the sample beaker and that the handling of the sample in the sample beaker does not change the measured drop size distribution.

3.4.3 Reproducibility of consecutive sampling

The maximum stable drop diameter for a wide range of operating conditions with agitation rates varied from 4.2 1/s to 10 1/s at an aeration rate of 0.7 vvm are presented in Figure 3.5. The solid lines represent the average values for the corresponding measurements. Samples were taken between 110 min and 190 min after oil addition or a step-change in agitation rate, respectively. No time-dependence of the maximum stable drop size was observed in the range of the measurement accuracy. The effect of turbulence intermittency does not seem relevant during this time span. Hence, the drop size distribution can be regarded as stable and consecutive samples can be treated as reproductions. Relative standard deviations for consecutive measurements of the maximum stable drop size for the different agitation rates were below 4 %. A good reproducibility of the measurement results was achieved over the whole range of typical agitation rates. The maximum stable drop size decreases with increasing agitation rate as expected.

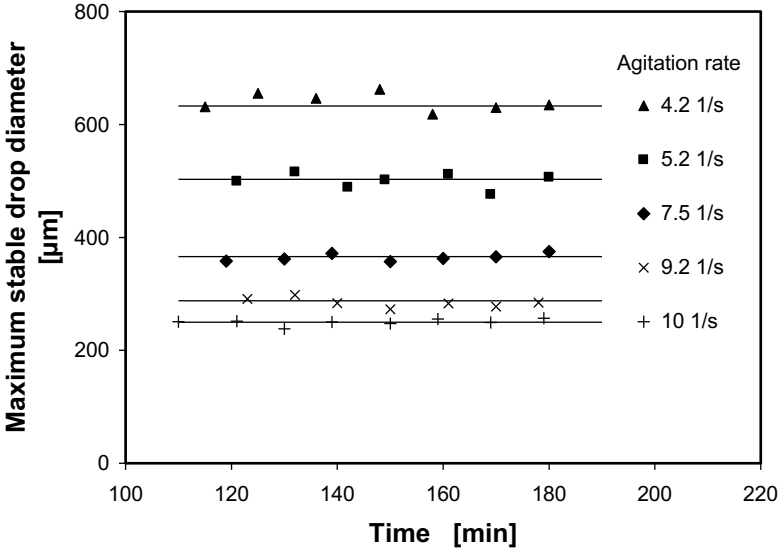

Figure 3.5: Reproducibility of consecutive measurements. Experimental conditions: reactor configuration A-1 (see Table 2.2), filling volume 0.035 m^3, dispersed phase concentration 0.003 L/L, agitation rate varied, aeration rate 0.7 vvm, measured between 120 min and 180 min after oil addition.

3.4.4 Drop size distributions for different agitation rates

Drop size distributions for different agitation rates and an aeration rate of 0.7 vvm are shown in Figure 3.6. Generally, the distributions become narrower (increased slope in probability plot) with increasing agitation rate and are shifted towards smaller drops. The solid lines in Figure 3.6 represent the fitted Gaussian distributions for the measured drop size frequencies. The larger drops above approx. the 10^{th} percentile of the distribution are essentially normally distributed which is reflected by the linear correlation in the probability plot. A normal distribution of drop sizes is in line with measurements in unaerated coalescence inhibited dispersions [9, 39, 72]. A fraction of small sized particles exists in all distributions that deviate from the normal distribution.

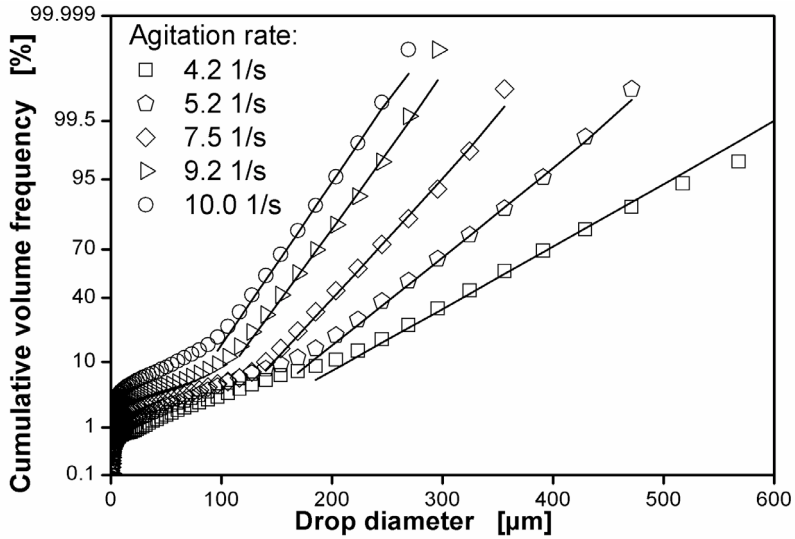

Figure 3.6: Drop size distributions for different operating conditions. Solid lines: fitted Gaussian distributions. Experimental conditions: reactor configuration A-1 (see Table 2.2), filling volume 0.035 m^3, dispersed phase concentration 0.003 L/L, agitation rate varied, aeration rate 0.7 vvm, measured between 120 min and 180 min after oil addition.

3.4.5 Experiment to experiment reproducibility

The reproducibility of independent experiments for different agitation rates is shown in Table 3.2. The maximum stable drop diameters reported are average values of at least 4 consecutive samples from the same experiment. The standard deviation for independent experiments is typically in the range of 10 % of the maximum stable drop size. The average maximum stable drop sizes for the similar agitation rates of 7.3 1/s and 7.5 1/s differ by 48 µm. Taking the standard deviation of the measurements into account it becomes obvious that this difference is not significant. This scatter in the data may be attributed to inaccuracies in operating conditions (control of agitation and aeration rate) and uncontrollable trace impurities introduced by either the liquids used, by the purged air or from the reactor surfaces although great care was taken to thoroughly rinse the tank before and after experiments. It is well known that liquid-liquid dispersions are extremely sensitive to impurities [49]. This difficulty may be expected to be less pronounced in larger reactors since surface area becomes smaller compared to the working volume in larger tanks.

Table 3.2: Experiment to experiment reproducibility. Experimental conditions: reactor configuration A-1 (see Table 2.2), filling volume 0.035 m^3, dispersed phase concentration 0.003 L/L, agitation rate varied, aeration rate 0.7 vvm.

Agitation rate [1/s]	4.0	5.0	7.3	7.5
No. of experiments	2	2	3	5
Maximum stable drop diameter [µm]	785	687	417	369
Standard deviation [µm]	104	44	41	34
Rel. standard deviation [%]	13	6	10	9

Eq. 3.1 allows a rough estimation of the difference in turbulence intensity that can be detected with a standard deviation in the drop size of 10 %: a reduction in maximum local energy dissipation rate by 21 % is necessary for an increase in maximum stable drop diameter of 10 % and an increase in maximum local energy dissipation rate by 30 % is necessary for a decrease in maximum stable drop diameter of 10 %. This range can be regarded as an approximation for the minimum difference in turbulence intensity that can be detected by the method. Given the facts that large differences in turbulence levels exist for different reactor configurations [38], that the characterization of turbulence intensity is extremely difficult with any method [73] and that a unique operating range with high gas hold-ups and power inputs can be characterized with the drop size based method it can be concluded that the approach presented here is very promising.

3.4.6 Conclusions

A method was presented that can be used to measure maximum stable drop sizes in aerated dilute liquid-liquid dispersions. Coalescence is inhibited by using a dilute dispersion in a continuous phase with low ionic strength and by incorporating a dispersed phase, paraffin oil, with a negative spreading coefficient which prevents coalescence as a consequence of drop-bubble interaction. This enables the possibility to compare levels of turbulence intensity under operating conditions that are hardly accessible by other methods like intense aeration and agitation in stirred tanks. Special attention was paid on the applicability of the method in scale-up experimentation. Relevant constraints for the application in large-scale experiments like usage of standard ports, safety and environmental considerations and the presence of high volumetric gas hold-ups were presented and accounted for during method

development. The measurement procedure consists of withdrawal of a sample from the mixing tank, stabilization of the drop size distribution by a surfactant in a sample beaker, separation of entrained air bubbles and subsequent measurement of the drop size distribution with a laser diffraction particlesizer. It was shown, that the sample withdrawn from the tank is representative and that the measurement procedure does not alter the drop size distribution. The sampling and measurement procedure was demonstrated to be highly reproducible. The standard deviation for independent experiments was in the range of 10 %.

The application of this method to investigate the influence of aeration on turbulence intensity and to compare turbulence intensity in reactors of different scales under operating conditions that are characterized by intense aeration and agitation will be presented in Chapters 5 and 6. The following Chapter 4 covers an analysis of the electrical power measurement in the 3 m^3 reactor that is the basis for a reliable impeller power input measurement for the evaluation of the drop-dispersion experiments in the subsequent work.

4 Verification of power input measurement in the 3 m^3 reactor

4.1 Introduction

Impeller power input is one of the most important parameters for processes involving stirred reactors. There are two major reasons for this: first, impeller power draw contributes significantly to operating costs and, therefore, to process economics. Second, impeller power draw correlates with many process parameters like heat and mass transfer and mixing efficiency which makes it an important parameter for reactor design and scale-up considerations. Impeller power input is of primary interest for the focus of this work because it is directly related to hydromechanical stress (see Section 5.2).

There are different possibilities to measure power input. A detailed and comprehensive review of the available methods was presented by Ascanio et al. [74]. Only a short overview of the most important methods based on this review will be given here: A method with high accuracy uses strain gauges that measure the strain of the impeller shaft due to the resistance of the liquid. Strain gauges are installed inside the tank directly on the impeller shaft. This offers the advantage that the measurement occurs behind the shaft sealing and bearing. Therefore, friction does not influence the measurement result when applying this method (provided that there are no shaft bearings inside the tank). Another possibility to measure power input is to measure the torque τ that is generated as the reaction to the resistance of the liquid by a torque meter. Power is related to torque by $P = 2 \cdot \pi \cdot n \cdot \tau$ (with P – power in [W], n – agitation rate in [1/s], τ – torque in [Nm]). The torque meter is coupled to the shaft between the engine and the bearing outside the tank. Friction losses in the sealing and in

bearings have to be taken into consideration for accurate measurements. Another possibility to make use of the torque is to mount the whole reactor on a low friction bearing and measure the force needed to hold the reactor in place. This method is referred to as the dynamometer method. Also this method measures the sum of impeller power input to the liquid and friction losses which demands for a correction for the friction losses to get reliable values for the power transferred to the liquid. These three methods need special instrumentation that is typically not available in process equipment in industries. Costly installations would be necessary to apply these measurement methods.

A method that only needs standard installations is based on the heat generated by stirring. Since all kinetic energy that is introduced by the impellers to the liquid dissipates into heat a heat balance can be used to measure impeller power input. This can be done in two ways. If the flow rate of cooling water and the cooling water inlet and outlet temperatures are known, the reactor temperature can be stabilized to a constant value at given operating conditions and the power input can be calculated from a stationary heat balance around the cooling system. Since there is a temperature difference between the cooling system and the environment, there is a heat exchange with the surrounding. This might be more relevant in lab scale and less pronounced in large reactors due to their lower surface area to volume ratio. But there is another important effect that is driven by the temperature difference that might be relevant for large reactors. When humidity is high in the surrounding, which is often the case in fermentation facilities, steam might condensate on the cool surface of the reactor which creates a large heat flow that will render the measurement results useless. Small reactors can be insulated to minimize these effects but this is normally not possible in large equipment. The second way to make use of a heat balance to measure power input is to disable the reactor cooling system and measure the temperature increase due to stirring without cooling. An instationary heat balance around the reactor volume can be solved to calculate the power input by stirring. Also in this case the heat exchange with the surrounding has to be minimized. But this can be done effectively by setting the reactor temperature close to the environmental temperature. This eliminates condensation of water on the reactor surface and heat exchange with the surrounding. Both methods are not applicable as in-process measurement of impeller power input.

A different possibility to measure power input is to use the electrical power that is consumed by the engine. In principal, this is a convenient method in large reactors because measurement of electrical power is a standard measurement in production facilities. The total electrical power consumed is the sum of power transferred to the liquid, friction losses

in sealings, bearings and gear belt and efficiency losses within the engine. The measured value of electrical power must be corrected to account for this additional load to the engine. Measurement of power input by electrical power in small reactors is generally regarded as inaccurate since the power introduced to the liquid is small compared to friction losses in the sealing and bearings [75]. However, in large reactors power losses are small compared to the power transferred to the liquid. If the power losses can be estimated, measurement of the electrical power is fast, convenient and can give good results. One simple way to approximate the power losses is to measure electrical power draw in an empty reactor. In this case the power input to the liquid is eliminated and all power drawn by the engine can be attributed to the power losses. However, this leads to a different load of the engine at a given agitation rate than in normal operation. This might cause inaccuracies because the efficiency of the engine is typically load dependent. Since the magnitude of this effect is not known, an independent method to measure the power losses would be useful to verify the results gained in these experiments. Additionally, measurement of electrical power in the typical industry reactors with 3-phase alternating current engines with frequency transformers is not straight forward and subject to systematic measurement errors. Reliability of the measured electrical power values should, therefore, be tested with an independent method before using the electrical power measurement. These control experiments can be conducted with the instationary temperature method. Applying the instationary temperature method as a control method also offers the possibility to establish a correlation for the power losses as the difference between the total electrical power draw and power input to the liquid measured by the instationary temperature method. Once a correlation for power losses is established, measurement of electrical power input can be corrected to directly yield the power input to the liquid.

This approach will be applied in the following chapter in a 3 m^3 reactor to ensure an accurate power measurement and to establish a correlation for power losses as a basis for the analysis of the drop dispersion experiments in the subsequent work. The instationary heat balance will be introduced in the next section (Section 4.2). After that, the experimental procedure will be explained (Section 4.3) followed by a discussion of the measurement results gained for two different impeller setups (4.4).

4.2 Instationary heat balance

Figure 4.1 depicts a schematic drawing of the reactor with the relevant sources of power input and rates of heat flow:

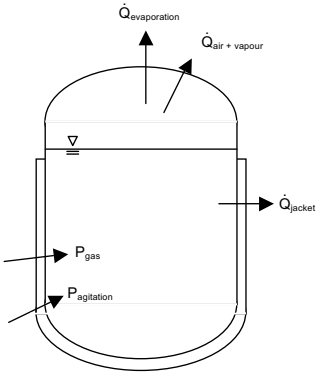

Figure 4.1: Schematic drawing of the reactor with all relevant heat flows for the instationary heat balance.

The kinetic energy introduced by the stirrer dissipates into heat in the reactor volume which is symbolized by $P_{agitation}$. This heat increases the temperature of the liquid inside the tank but also the temperature of the tank itself which is made of steel. An additional power input stems from the pneumatic power from the rising gas bubbles P_{gas} in the case of aerated operating conditions. Heat flows leaving the balance volume can be heat loss to the surrounding $\dot{Q}_{jacket}$. If experiments are conducted with aeration additionally the energy necessary to heat or cool the incoming gas flow to the actual reactor temperature has to be accounted for. The incoming gas flow consists of air with some vapour content. The heat flow for tempering the incoming gas is depicted as $\dot{Q}_{air+vapour}$. When the air bubbles through the liquid, water evaporates into the air. It is assumed that gas leaving the reactor is completely saturated with water vapour at the temperature of the liquid. Evaporation contributes to the heat balance as $\dot{Q}_{evaporation}$. The cooling system is not active. So there is no heat flow to the cooling system. Further assumptions are that all heat flows are quasi-stationary. I.e. the temperature rise due to stirring is by far the slowest process and is rate limiting. Heat introduced by friction at the shaft sealing and bearings is neglected in the balance.

The heat balance can thus be formulated as:

$$\left(c_{p,water} \cdot m_{water} + c_{pV,steel} \cdot V_{steel}\right) \cdot \frac{dT}{dt} = P_{agitation} + P_{gas} - \dot{Q}_{jacket} - \dot{Q}_{air+vapour} - \dot{Q}_{evaporation} \qquad (4.1)$$

with the specific heat capacity of water $c_{p,water}$, the total amount of liquid in the tank m_{water}, the heat capacity of steel $c_{pV,\,steel}$ and the total volume of the steel of the reactor jacket V_{steel}. The volume of the jacket is approximated by the volume of a cylinder with wall thickness d_{steel}:

$$V_{steel} = \pi \cdot d_{steel} \cdot \left(D_R + d_{steel}\right) \cdot H_{jacket} \cdot F \qquad (4.2)$$

where H_{jacket} is the height of the cylinder and F is a correction factor that is introduced to correct for interiors and bottom and top of the reactor.

4.2.1 Pneumatic power

The pneumatic power input due to the rising gas can be calculated from [76]:

$$P_{gas} = \rho_c \cdot g \cdot H \cdot Q_g \qquad (4.3)$$

with the density of the continuous phase ρ_c, the gravitational acceleration g, the liquid height H and the gas flow rate Q_g.

4.2.2 Evaporation

The heat of evaporation can be calculated from

$$\dot{Q}_{evaporation} = \dot{n}_{vapour} \cdot \Delta h_v \qquad (4.4)$$

$\dot{n}_{vapour}$ is the molar flow of water that evaporates into the gas flow and Δh_v is the evaporation enthalpy of water. $\dot{n}_{vapour}$ can be calculated from a gas balance of the reactor volume which is depicted in Figure 4.2:

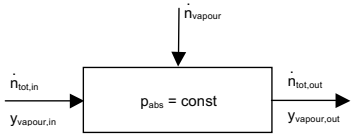

Figure 4.2: Schematic drawing of the gas balance with all relevant parameters.

$\dot{n}_{tot,in}$ and $\dot{n}_{tot,out}$ are the molar flows of gas entering and leaving the reactor. $y_{vapour,in}$ and $y_{vapour,out}$ are the molar fractions of water in the respective flows. p_{abs} is the absolute pressure in the reactor which is constant. $\dot{n}_{tot,in}$, $y_{vapor,in}$ and p_{abs} are measured values. $y_{vapor,out}$ can be calculated from the saturation vapour pressure if the temperature is known. $\dot{n}_{tot,out}$ and $\dot{n}_{vapour}$ must be calculated. The water balance reads:

$$y_{vapour,out} \cdot \dot{n}_{tot,out} = y_{vapour,in} \cdot \dot{n}_{tot,in} + \dot{n}_{vapour} \tag{4.5}$$

and the total molar balance for the gas phase:

$$\dot{n}_{tot,out} = \dot{n}_{tot,in} + \dot{n}_{vapour} \tag{4.6}$$

Thus:

$$y_{vapour,out} \cdot \left(\dot{n}_{tot,in} + \dot{n}_{vapour}\right) = y_{vapour,in} \cdot \dot{n}_{tot,in} + \dot{n}_{vapour} \tag{4.7}$$

Which can be transformed to yield the total molar flow of water that evaporates

$$\dot{n}_{vapour} = \dot{n}_{tot,in} \frac{\left(y_{vapour,in} - y_{vapour,out}\right)}{\left(y_{vapour,out} - 1\right)} \tag{4.8}$$

with $y_{vapour} = p_{vapour} / p_{abs}$, $\dot{n}_{tot,in} = \dot{V}^{N}_{tot,in} / V_{mo}$ and the relative humidity $\varphi = p_{vapour} / p^{S}_{H_2O}$ this can be transformed into:

$$\dot{n}_{vapour} = \frac{\dot{V}^{N}_{tot,in}}{V_{mo}} \frac{p^{S}_{H_2O,out} - \varphi_{in} \cdot p^{S}_{H_2O,in}}{p_{abs} - p^{S}_{H_2O,out}} \tag{4.9}$$

Combination of Eq. 4.9 with Eq. 4.4 results in:

$$\dot{Q}_{evaporation} = \frac{\dot{V}^{N}_{tot,in}}{V_{mo}} \cdot \frac{p^{S}_{H_2O,out}(T_{out}) - \varphi_{in} \cdot p^{S}_{H_2O,in}(T_{in})}{p_{abs} - p^{S}_{H_2O,out}(T_{out})} \cdot \Delta h_v \tag{4.10}$$

The saturation vapour pressure as a funtion of temperature can be calculated from

$$p^{S}_{H_2O}(T) = 5.9 \cdot (T - 273.15)^2 - 104.2 \cdot (T - 273.15) + 2063.1 \tag{4.11}$$

with $p^{S}_{H_2O}(T)$ in Pa and T in Kelvin. Eq. 4.11 approximates Hardy's equation for water vapour pressure based on the ITS-90 standard [77] within ±0.8 % in the temperature range 20°C – 40°C and within 2.9 % in the range 40°C to 45°C.

4.2.3 Air flow temperature change

The heat flow due to the temperature change of the incoming air flow can be calculated from:

$$\dot{Q}_{air+vapour} = \left(c_{p,air} \cdot \dot{m}_{air} + c_{p,vapour} \dot{m}_{vapour,in}\right) \cdot \left(T_{out} - T_{in}\right) \tag{4.12}$$

With $\dot{m} = \dot{V}^{N} / V_{mo} \cdot MW$ and

$$\dot{V}^{N}_{vapour,in} = y_{vapour,in} \cdot \dot{V}^{N}_{tot,in} = \varphi_{in} \cdot \frac{p^{s}_{H_2O,in}}{p_{abs}} \cdot \dot{V}^{N}_{tot,in} \tag{4.13}$$

follows:

$$\dot{m}_{vapour,in} = \varphi_{in} \cdot \frac{p^{s}_{H_2O,in}}{p_{abs}} \cdot \frac{\dot{V}^{N}_{tot,in}}{V_{mo}} \cdot MW_{water} \tag{4.14}$$

The air flow can be calculated from:

$$\dot{V}^{N}_{air} = \dot{V}^{N}_{tot,in} - \dot{V}^{N}_{vapour,in} = \left(1 - \varphi_{in} \cdot \frac{p^{s}_{H_2O,in}}{p_{abs}}\right) \cdot \dot{V}^{N}_{tot,in} \tag{4.15}$$

Approximating the composition of air with 79% nitrogen and 21% oxygen, this is equivalent with:

$$\dot{m}_{air} = \left(1 - \varphi_{in} \cdot \frac{p^{s}_{H_2O,in}}{p_{abs}}\right) \cdot \frac{\dot{V}^{N}_{tot,in}}{V_{mo}} \cdot \left(0.79 \cdot MW_{N_2} + 0.21 \cdot MW_{O_2}\right) \tag{4.16}$$

Combining Eqs. 4.14 and 4.16 with 4.12 results in:

$$\dot{Q}_{air+vapour} = \left(c_{p,air} \cdot \left(1 - \varphi_{in} \cdot \frac{p^{s}_{H_2O,in}}{p_{abs}} \right) \cdot \frac{\dot{V}^{N}_{tot,in}}{V_{mo}} \cdot \left(0.79 \cdot MW_{N_2} + 0.21 \cdot MW_{O_2} \right) \right) \cdot \left(T_{out} - T_{in} \right) + \left(c_{p,vapour} \cdot \varphi_{in} \cdot \frac{p^{s}_{H_2O,in}}{p_{abs}} \cdot \frac{\dot{V}^{N}_{tot,in}}{V_{mo}} \cdot MW_{water} \right) \cdot \left(T_{out} - T_{in} \right) \quad (4.17)$$

with $c_{p,air} = 1 \frac{kJ}{kgK}$ and $c_{p,vapour} = 2.02 \frac{kJ}{kgK}$.

If the due point of the inlet air T_d is measured (at the pressure of the inlet air p_{in}), the relative humidity can be calculated from:

$$\varphi_{in} = \frac{p^{s}_{H_2O}(T_d)}{p^{s}_{H_2O,in}(T_{in})} \cdot \frac{p_{abs}}{p_{in}} \quad (4.18)$$

The water vapour pressure can be calculated with Eq. 4.11. The outlet temperature T_{out} can be assumed to be equivalent with the reactor temperature $T_{reactor}$.

4.2.4 Heat flow to the environment

The heat flow through the reactor jacket to the environment can be modelled assuming that the conductive heat flow in the metal jacket of the reactor is much faster than the convective heat flow to the environment. In this case, the heat flow to the environment is rate limiting and the temperature at the outside jacket surface is equal to the liquid temperature. All fluxes are assumed quasi-stationary which means that the temperature change due to stirring occurs much slower than the convective heat-flow to the environment. The heat flow to the environment can thus be calculated as:

$$\dot{Q}_{jacket} = Nu \cdot \lambda_{air} \cdot \frac{A_{jacket}}{L} \cdot \left(T_{reactor} - T_{environment} \right) \quad (4.19)$$

where the Nusselt number $Nu = \alpha \cdot H_{jacket} \lambda^{-1}_{air}$ is the dimensionless heat transfer coefficient, α is the heat transfer coefficient and λ_{air} is the heat conductivity of air. Nu is calculated with the height of the reactor as the characteristic length. The Nusselt number can be estimated based on a model for free convection on a vertical surface [78]. The complex geometry of the reactor is approximated by reducing the reactor to the cylindrical outside surface and neglecting the dished top and bottom. For a cylindrical geometry Nu can be calculated from:

$$Nu = Nu_{plate} + 0.435 \cdot \frac{H_{jacket}}{D_R} \tag{4.20}$$

with

$$Nu_{plate} = \left(0.825 + 0.387 \cdot \left[Gr \cdot Pr \cdot \left(1 + \left(\frac{0.492}{Pr} \right)^{\frac{9}{16}} \right)^{-\frac{16}{9}} \right]^{\frac{1}{6}} \right)^2 \tag{4.21}$$

Gr is the Grashof number $Gr = g \cdot H_{jacket}^3 \cdot \nu_{air}^{-2} \cdot \left(T_{environment} - T_{reactor}\right) \cdot T_{environment}^{-1}$ and Pr is the Prandtl number $Pr = \nu_{air} \cdot c_{p,air} \cdot \rho_{air}^{-1} \cdot \lambda_{air}^{-1}$.

The parameters ν_{air}, λ_{air} and Pr are temperature dependent and have to be determined at the average temperature T_{avg}:

$$T_{avg} = \frac{1}{2} \cdot \left(T_{environment} + T_{reactor}\right) \tag{4.22}$$

The temperature dependence of these parameters is approximated by a linear interpolation of the tabulated data from the [78] for 30°C, 40°C and 50°C:

$$\nu_{air} = 9{,}8 \cdot 10^{-8} \cdot T_{avg} - 1{,}3452 \cdot 10^{-5} \tag{4.23}$$

$$\lambda_{air} = 7{,}32 \cdot 10^{-5} \cdot T_{avg} - 4{,}4288 \cdot 10^{-3} \tag{4.24}$$

$$Pr = -1{,}15 \cdot 10^{-4} \cdot T_{avg} - 7{,}4165 \cdot 10^{-1} \tag{4.25}$$

$\dot{Q}_{jacket}$ can be calculated from Eqs. 4.19 to 4.25 when the temperatures inside the reactor $T_{reactor}$ and in the environment of the reactor $T_{environment}$ are measured.

4.3 Materials and methods

The experiments were conducted in the 3 m^3 reactor that is described in Chapter 2 (Figure 2.1, Table 2.1). The two different setups of Ekato Phasejet and Combijet impellers B-4 and B-5 were used for the experiments (see Table 2.3 and Figure 2.2). The different number of impellers in the two different setups allows a variation of the engine load at the same

agitation rate. This allows testing of the influence of engine load on the correlation for power loss.

Water was used as the working medium. The filling volume was 2.4 m^3. A weight measurement allowed the determination of the filling volume. A due point measurement was installed in the inlet air to measure the moist content of the air. The due point was essentially constant in the range of 6°C to 8°C throughout the experiments and the average value over the course of each experiment was used for the analysis of the data. Reactor and environmental temperatures were measured with standard Pt100 temperature sensors. The internal temperature sensor was installed at the bottom of the reactor. The initial temperature was set to less than 5°C below the environmental temperature to avoid condensation of humidity on the surface of the reactor. The external temperature sensor was installed approximately in the middle of the reactor height at 0.3 m from the tank outer surface. An average value of external temperature over the course of the experiment was used for data analysis. Operating conditions were kept constant for several hours depending on the experimental conditions and the reactor temperature was logged. Power input from agitation was then estimated based on the set of equations presented in Section 4.2. The ordinary differential equation system was implemented and solved in ModelMaker (Version 3, Cherwell Scientific Publishing, Oxford, UK). The parameters used for the calculations are listed in Table 4.1.

Measurement of power loss by electrical power measurement was conducted by setting different agitation rates when the reactor was filled with water to a level below the lowest impeller. The bottom shaft bearing had to be immersed in water to ensure sufficient cooling for the bearing.

Table 4.1: Parameter values used for the estimation of impeller power input from instationary temperature experiments.

Parameter	Value	Dimension
A_{jacket}	12	m^2
$c_{p,air}$	1.005	$kJ \cdot kg^{-1} \cdot K^{-1}$
$c_{p,vapour}$	2.02	$kJ \cdot kg^{-1} \cdot K^{-1}$
$c_{pV,steel}$	3713	$kJ \cdot m^3 \cdot K^{-1}$
$c_{p,water}$	4.183	$kJ \cdot kg^{-1} \cdot K^{-1}$
d_{steel}	$5 \cdot 10^{-3}$	m
F	1.3	-
H_{jacket}	2.5	m
H_L	2.12	m
Δh_v	40.7	$kJ \cdot mol^{-1}$
L	0.02	m
MW_{water}	18	g/mol
MW_{N2}	28	g/mol
MW_{O2}	32	g/mol
p_{in}	2.6	bar
p_{abs}	1	bar
V_L	2.4	m^3
V_{mo}	22.414	L/mol

4.4 Results and discussion

The relative importance of the different heat flows and the pneumatic power input from aeration that contribute to the heat balance can be evaluated by calculating their magnitude for typical conditions. Results for an environmental temperature of 42°C and a reactor temperature of 37°C, a reactor pressure of 1 bar, a dew point of the inlet air of 8°C (at 2.6 bar system pressure of the inlet air), an inlet air temperature of 35°C and a specific aeration rate of 0.7 vvm are depicted in Figure 4.3. The heat flow over the reactor jacket and the heat flow for tempering the inlet air are very small with 0.1 kW and -0.1 kW, respectively.

Pneumatic power contributes to the heat balance with 0.6 kW and heat of evaporation has a value of 3.2 kW which is in the same order of magnitude as the typical power input from agitation. While the heat flow over the reactor jacket and the heat for tempering the inlet air are small enough to be neglected, a good estimation of pneumatic power input and particularly of the heat of evaporation is necessary to be able to get reliable estimations for power input from agitation. Since all necessary parameters to calculate pneumatic power input and heat of evaporation are known or can be measured directly with high accuracy, it can be assumed that these parameters can generally be determined with high precision.

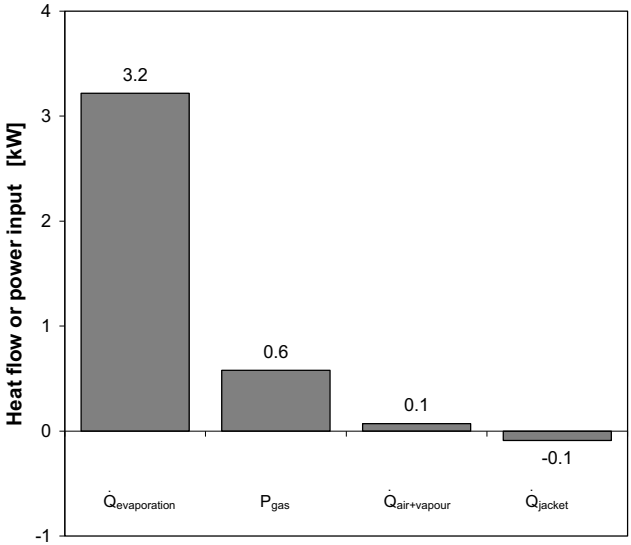

Figure 4.3: Magnitude of different heat flows and pneumatic power input from aeration at typical parameter values: environmental temperature 42°C, reactor temperature 37°C, reactor pressure 1 bar, dew point of the inlet air 8°C (at 2.6 bar), inlet air temperature 35°C, specific aeration rate 0.7 vvm.

A typical experimental result for reactor configuration B-5 with an agitation rate of n = 230 1/min and a specific aeration rate of 0.7 vvm is depicted in Figure 4.4. The external temperature is essentially constant at 42°C. The experiment starts at approximately 5°C below the environmental temperature. The reactor temperature rises to 41.8 °C within 3

hours of agitation. The temperature increase is not linear although power input from agitation is constant due to the constant operating conditions. The slope of the temperature rise decreases over time. This is caused by an increasing heat of evaporation due to the higher saturation vapour pressure at higher temperatures (Eq. 4.11). Power input due to agitation was estimated to 7.8 kW in this experiment. Measured and calculated temperatures are very well in agreement.

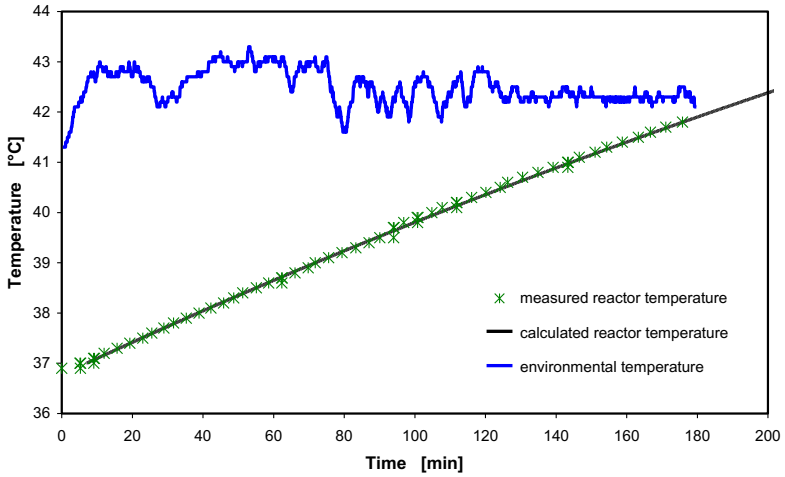

Figure 4.4: Comparison of measured and calculated reactor temperature. 3 m^3 reactor, impeller setup B-5 (see Table 2.1 and Table 2.3 for details). Operating conditions: agitation rate n = 230 1/s, specific aeration rate q_g = 0.7 vvm. Power input from parameter estimation based on instationary heat balance: 7.8 kW (P/V_L = 3.3 kW/m^3).

The total electrical power input for this experiment was 9.5 kW. This results in an estimate for power loss under these conditions of 1.7 kW. Therefore, power input would be overestimated by 18 % if the electrical power input was not corrected for the power losses. This shows the importance of a good estimation of power losses for a reliable power input measurement. And the correction becomes even higher at lower values of power input. This can be seen in Figure 4.5 where the measured values for electrical power input and for power loss are shown for different impeller setups and operating conditions. Figure 4.5 shows data for impeller setups B-4 and B-5. Due to the higher number of impellers in setup B-5, the total power input at the same agitation rate is higher for setup B-5 than for setup B-

4. In addition to the data for power loss based on the instationary temperature method also results for power loss from electrical power measurement in the empty reactor are shown.

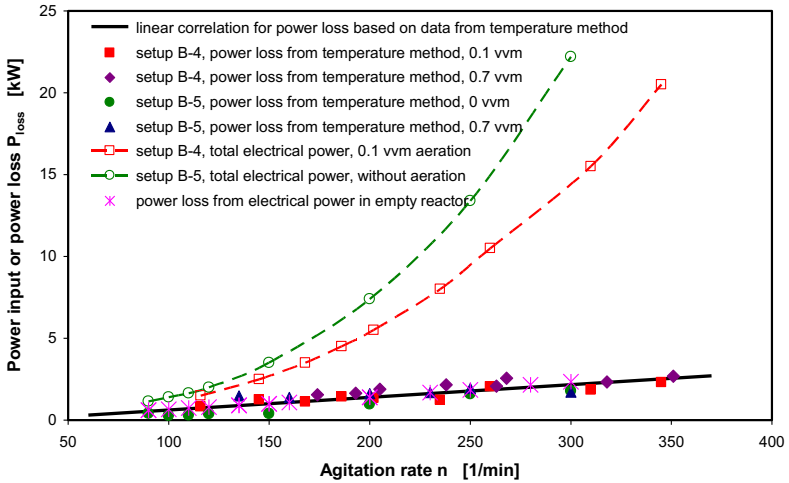

Figure 4.5: Power input from electrical power measurement and power loss as the difference between measured electrical power and power input from instationary temperature method for impeller setups B-4 and B-5 (see Table 2.3 for details) and different aeration rates. Power loss from measurement of electrical power in the empty reactor is also shown. Solid line: linear correlation of power loss.

The data for power losses for the two impeller setups with different operating conditions and also the results from electrical power measurement in the empty reactor are in good agreement with each other. That means power loss at a given agitation rate is essentially independent of the load of the engine. This allows the application of the correlation independently of the power characteristics of the impeller setup. Power loss can be correlated linearly with the following correlation:

$$P_{loss} = 463 \cdot n - 147 \qquad (4.26)$$

with power losses P_{loss} in W and agitation rate n in 1/s. R^2 for this correlation is 0.73 and the standard deviation of the residual between measured and calculated power loss is 0.17 kW.

4.5 Conclusions

Impeller power input in a 3 m^3 reactor was measured by electrical power measurement and by an instationary temperature method. The temperature method estimates the impeller power input due to stirring by solving an instationary heat balance around the reactor volume. Impeller power input, pneumatic power input due to aeration, heat flow due to evaporation, temperature change of the inlet air and heat exchange with the environment due to the temperature difference between the reactor and the environment are incorporated in the heat balance. An estimation of the magnitude of the different heat flows and the pneumatic power input for typical parameter values showed that the heat flow due to the temperature change of the inlet air $\dot{Q}_{air+vapour}$ and the heat exchange with the environment $\dot{Q}_{jacket}$ are very small under typical conditions while the pneumatic power input and particularly heat of evaporation contribute considerably to the heat balance. Heat of evaporation is of the same order of magnitude as typical values for impeller power input.

The temperature change in the reactor could be modelled successfully with the heat balance with fitted values for impeller power input. The difference between total electrical power and the value for impeller power input from the instationary temperature method are the power losses. Based on experiments with two different impeller setups with different power characteristics (setups B-4 and B-5, see Table 2.1 and Table 2.3) the linear correlation $P_{loss} = 463 \cdot n - 147$ (power loss P_{loss} in [W], agitation rate n in [1/s]) of power loss vs. agitation rate could be established.

The correlation for power loss can be used to correct values from electrical power measurement to give an accurate value of agitation power input in the 3 m^3 reactor. This is an important basis for the analysis of the drop dispersion experiments to measure hydromechanical stress. The next chapter will incorporate this refined electrical power measurement for the investigation of the influence of aeration on hydromechanical stress in the 3 m^3 reactor with two different sets of Rushton type impellers.

5 Influence of aeration on hydromechanical stress in aerated stirred tanks

5.1 Introduction

The newly developed measurement procedure described in Chapter 3 gives experimental access to hydromechanical stress in aerated stirred tanks. The establishment of the method was done in a 50 L reactor. It is the aim of the following chapter to prove the applicability of this measurement principle to large equipment of m^3-scale where the application of other methods is difficult. This will be done by the comparison of the ratio of maximum to specific energy dissipation rate ϕ of two different Rushton type impellers in a 3 m^3 pilot scale reactor under unaerated conditions where a comparison with literature data is possible. Even more importantly, the second aim of this chapter is to apply this method under conditions of intense aeration and agitation to evaluate the influence of aeration on turbulence intensity under conditions that are comparable to process conditions. First, the theoretical background will be introduced shortly (Section 5.2). Then, the materials and methods used for the experiments will be described (Section 5.3). After that, results for unaerated and aerated experiments will be presented and discussed (Sections 5.4.1 and 5.4.3).

5.2 Estimation of the ratio of maximum to specific energy dissipation rate ϕ from the maximum stable drop size d_{max}

When an insoluble organic liquid phase is added to a waterlike continuous phase and stirred in an agitated tank, drops will be formed by the action of the turbulent eddies of the continuous phase. In dilute dispersions, coalescence rate of drops is small and the dispersion can be regarded as break-up dominated. The break-up process was modelled mechanistically by Kolmogorov [52] and Hinze [2] and extended to viscous dispersed phases by Arai [53] by a balance of deforming stresses from turbulent velocity fluctuations and cohesive stresses from surface tension and viscosity. Based on this theory, the maximum stable drop diameter d_{max} is related to the maximum local energy dissipation rate ε_{max} by:

$$d_{max} = K_1 \cdot \left(\frac{\sigma}{\rho_c}\right)^{0.6} \cdot \varepsilon_{max}^{-\alpha} \cdot \left(1 + K_2 \cdot \frac{\eta_d}{\sigma}\left(\varepsilon_{max} \cdot d_{max}\right)^{\frac{1}{3}}\right)^{0.6} \tag{5.1}$$

α follows from turbulence theory as $\alpha = 0.4$. Baldyga and Podgórska [79] derived a value of $K_1 = 0.23$ from diverse literature data. Liepe [40] report a value of $K_2 = 2.5$ for the constant in the viscosity correction term. With

$$\varepsilon_{max} = \phi \cdot \varepsilon_{Ø} \tag{5.2}$$

ϕ can be found iteratively on the basis of measured maximum stable drop sizes d_{max} and the corresponding measured volume averaged energy dissipation rates $\varepsilon_{Ø}$.

Different literature correlations can be applied to estimate ϕ for Rushton impellers of different geometry for single-phase operation. These correlations were introduced in Section 1 and are collected in Table 6.1. McManamey's equation [42] relates the total energy dissipation to the impeller swept volume to estimate maximum energy dissipation. This equation is one of the most commonly used equations for the estimation of hydromechanical stress. Jüsten et al. used this apprach to calculate the energy dissipation to circulation function EDCF [14-16]. [80] and [50] used the principle to correlate drop sizes for stirred tanks with different other mixing devices, [81] used this approach to correlate particle stress in stirred tanks. Kresta and Brodkey [49] recommend this approach "as the best practice estimate" to calculate maximum energy dissipation.

Table 5.1: Literature correlations for the estimation of the ratio of maximum to volume-averaged energy dissipation rate ϕ for Rushton impellers for single-phase, unaerated operating conditions.

McManamey [42]	$\phi = \frac{4}{\pi} \cdot \frac{V_L}{d^2 \cdot h}$	(5.3)
Okamoto et al. [41]	$\phi = 0.85 \cdot \left(\frac{h}{D_R}\right)^{-1.38} \cdot e^{-2.46 \cdot d/D_R}$	(5.4)
Liepe et al. [40]	$\phi = \frac{0.1 \cdot \pi^3}{Po} \cdot \frac{V_L}{d^2 \cdot h}$	(5.5)
Liepe et al. [40]	$\phi = 0.11 \cdot \pi^3 \cdot \frac{V_L}{d^3}$	(5.6)

5.3 Materials and methods

The choice and combination of the continuous and dispersed phases are a decisive factor for a successful application of a break-up controlled dispersion under aerated operating conditions. Details on the rationale for the continuous and dispersed phases used and on the development of the method applied for measuring maximum stable drop size under aerated conditions were discussed in detail in Chapter 3. Only the experimental details specific for the experiments reported in this chapter will be discussed in the next paragraphs.

5.3.1 Reactor and agitators

The experiments were conducted in a 3 m^3 reactor as depicted in Figure 2.1. Geometrical details of the reactor are given in Table 2.1. The filling volume was 2.4, 2.6 or 2.8 m^3, respectively. The filling volume depended on the operating conditions for the experiments as discussed below. A weight measurement allowed the determination of the filling volume. Impeller setups B-1 and B-3 with 6-bladed Rushton type impellers were used. The geometrical details of the impellers are given in Table 2.2. Temperature was controlled at 25°C for all drop dispersion experiments.

5.3.2 Power measurement and impeller power number

Impeller power was measured by electrical power drawn by the engine. Friction and other power losses were corrected for as described in Chapter 4. For estimation of individual power input of the different impeller stages, it was assumed for simplification that power input was evenly distributed between impellers. Power numbers were measured for both impellers. The values are given in Table 2.2.

5.3.3 Continuous and dispersed phase

The continuous phase consisted of 1 mM PO_4-buffer at pH 7.3. The buffer was prepared by adding 224.5 mmol/m^3 NaH_2PO_4 x 2 H_2O (Merck, Darmstadt, Germany, >99% purity) and 775.4 mmol/m^3 Na_2HPO_4 x 12 H_2O (Merck, Darmstadt, Germany, >99% purity) to deionised water directly in the tank. The density of the continuous phase was taken as 1000 kg/m^3.

The same batch of Paraffin oil (Weissöl Ph Eur., Brenntag, Germany) that was applied in the experiments presented in Chapter 3 was used in all experiments discussed in this chapter. The typical range of the volumetric fraction of the dispersed phase in the experiments was 0.001 – 0.003 m^3/m^3.

5.3.4 Measurement of maximum stable drop size

The organic phase was poured into the tank through the manway opening on top of the tank after constant temperature, aeration and agitation rate were established. The oil was completely suspended in the liquid due to the intense flow conditions for all operating conditions and no oil film was present on the surface despite the lower density of the organic phase compared to water. The sampling port was located 2.1 m above the tank bottom at 45° between two baffles. Sampling, sample handling, measurement of the drop size distribution and data analysis were conducted as described in Chapter 3. The operating conditions were held constant for 3 h after oil addition or a step-change in the agitation rate. Increasing the agitation rate allowed a more economic utilization of the tank compared to refilling the tank after each operating condition and yielded identical results. The drop size reached a stable value within 90 min and did not change any more during the time of measurement within the measurement accuracy (cf. Section 3.4.3). The average value of at least 3 individual samples between the 2nd and 3rd hour of an experiment is given as the

measured value for each operating condition. It is well known that drop dispersions do not reach a real equilibrium due to the intermittent character of turbulence [82] but this effect was not significant within the time-frame relevant for this study. Long-term experiments showed a further decrease of the maximum stable drop size in the range of 10 % between hours 3 and 9 after oil addition. This is exemplified in Figure 5.1 (experiment conducted with reactor configuration B-5 at an agitation rate of n = 160 1/min and a aeration rate of 1.3 vvm) where the measured maximum stable drop size decreases from 377 µm after 3 h to 348 µm after 9 h. This is equivalent to a decrease of 8%.

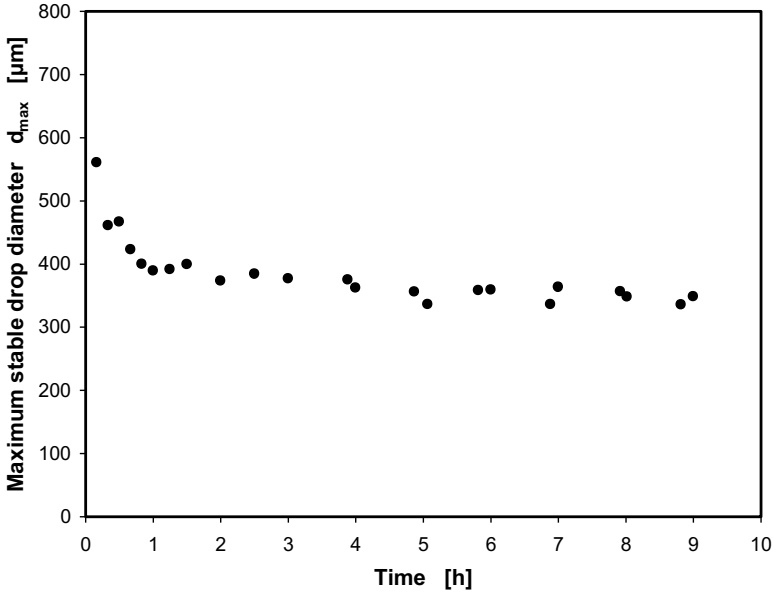

Figure 5.1: Evolution of maximum stable drop size over long dispersion times. Dispersion of paraffin oil in 1 mM PO_4-buffer at pH 7.3. Impeller setup B-5 (Table 2.3). Agitation rate n = 160 1/min, aeration rate q_g = 1.3 vvm.

The start of an experiment was marked either by the addition of the organic phase to the tank or by the step-change in the agitation rate. The filling volume had to be slightly adjusted for the different operating conditions used. Experiments without aeration were conducted with a filling volume of 2.8 m^3. Lower filling volumes resulted in surface aeration due to the low liquid level, which had to be avoided for the unaerated experiments.

Aerated experiments with high aeration rates were conducted with filling volumes of 2.6 m^3 or 2.4 m^3 to avoid a spill-over of the liquid due to the high gas hold-up in the tank for the higher agitation rates. The results shown in Figure 5.2 confirm that the reduction of the filling volume from 2.8 m^3 to 2.4 m^3 has no measurable influence on the maximum stable drop size for the example of the setup B-1 (see Table 2.2) at an agitation rate of 205 1/min and an aeration rate of 0.4 vvm:

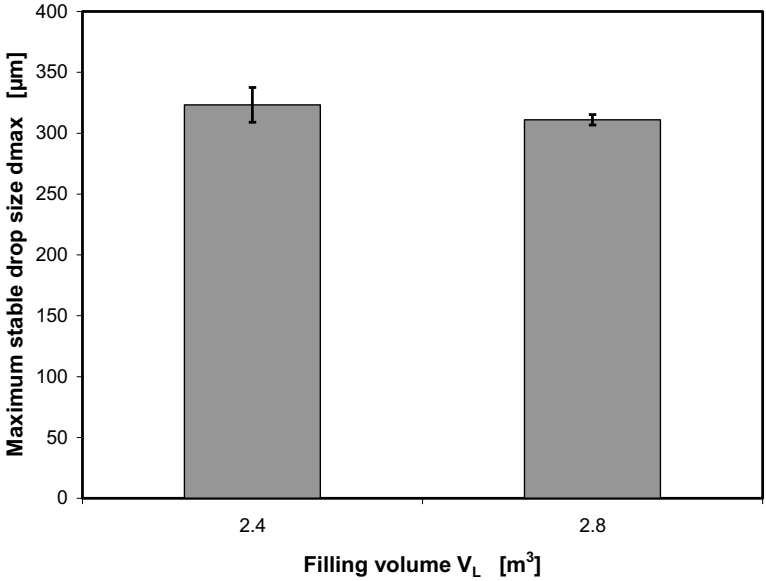

Figure 5.2: Influence of filling volume on measured maximum stable drop size. Dispersion of 0.002 L/L paraffin oil in 1 mM PO_4-buffer at pH 7.3. Impeller setup B-1 (Table 2.2). Agitation rate n = 205 1/min, aeration rate q_g = 0.4 vvm.

5.4 Results and Discussion

5.4.1 Turbulence characteristics

Application of the theory of turbulent drop dispersion as expressed in Eqs. 5.1 and 5.2 implies a fully turbulent flow field with Reynolds number Re > $5 \cdot 10^3$, drop sizes between the macroscale of turbulence $\Lambda = 0.4$ h and the microscale of turbulence $\lambda = \left(\nu^3/\varepsilon\right)^{1/4}$ and the existence of an inertial subrange (see also Section 3.1). The inertial subrange is developed when $\Lambda/\lambda > 150$. An approximate validity range for the drop size may be given by $d_{max}/\lambda >$ 10 and $\Lambda/d_{max} > 10$ [40]. Table 5.2 shows that these parameter ranges were satisfied for all experiments presented in this chapter:

Table 5.2: Ranges of turbulence parameters for all operating conditions applied in the experiments.

Reactor configuration	Re	λ	λ/Λ	d_{max}/λ	Λ/d_{max}
	-	µm	-	-	-
B-1	$2.5 - 9.7 \cdot 10^5$	11 – 23	$1.5 - 3.2 \cdot 10^3$	14 – 23	71 – 211
B-3	$2.6 - 11 \cdot 10^5$	11 – 25	$1.9 - 4.4 \cdot 10^3$	15 – 24	82 – 261

The microscale of turbulence was estimated with maximum local energy dissipation rates for the individual experiments based on Eq. 5.2 with values for ϕ from Table 5.4 and measured values for $\varepsilon_{Ø}$.

5.4.2 Ratio of maximum to specific energy dissipation rate ϕ without aeration

Figure 5.3 depicts the results for the maximum stable drop size without aeration for the two different impeller configurations as a function of the volumetric power input. The dashed and solid lines represent the calculated maximum stable drop sizes with fitted values for ϕ for setup B-1 ($\phi = 33$) and setup B-3 ($\phi = 17$), respectively. The ± 10 % ranges (dash-dot lines and dotted lines) indicate that the majority of the data lies around the theoretical curve within the typical standard deviation of independent experiments which is approximately 10 % (see Section 3.4.5). The general trend of the measured data is well in agreement with the model based on Eq. 5.1 with the literature values for K_1 (0.23), K_2 (2.5) and $\alpha = 0.4$. It is

evident from the data that a higher volumetric power input is necessary to achieve the same maximum stable drop size for the larger impeller in setup B-3 than for the smaller impeller in setup B-1.

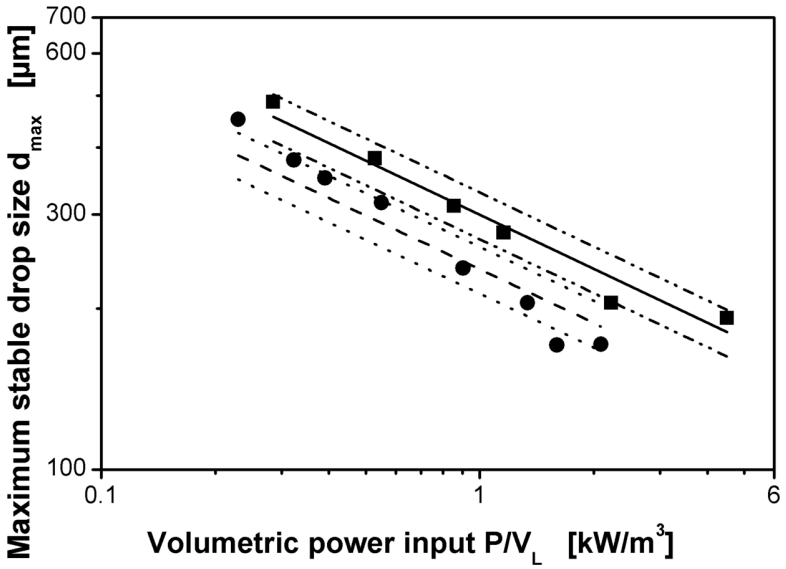

Figure 5.3: Correlation of the maximum stable drop diameter for unaerated experiments. Dispersion of paraffin oil in 1 mM PO_4-buffer at pH 7.3. Maximum stable drop diameter measured after 3 h agitation. Solid line and dash-dot lines: theoretical drop size with ϕ = 17 for the d/D_R = 0.43 agitator and limits for ± 10 % range; dashed line and dotted lines: theoretical drop size with ϕ = 33 for the d/D_R = 0.34 agitator and limits for ± 10 % range; calculated after Eq. 5.1 with K_1 = 0.23, K_2 = 2.5 and α = 0.4.

This is also reflected in the calculated values for ϕ that are given in Table 5.3 together with the values calculated with different literature correlations. For comparison of the measured data with literature results, the different reactor geometry has to be accounted for. The literature results are based on a geometry with a single impeller and an aspect ratio of H/D_R = 1, which results in a different liquid volume per impeller stage than used in the present study. As a first approximation, it is reasonable to assume that the turbulence intensity in the direct vicinity of the stirrer and the impeller power input are not affected by a reasonable change in liquid volume. Hence, ϕ changes directly proportional to V_L. This can also be derived from Eq. 5.3.

Table 5.3: Comparison of ϕ calculated from the experimental data for unaerated experiments with results from literature correlations. The measured values were recalculated to reflect the standard aspect ratio of $H/D_R = 1$ and single impeller setup for comparison with the literature correlations.

	Experiment (V_L = 2.8 m^3)	Experiment recalculated for $H/D_R = 1$	McManamey [42] Eq. (5.3)	Okamoto [41] Eq. (5.4)	Liepe [40] Eq. (5.5)	Liepe [40] Eq. (5.6)
ϕ for B-1 [-]	33	49	114	13	57	67
ϕ for B-3 [-]	17	24	55	7	23	34
Ratio	2.0	2.0	2.1	1.9	2.5	2.0

Due to this volume adjustment, the resulting calculated values for ϕ are 45 % larger than the values calculated with the real liquid volume (Table 5.3). The geometry of the smaller impeller setup B-1 is very similar to the standard impeller with d/D_R (+4%), h/d (+10%) and w/d (+12%) being only slightly larger. A similar value for ϕ can, therefore, be expected and the value of 49 (recalculated for $H/D_R = 1$) is in fact very well in the range reported in Table 1.1 for the standard impeller. The absolute values for ϕ calculated with the literature correlations are different for each correlation as already discussed in the introductory part for the standard geometry impeller. However, it is very interesting to note that all four equations predict very similar relative differences between the two impeller geometries that agree very well with the value of 2.0 calculated from the values for ϕ that were derived from the measurements for the two agitator configurations.

In conclusion, the results gained for the two-impeller configurations for unaerated operating conditions are very well in agreement with available data from literature and with the theoretical dependence of maximum stable drop size on operating conditions and physical properties of the dispersed and liquid phases as expressed in Eq. 5.1. This confirms that the method applied is well suited for the comparison of turbulence intensity in large scale equipment where other methods cannot easily be applied.

5.4.3 Ratio of maximum to specific energy dissipation rate ϕ under aerated operating conditions

Volumetric power input was varied between 0.2 – 4.3 kW/m^3 and aeration rates were varied between 0.1 vvm and 1.0 vvm for impeller setup B-1. For the impeller setup B-3, volumetric power input was varied in the range of 0.3 – 6.3 kW/m^3 and aeration rate was varied in the range of 0.1 - 0.7 vvm. The range of aeration rates and volumetric power input were chosen to reflect typical values in aerobic fermentations. If not otherwise stated, volumetric power input was calculated with 2.4 m^3 liquid volume for all operating conditions to avoid a bias in the data that would be caused by the slightly different filling volumes used in the experiments as already discussed in the previous section. Operating conditions for the two impeller setups were in the loading and complete dispersion regimes with two exceptions. These were the lowest agitation rates at 0.7 vvm and 1.0 vvm for the d/D_R = 0.34 impeller where the lowest impeller stage was in the flooding regime (flow regimes calculated with the equations given in [83] based on real volumetric gas flows). The upper impellers experience only about half the gas rate of the lowest impeller [83]. Therefore, the upper impellers were not flooded under these conditions and it might be expected that these impellers govern drop dispersion when the lowest impeller is flooded.

The maximum stable drop sizes measured under aerated operating conditions are depicted in Figure 5.4A for impeller setup B-1 and in Figure 5.4B for impeller setup B-3 together with the data from unaerated operating conditions from Figure 5.3. For both agitator configurations, the data for aerated operating conditions exhibit the same general trend as the data for unaerated operating conditions but show a parallel translation towards larger drop sizes for the same volumetric power input. Within the accuracy of the maximum stable drop size measurement, the data for the different aeration rates collapse to a single line when correlated with the volumetric power input. Based on Eq. 5.1 this data indicates a strong attenuation of the maximum local energy dissipation rate for aerated compared to unaerated operating conditions at the same volumetric power input.

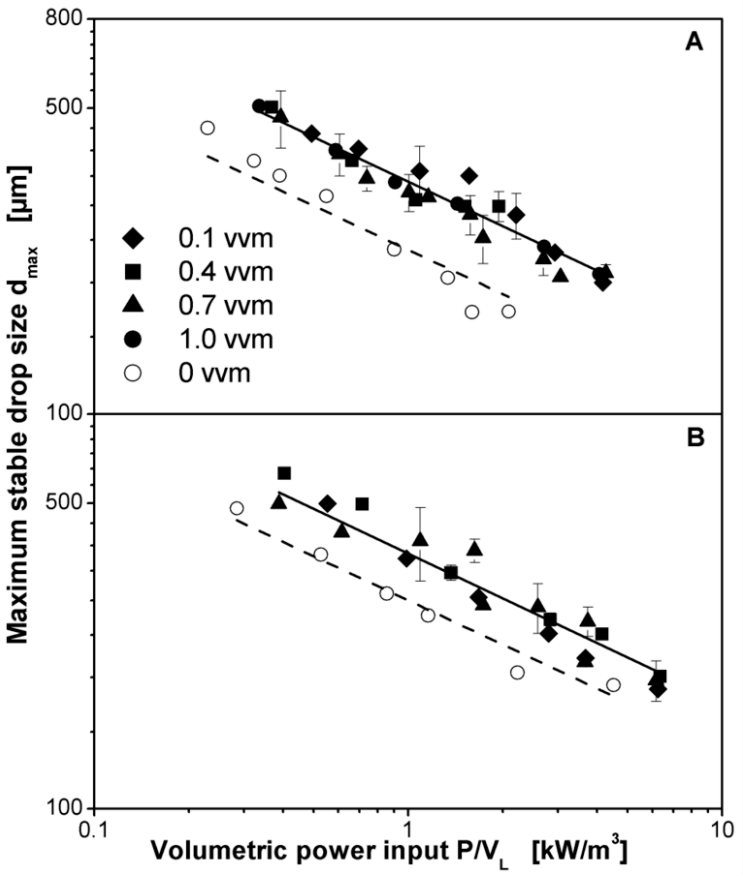

Figure 5.4: Correlation of the maximum stable drop size for aerated and unaerated experiments. Dispersion of paraffin oil in 1 mM PO_4-buffer at pH 7.3. Volumetric power input calculated with 2.4 m^3 filling volume. Maximum stable drop diameter measured after 3 h agitation. (A) Impeller setup B-1. Dashed line: theoretical drop size with ϕ = 28.6 for the unaerated operating conditions and solid line: theoretical drop size with ϕ = 9.9 for the aerated operating conditions; (B) Impeller setup B-3. Dashed line: theoretical drop size with ϕ = 14.4 for the unaerated operating conditions and solid line: theoretical drop size with ϕ = 6.9 for the aerated operating conditions. Values for ϕ calculated after Eq. 5.1 with K_1 = 0.23, K_2 = 2.5 and α = 0.4.

Given the fact that the drop dispersion based measurement method is an indirect way to assess hydromechanical stress, it is important to ensure that hypothetically possible interfering physical or chemical effects caused by the addition of air to the system do not

bias the interpretation of the experimental results. Therefore, different control experiments were conducted to ensure that an interpretation of the results based on Eq. 5.1 is justified.

Experiments with varied dispersed phase concentrations with the two impeller setups for aerated and unaerated operating conditions were conducted to verify that the dispersion is break-up controlled and coalescence is negligible. The results are shown in Figure 5.5. The operating conditions for these experiments were chosen to result in a maximum stable drop size that is approximately in the middle of the range found in the dispersion experiments. The dispersed phase concentration was increased by up to a factor of 20. All datasets exhibit basically constant maximum stable drop sizes independent of the dispersed phase concentration. Individual values vary around the average within the standard deviation of the experimental technique which was determined to approximately 10 % (see Section 3.4.5). The maximum stable drop diameter for the highest dispersed phase concentration of 0.01 L/L for impeller setup B-1 without aeration (Figure 5.5A) deviates from the average towards an increased drop size. However, also this deviation lies within one standard deviation with d_{max} = 358 µm compared to an average value for this dataset of d_{max} = 325 µm (equivalent to 10 % difference). It has to be expected that for a strong increase of the dispersed phase concentration, coalescence will eventually become a significant effect for the development of the maximum stable drop size. For the range of concentrations used in the current experiments this is not the case. This is in good agreement with literature on liquid-liquid dispersion without aeration where dilute systems with insignificant coalescence are reported when the dispersed phase concentration is kept below 0.01 m^3/m^3 [49, 53, 54, 63, 64].

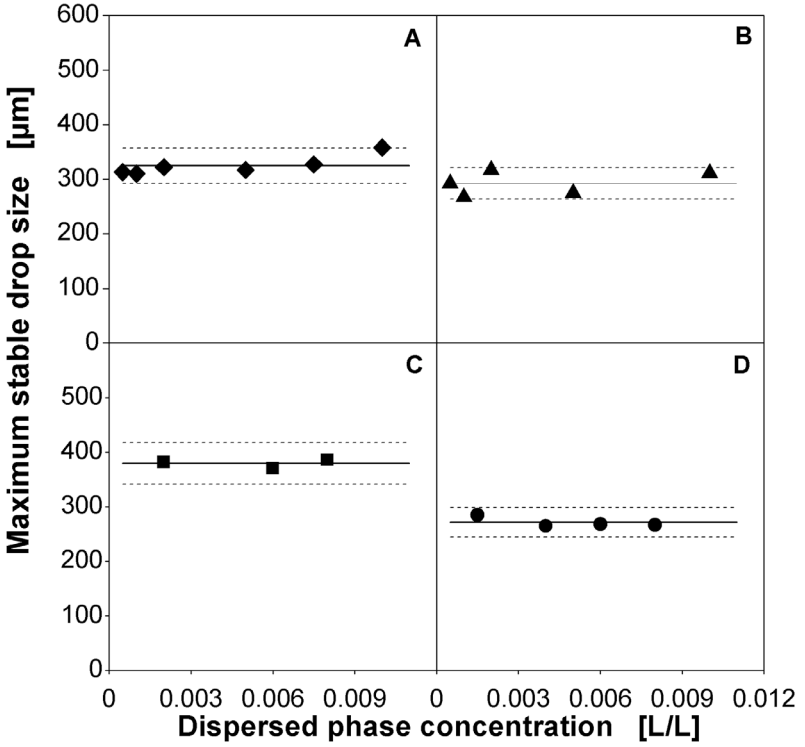

Figure 5.5: Maximum stable drop size with varied dispersed phase concentrations for aerated and unaerated operating conditions. A: setup B-1, q_g = 0 vvm, n = 2.0 1/s; B: setup B-1, q_g = 0.4 vvm, n = 2.7 1/s. C: setup B-3, q_g = 0 vvm, n = 1.3 1/s; D: setup B-3, q_g = 0.4 vvm, n = 2.7 1/s. Symbols: results from individual experiments, solid lines and dotted lines: average value for dataset and ± 10 % range. Dispersion of paraffin oil in 1 mM PO_4-buffer at pH 7.3. Maximum stable drop diameter measured after 3 h agitation.

It is particularly important to emphasize that there is no change in behaviour between aerated and unaerated experiments. The experiments for aerated operating conditions do not exhibit a tendency for stronger coalescence than the experiments without aeration. It is, therefore, concluded that the maximum stable drop size is primarily controlled by drop break-up processes and that coalescence can be neglected under unaerated as well as aerated operating conditions as assumed during method development (see Section 3.4.1).

Theoretically, it could also be possible that oxygen or carbon dioxide from aeration or unknown traces of impurities that might be introduced into the system by aeration may alter

the dispersion behaviour and lead to the larger drop sizes under aerated conditions. To test these hypotheses aeration was switched from air sparging to sparging with inert nitrogen to assess a possible influence of the sparged gas on the measured maximum stable drop size. Due to safety restrictions the experiments had to be conducted in the 50 L scale. Results for impeller setup A-4 at an agitation rate of 270 1/min and an aeration rate of 0.7 vvm are shown in Figure 5.6:

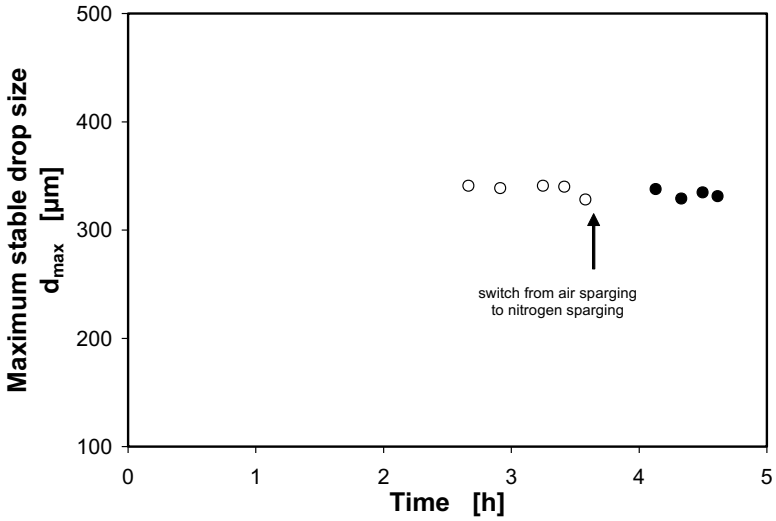

Figure 5.6: Influence of sparged gas on measured maximum stable drop size. Arrow indicates time when sparging was switched from air to nitrogen. Dispersion of paraffin oil in 1 mM PO_4-buffer at pH 7.3. 50 L reactor, impeller setup: A-4 (see Table 2.2). Agitation rate n = 270 1/min, aeration rate q_g = 0.7 vvm.

The experiment was started with air as the sparged gas. After 3.6 h, sparging was switched to nitrogen and the maximum stable drop size was measured over the next hour. The exchange of air by nitrogen had no effect. Maximum stable drop size did not change and the data with nitrogen sparging fell on the line of the aerated experiments.

A further experiment was conducted to verify that the transition of the characteristic behaviour for aerated and unaerated operating conditions is reversible within the same experiment. Therefore, a dispersion experiment with impeller setup B-1 without aeration was started with 0.3 kW/m^3 power input. After 3 h of stirring, 0.4 vvm aeration was

switched on and the agitation rate was increased at the same time, which resulted in a volumetric power input of 1.3 kW/m^3. Based on the previous experiments a decrease in maximum stable drop diameter was expected with the new operating conditions. After another period of 3 h, agitation and aeration were stopped to allow the gas to disengage. Agitation was then turned on again without aeration with a power input of 1.4 kW/m^3. The relatively low agitation and aeration rates in this experiment allowed applying the same filling volume of 2.8 m^3 during aerated and unaerated operating conditions. The experiment was repeated twice. The results are depicted in Figure 5.7. The lines represent the trends taken from the data shown in Figure 5.4A (with 2.8 m^3 filling volume). It is evident from this data that the differences in the behaviour under aerated and unaerated operating conditions as described above are also observed within the same experiment. Switching back from aerated to unaerated operating conditions results in a maximum stable drop size that is in accordance with the characteristic line for the unaerated experiments.

Taking these results together it can be concluded that there is no evidence that interfering effects might be present that bias the interpretation of the results on the basis of the theory for break-up controlled dispersion in turbulent flow. It follows that the introduction of air reduces the hydromechanical stress that is experienced by the oil drops. Based on Eq. 5.1 this is equivalent with an attenuation of the maximum local energy dissipation rate due to the presence of air. Within the range of measurement accuracy, there seems to be no influence of aeration intensity on this effect in the range of aeration rates tested. Alves et al. [84] present data on bubble sizes in aerated stirred tanks in non-coalescent media and were able to correlate Sauter mean diameter with power input. They did not find an influence of aeration intensity on bubble size, which supports the results found here for drop dispersion. Even the data for the lowest aeration rate of 0.1 vvm falls on the trend for the aerated operating conditions. For practical applications, the value of 0.1 vvm is already below the typical range of aeration rates used. A further reduction of aeration rate was not possible due to technical restrictions in the available equipment. It might be assumed that there is a transitional range of aeration rates for very low aeration where the trend for the aerated operating conditions converges towards the trend for unaerated operating conditions. In the present data, however, the gas hold-up around the impellers seems to be high enough to strongly reduce turbulence intensity already at 0.1 vvm.

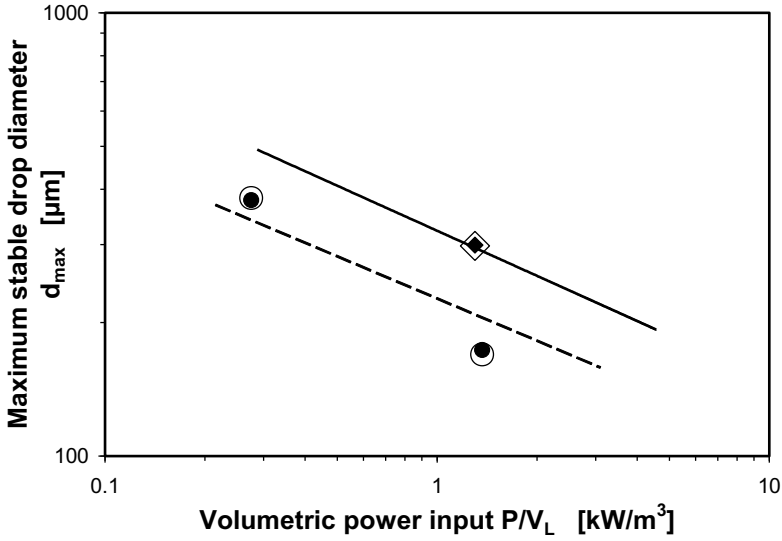

Figure 5.7: Step-change of operating conditions from unaerated (0.3 kW/m^3) to aerated (1.3 kW/m^3) to unaerated (1.4 kW/m^3) conditions within one experiment for impeller setup B-1. Dispersion of paraffin oil in 1 mM PO_4-buffer at pH 7.3. Volumetric power input calculated with 2.8 m^3 filling volume. Maximum stable drop diameter measured after 3 h agitation. Full symbols: first experiment; open symbols: repetition. Circles: no aeration; diamonds: 0.4 vvm aeration. Solid line: theoretical drop size with ϕ = 33 for the unaerated operating conditions and dashed line: ϕ = 11.6 for the aerated operating conditions; calculated after Eq. 5.1 with K_1 = 0.23, K_2 = 2.5 and α = 0.4.

For cell culture processes, not only the effect of maximum energy dissipation induced by the flow field is relevant for cell damage [85, 86]. More importantly, bubble formation at the sparger and bubble rupture at the liquid surface are known to be the major cause for cell death by hydrodynamic forces in these processes [87-89]. Attachment of cells to bubbles plays an important role in the lethal effects of bursting bubbles in cell culture processes [90, 91]. There is no evidence that these effects may have an influence on the maximum stable drop size. Measurements were conducted with aeration rates varied from 0.1 vvm to 1 vvm. If bubble rupture had a considerable influence on the maximum stable drop size a correlation of maximum stable drop size with aeration intensity migh be expected. Additionally, when unaerated and aerated data are compared with each other, maximum stable drop size is smaller without aeration than with aeration (with the same volumetric power input). Hence, it can be concluded that the experimental results shown in this study are not influenced by the effects of bursting bubbles.

Table 5.4 shows a comparison of the resulting values for ϕ for the two impeller configurations for aerated and unaerated experiments. The reduction of ϕ between aerated and unaerated experiments is more pronounced for impeller setup B-1 with a factor of 2.8 than for the impeller setup B-3 with a factor of 2.1. This means that compared on the basis of equal volumetric power input the maximum local energy dissipation rate is reduced by 64 % for the impeller setup B-1 and by 52 % for impeller setup B-3 by the presence of air. Therefore, energy dissipation is distributed much more evenly in aerated stirred tanks than in unaerated stirred tanks with the same impeller.

Table 5.4: Comparison of ϕ for aerated and unaerated operating conditions. All values calculated on the basis of a filling volume of 2.4 m^3.

	unaerated	aerated	Ratio unaerated/aerated [-]
ϕ for B-1 [-]	28.6	9.9	2.8
ϕ for B-3 [-]	14.4	6.9	2.1
Ratio between impellers [-]	2.0	1.4	

Experimental evidence and theoretical models show that turbulence may be both increased or reduced by particles and bubbles [92] depending on flow conditions, dispersed phase properties and particle loading or gas hold-up, respectively. Different mechanisms of interphase coupling that modulate turbulence are discussed in literature. Most available data and analysis is related to pipe or jet flows with low dispersed phase concentrations. In how far these results can contribute to the understanding of the mechanisms dominant in a highly turbulent flow field around a stirred tank impeller is not known. Additionally, published results are largely contradictory [93-95]. Computational fluid dynamics might be a useful tool to throw light onto the processes involved. There have been successes in modelling bubble size distributions in stirred tanks [96]. But the results of these simulations strongly depend on the assumptions used for the fine-scale turbulence model and the bubble break-up model [26]. Recently, Balachandar and Eaton [95] comprehensively reviewed the current understanding of turbulence modulation in multiphase dispersed flows and come to the conclusion that “the mechanisms of turbulence modulation and their parametric dependence are poorly understood and are wide open for fundamental investigation.” A theoretical explanation for the experimental results is therefore out of reach at the time being. It might be speculated that already the primary turbulence production by the impellers is less inhomogeneous in the presence of air bubbles. An absorption of local high energy bursts by

bubbles due to their compressibility and the mobility of their interface might also contribute to turbulence attenuation.

Other experimental data on effects of aeration on turbulence intensity in stirred tanks that is directly comparable to the results presented in this study is very scarce. Fort et al. [97] used a piezoelectric pressure transducer in an agitated gas-liquid stirred reactor. The transducer was positioned at different locations inside the tank to measure the mean kinetic energy of turbulence, which was used to calculate the energy dissipation rate. Results for aerated and unaerated operating conditions were compared and a significant suppression of energy dissipation in the impeller discharge flow was reported which is qualitatively in agreement with the results found in this work. However, the comparison was made at constant agitation rate rather than at constant volumetric power input which prevents a direct comparison of the magnitude of the effect with the data found in this work.

Bourne [98] published results from experiments with a chemical method to measure micromixing in a stirred tank that was applied under aerated operating conditions. Since micromixing efficiency depends on the local energy dissipation rate, Bourne was able to draw conclusions on the influence of aeration on local energy dissipation rate. He found no influence of aeration on local energy dissipation rate close to the impeller when the volumetric power input was kept constant under aeration by increasing the agitation rate. Recently, Hofinger et al. [99] applied a similar technique and supports the results of Bourne [98] with respect to the micromixing efficiency. Brilman et al. [100] also worked with a micromixing-sensitive reaction system. They applied various aeration rates up to 10 vvm. Their results show essentially no effect of aeration on product distribution and local energy dissipation rate when agitation rates were kept constant. These results seem to be in contrast to the results found in this work. However, Assirelli et al. [30] pointed out that results gained by chemical techniques strongly depend on the feeding point for the reactants and reflect an average value of local energy dissipation over the volume that is passed by the reactants until the reaction is completed. They present a detailed analysis of these effects for single-phase measurements and come to the conclusion that specifically measurements in the region where the maximum local energy dissipation rate is expected are flawed because the reactants are swept away from the region of maximum local energy dissipation rate before the reaction is completed. They estimate the reaction zone to a length of about $3 \cdot 10^{-3}$ m. Hilber [101] calculated the length of the reaction zone for his experiments (on which the analysis of Bourne [98] is based on) to $1.6 \cdot 10^{-2}$ m to $7.1 \cdot 10^{-2}$ m depending on the feeding point and operating conditions. The spatial resolution of these techniques is, therefore,

restricted to these length scales which might be too large to resolve the region of maximum local energy dissipation rate. The spatial resolution of the drop size based measurements of this work may be estimated to be in the range of the maximum stable drop size which is approximately an order of magnitude smaller than the value reported by Assirelli et al. [30].

Aeration strongly influences the flow field in the impeller region. The vortexes behind the impeller blades are bend upwards in the presence of air [102, 103]. It can be expected that the location where the maximum local energy dissipation rate occurs depends on aeration and agitation rate and is not constant relative to the reactor or the agitator when operating conditions are changed. Therefore, it is questionable if the maximum local energy dissipation rate can be resolved for changing operating conditions with methods where the measurement point is constant. It can be argued that a drop dispersion technique, on the other hand, has the advantage that drops will eventually pass the zone of maximum local energy dissipation rate. It is, therefore, not necessary to know the exact position where maximum local energy dissipation rate occurs to conduct the measurement.

Overall, it seems that due to the unique characteristics of the method applied the results presented in this study may be ~~a~~ the first set of data that quantitatively capture the effect of aeration on ϕ in stirred tanks.

5.5 Conclusions

Drop dispersion experiments were conducted in a 3 m^3 pilot scale stirred tank reactor with 1.2 m inner diameter with a measurement technique that allows the measurement of the maximum stable drop size and the characterization of the maximum local energy dissipation rate at intense aeration. The dispersion is break-up controlled under aerated operating conditions. Experiments with two different setups of 6-bladed Rushton turbines with diameters of d/D_R = 0.34 (setup B-1) and d/D_R = 0.43 (setup B-3) in a 3 impeller configuration were conducted. Experiments without aeration showed that the results gained are well in agreement with the existing literature on drop dispersion. ϕ, which is the ratio of the maximum to the volume-averaged energy dissipation rate, for impeller setup B-1 was in the range reported in literature for similar impeller geometries. The value of ϕ for the smaller impeller setup B-1 was 2.0 times larger than for setup B-3 which was shown to be well in agreement with results from existing literature correlations for the influence of impeller geometry on ϕ. Experiments with aeration showed a remarkable influence of the

presence of bubbles on the maximum stable drop size compared to unaerated operating conditions at the same volumetric power input for both impellers. It was shown that coalescence can be neglected under unaerated as well as aerated operating conditions, that the parallel translation of the characteristic trend for aerated compared to unaerated experiments is reversible and that the exchange of air by nitrogen sparging has no influence on the result for maximum stable drop size. This shows that there is no interfering effect that might bias the interpretation of the results on the basis of the theory for break-up controlled dispersions in turbulent flow. It is, therefore, concluded that the results shown in this study indicate a strong attenuation of turbulence intensity in stirred tank reactors by the presence of air under intense operating conditions. The ratio between maximum and volume-averaged energy dissipation rate was reduced by 64 % for setup B-1 and by 52 % for setup B-3 by the presence of air when compared on the basis of equal volumetric power input. The value of the aeration rate had no measurable effect in the range of aeration rates used, which was between 0.1 vvm and 1 vvm. A review of existing literature results on the effect of aeration on turbulence in stirred tanks showed that the results presented in this chapter are new due to the unique character of the measurement technique applied. It was possible for the first time to detect and quantify the effect of turbulence attenuation in stirred tanks under conditions of intense aeration and agitation.

The dataset for aerated operating conditions presented in this chapter will be extended in the next chapter by data for Rushton type impellers in two additional scales of 50 L and 40 m^3 nominal volume and by additional data in the 3 m^3 reactor with a further Rushton impeller setup and an Ekato Phasejet/Combijet impeller setup to investigate the influence of geometry and scale on hydromechanical stress.

6 Influence of geometry and scale on hydromechanical stress in aerated stirred tanks

6.1 Introduction

After successfully applying the measurement method developed in Chapter 3 in the 3 m^3 pilot scale reactor to evaluate the influence of aeration on turbulence intensity the method will be applied in the current chapter with 8 different reactor configurations with Rushton type impellers in reactors of scales 50 L, 3 m^3 and 40 m^3 in a wide range of operating conditions. It is the goal of this chapter to provide a broad data basis to demonstrate the applicability of this method to real life equipment of different scales, to characterize different reactor configurations with respect to hydromechanical stress as a basis for successful scale-up or scale-down under aerated operating conditions and to test whether established literature correlations for the estimation of hydromechanical stress for different impellers can be applied with acceptable accuracy. The chapter is organized as follows: first, in Section 6.2 the basic equations needed for the interpretation of the experimental results will be briefly introduced. Then, the materials and methods specific for the experiments in this chapter will be presented (Section 6.3). The results section starts with a comparison of drop size distributions in the different scales (Section 6.4.1). This is followed by an analysis of the correlation of the drop size data with impeller tip speed (Section 6.4.3) and impeller power input (Section 6.4.4). The chapter closes with the estimation of the ratio of maximum to specific power input under aerated operating conditions for the different impeller setups and scales (Section 6.4.5).

6.2 Calculation of the ratio of maximum to volume averaged energy dissipation rate ϕ

Kinetic energy is introduced to the liquid by the action of the impeller. This energy dissipates in the reactor volume inhomogeneously. A maximum local value of energy dissipation, ε_{max}, exists in the impeller region that defines the most severe action of the flow field on dispersed drops, bubbles or microorganisms. The ratio of maximum local energy dissipation rate to volume-averaged energy dissipation rate is given by:

$$\phi = \frac{\varepsilon_{max}}{\varepsilon_{\emptyset}} \tag{6.1}$$

where $\varepsilon_{\emptyset}$ is the average energy dissipation rate in the reactor volume per unit mass. ϕ is constant for a given impeller, i.e. independent of agitation rate in single-phase operation [38]. It, therefore, characterizes a given reactor configuration in terms of hydromechanical stress. ε_{max} can be related to the maximum stable drop size in a break-up controlled dispersion by [40]

$$d_{max} = K_1 \cdot \left(\frac{\sigma}{\rho_c}\right)^{3/5} \cdot \varepsilon_{max}^{-2/5} \cdot \left(1 + K_2 \cdot \frac{\eta_d}{\sigma}\left(\varepsilon_{max} \cdot d_{max}\right)^{\frac{1}{3}}\right)^{3/5} \tag{6.2}$$

with K_1 = 0.23 [79] and K_2 = 2.5 [40]. If d_{max} and $\varepsilon_{\emptyset}$ are known, ϕ can be calculated iteratively from Eqs. 6.1 and 6.2.

There are different correlations available in literature that allow an estimation of ϕ for single-phase operation without aeration as a function of the impeller geometry for Rushton type impellers. These were introduced in Section 1 and are compiled in Table 6.1. Probably the most commonly used approach [49] is McManamey's equation [42] that estimates the maximum energy dissipation by relating the total impeller power to the volume swept by the impeller.

Table 6.1: Literature correlations for the estimation of the ratio of maximum to volume-averaged energy dissipation rate ϕ for Rushton impellers for single-phase, unaerated operating conditions.

McManamey [42]	$\phi = \frac{4}{\pi} \cdot \frac{V_L}{d^2 \cdot h}$	(6.3)
Okamoto et al. [41]	$\phi = 0.85 \cdot \left(\frac{h}{D_R}\right)^{-1.38} \cdot e^{-2.46 \cdot d/D_R}$	(6.4)
Liepe et al. [40]	$\phi = \frac{0.1 \cdot \pi^3}{Po} \cdot \frac{V_L}{d^2 \cdot h}$	(6.5)
Liepe et al. [40]	$\phi = 0.11 \cdot \pi^3 \cdot \frac{V_L}{d^3}$	(6.6)

6.3 Materials and methods

6.3.1 Reactor and impeller configurations

A schematic drawing of the reactors used in the experiments is depicted in Figure 2.1. Geometrical details of the reactors are given in Table 2.1. The filling volume was chosen to result in equivalent ratios of unaerated liquid height to tank diameter of approx. 1.8 in all three scales. The sampling ports were at different positions in all three reactors. It was not possible to align the sampling ports in the three reactors because additional ports could not be installed. Since the dispersion is break-up controlled it can be assumed that the reactor is homogeneous with respect to the drop size distribution. The sampling positions should, therefore, not be relevant. This was tested in the 3 m^3 tank where a second sampling point was available on the bottom of the reactor and direct sampling through the manway opening at the top was also possible. Comparison of samples from these alternative sampling positions with the results from the standard sampling point showed no influence of the sampling position on the measured drop size distribution (data not shown). In the 50 L reactor the sampling port was located at 0.24 m from the tank bottom between the middle and the upper impeller. In the 3 m^3 reactor, the sampling port was at 2.1 m from the bottom close to the unaerated liquid surface above the upper impeller and in the 40 m^3 reactor it was at 3.5 m from the tank bottom above the second impeller. All sampling ports were half

way between two baffles or cooling pipe installations, respectively. Rushton type 6-bladed impellers with different geometries were used in the experiments. The Rushton impellers were installed in a three impeller configuration which is typical for high aspect ratio reactors. In the 3 m^3 reactor, an impeller setup with an Ekato Phasejet and four Ekato Combijet impellers was used in addition to the Rushton setups. The geometrical details of the impellers are given in Table 2.2 and Table 2.3. Temperature was controlled at 25°C for all drop dispersion experiments.

6.3.2 Measurement of drop size distributions and maximum stable drop size

The development of the experimental procedure to measure drop size distributions and maximum stable drop size including the rationale for the dispersed and continuous phases used for the dispersion experiments were described in Chapter 3. Details on the preparation of the 50 L reactor were also given there. Experimental details specific for the 3 m^3 reactor were presented in Section 5.3. The experiments in the 40 m^3 reactor were conducted in the same way as explained for the 3 m^3 reactor in Section 5.3.4. All experiments were conducted with the same production batch of paraffin oil (Weissöl Ph Eur., Brenntag, Germany).

6.3.3 Power input and power number Po

Power input was determined in different ways for the three reactors due to different technical limitations in the different scales. The 50 L reactor was not equipped with power measurement. The power input was estimated using the equation from Middleton and Smith [83]:

$$P = 0.18 \cdot Fl^{-0.2} \cdot Fr^{-0.25} \cdot P_0 \tag{6.7}$$

with power input under aeration P, the impeller flow number Fl, impeller Froude number Fr and the unaerated power input P_0 that can be calculated from

$$P_0 = Po \cdot \rho_c \cdot n^3 \cdot d^5 \tag{6.8}$$

where Po is the power number, ρ_c the continuous phase density, n the agitation rate and d the impeller diameter. Power numbers were estimated using the equation of Liepe et al. [40]:

$$Po = 5.9 \cdot \left(n_{bl}^{0.8} \cdot \frac{h}{d} \right)^{0.9} \tag{6.9}$$

where n_{bl} is the number of impeller blades and h is the impeller blade height, except for impeller configurations B-1 and B-3 where the power numbers were measured based on experiments without aeration. The reliability of this correlation can be tested by comparing the measured values for B-1 and B-3 with the calculated power numbers for these impeller configurations. The calculated power number for configuration B-1 is 5.5 vs. the measured value of 4.9 (+12%) and for configuration B-3 5.8 vs. the measured value of 5.9 (-2%). Both values are in reasonable agreement with the measured values. This correlation for power number can be considered very helpful and reliable within engineering accuracy and within the accuracy needed for the power data for the analyses conducted in this work. It resembles correctly the relative influence of blade height and impeller diameter. Power input in the 3 m^3 and in the 40 m^3 reactors were measured through the electrical power draw for the engine. For the 3m^3 reactor the power input to the liquid was calculated from the raw value by a linear correction function as described in Chapter 4. Power losses were evaluated by an instationary temperature method that is completely independent of the electrical power measurement. The correlation for power losses was tested against electrical power measurement in the empty reactor and both measurements of power loss were in good agreement. Reproducibility of the electrical power measurement was very good with a standard deviation of 5%. Volumetric power input of the Phasejet impeller in impeller setup B-5 was estimated from measured total power input P by

$$\left(\frac{P}{V_L} \right)_{Phasejet} = \frac{Po_{Phasejet} \cdot d_{Phasejet}^5}{4 \cdot Po_{Combijet} \cdot d_{Combijet}^5 + Po_{Phasejet} \cdot d_{Phasejet}^5} \cdot \frac{P}{\frac{1}{5} \cdot V_L} \tag{6.10}$$

This is valid under aerated operating conditions when differences in relative power demand under aeration can be neglected at the same operating conditions. This is true for the Ekato impellers that exhibit only minor reduction of power input due to aeration (according to the manufacturer power reduction due to aeration is in the range of 10-20% for both impeller types). For the 40 m^3 reactor a linear correlation of the power data with n^3 showed a good correlation of the data with an R^2 of 0.99. This can be expected if the relative power demand P/P_0 is fairly constant in the range of operating conditions considered and if friction losses are relatively constant or unimportant compared to total power input by agitation. The latter might be expected for large reactors. The offset calculated from the linear correlation was determined to 25.2 kW. It is unlikely that this high value does really reflect friction losses. It

may rather be attributed to an offset in the calibration of the power measurement. The resulting values for power input with consideration of a constant offset of 25.2 kW were tested against the results for relative power demand P/P_0 that can be calculated from Eq. 6.7. The results are shown in Figure 6.1:

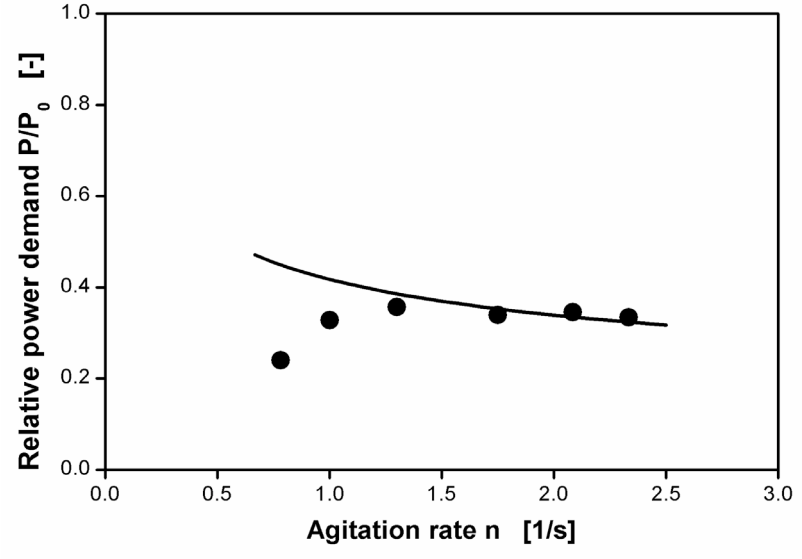

Figure 6.1: Comparison of calculated (solid line) and measured (●) relative power demand for the 40 m^3 reactor (reactor configuration C-1). All operating conditions at 0.7 vvm aeration. Calculated values were determined with Eq. 6.7. The two smallest agitation rates correspond to measured values of volumetric power input of 0.13 kW/m^3 (n = 0.78 1/s) and 0.36 kW/m^3 (n = 1.0 1/s).

For higher agitation rates, calculated and measured values for relative power demand are in very good agreement. Only the values for the two smallest agitation rates deviate considerably from the calculated values. The absolute values for the specific power input for the two smallest agitation rates were measured to 0.13 kW/m^3 (n = 0.78 1/s) and 0.36 kW/m^3 (n = 1.0 1/s). It is clear that for such small values of power input the measurement error in a production scale reactor is high compared to operating conditions with higher power inputs. The calculated values may give a more realistic value for power input in that low range of agitation rates. Therefore, the power input for the 40 m^3 reactor was determined by correcting the measured electrical power input by a constant offset of 25.2

kW except for the two smallest agitation rates, for which the calculated values for power input were used instead of the measured values.

6.4 Results and Discussion

6.4.1 Turbulence characteristics

The theory of turbulent drop dispersion (Eqs. 6.1 and 6.2; see also Section 3.1) is valid if the flow field is fully turbulent and the drop size is much smaller than the macroscale of turbulence $\Lambda = 0.4\ h$ ($\Lambda/d_{max} > 10$) and much larger than the microscale of turbulence $\lambda = \left(\nu^3/\varepsilon\right)^{1/4}$ ($d_{max}/\lambda > 10$). The flow field is fully turbulent when the Reynolds number is $Re > 5 \cdot 10^3$ and $\Lambda/\lambda > 150$ [40]. Table 6.1 shows the range of values of these parameters for all experiments presented in this study:

Table 6.1: Ranges of turbulence parameters for all operating conditions applied in the experiments. For geometrical details see Table 2.2.

Reactor configuration	Re	λ	λ/Λ	d_{max}/λ	Λ/d_{max}
	-	µm	-	-	-
A-1	$4.3 – 12 \cdot 10^4$	16 – 32	286 – 571	14 – 28	11 – 39
A-2	$8.1 – 18 \cdot 10^4$	13 – 23	400 – 688	17 – 21	19 – 40
A-3	$9.6 – 21 \cdot 10^4$	14 – 23	402 – 674	17 – 21	19 – 39
A-4	$1.0 – 2.2 \cdot 10^5$	13 – 23	396 – 695	17 – 21	19 – 42
B-1	$2.5 – 9.7 \cdot 10^5$	11 – 23	$1.5 – 3.2 \cdot 10^3$	14 – 23	71 – 211
B-2	$3.7 – 10 \cdot 10^5$	11 – 23	$1.5 – 3.2 \cdot 10^3$	15 – 26	64 – 185
B-3	$2.6 – 11 \cdot 10^5$	11 – 25	$1.9 – 4.4 \cdot 10^3$	15 – 24	82 – 261
B-5	$5.0 – 10 \cdot 10^5$	13 – 22	$1.6 – 2.8 \cdot 10^3$	15 – 23	70 – 172
C-1	$1.1 – 3.3 \cdot 10^6$	11 – 22	$3.9 – 8.3 \cdot 10^3$	13 – 24	163 – 652

The microscale of turbulence was calculated with maximum local energy dissipation rates based on Eq. 6.1 with values for ϕ from Table 6.4. All parameters are within the validity ranges for the application of the theory of turbulent drop dispersion.

6.4.2 Drop size distributions in different scales

The shape of a drop size distribution reveals important insight into the nature of the processes that formed the distribution. It was argued that a similarity of drop size distributions for different operating conditions or different equipment is a strong indication that the micro processes involved in forming the drop size distribution are comparable. Brown and Pitt [104], Chen and Middleman [39], Konno et al. [105], and Peter et al. [9], e.g., showed that a plot of a normalized drop diameter versus the cumulative volume distribution reveals invariant drop size distributions with respect to agitation rate and dispersion time. Normalization was done either by the Sauter mean diameter or the maximum stable drop size. Invariance of normalized drop size distributions is referred to as self-similarity. Pacek et al. [106] point out that the observation of self-similarity might partly be due to a smoothing of fine differences by the cumulative distribution that is typically used for these plots. They argue that differences in drop size distributions might be clearer recognized in volume density distributions. Therefore, these will be used in this work.

Volume density distributions for all three reactor sizes used in this study are compared with each other in Figure 6.2. Configuration A-2 is shown for the 50L reactor, B-3 for the 3 m^3 reactor and C-1 for the 40 m^3 reactor. It must be emphasized that the reactor configurations are not geometrically similar. Agitation rates and volumetric power inputs differed strongly for the experiments shown (values are given in the caption of Figure 6.2). The three drop size distributions with the smallest drop sizes, e.g., did occur at 11 kW/m^3 in the 50 L reactor (A-2), at 6.2 kW/m^3 in the 3 m^3 reactor (B-3) and at 2.0 kW/m^3 in the 40 m^3 reactor (C-1). The drop size distributions shown were chosen to represent comparable maximum stable drop sizes in all three scales. The drop size distributions are governed by a strong main peak that can be fit very well by a normal distribution (solid lines in the graph). There is a slightly increased tendency to bimodal distributions with increasing scale. This results in a reduced maximum value of the main peak of the volume density distributions because the integral of the volume density distribution is unity by definition. A second peak in the small diameter range, therefore, reduces the area of the main peak.

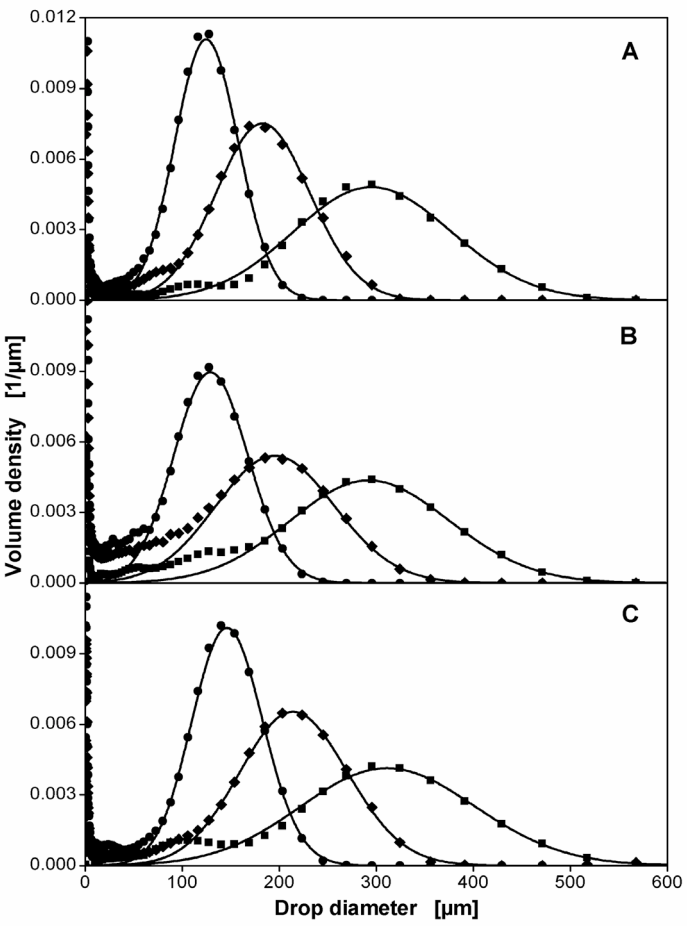

Figure 6.2: Measured drop size distributions with similar maximum stable drop sizes in three different scales with different reactor configurations. Dispersion of paraffin oil in 1 mM PO_4-buffer at pH 7.3. A: A-2 (50 L reactor), B: B-3 (3 m^3 reactor), C: C-1 (40 m^3 reactor). See Table 2.2 for details on geometry. Aeration rates in all measurements 0.7 vvm. Symbols: measured values for agitation rates: A: (●) 8.0 1/s (11 kW/m^3), (♦) 5.2 1/s (4.4 kW/m^3), (■) 3.6 1/s (1.3 kW/m^3); B: (●) 3.7 1/s (6.2 kW/m^3), (♦) 2.3 1/s (1.7 kW/m^3), (■) 1.3 1/s (0.6 kW/m^3); C: (●) 1.8 1/s (2.0 kW/m^3), (♦) 1.3 1/s (0.9 kW/m^3), (■) 0.8 1/s (0.2 kW/m^3). Solid lines: fitted normal distributions.

Very small drops in the range < 50 µm are also present that might be daughter drops that developed during break up of larger drops and did not coalesce to larger droplets any more. These small droplets are not relevant for the subject of this work as described in [9] and in

Chapter 3. Table 6.2 compares characteristic values for the main peaks of the distributions that were calculated from the fitted normal distributions. The ratio of d_{32}/d_{max} falls within a narrow range of 0.56 to 0.61 for all the distributions from the three scales. This shows that the drop size distributions for the different operating conditions and scales are self-similar. The values found for d_{32}/d_{max} are well in agreement with data from other groups found in break-up controlled single-phase experiments without aeration. Calabrese et al. [54], e.g., found values of 0.6 for moderately viscous dispersed phases. This is an important experimental verification that the mechanisms that shape drop size distributions in aerated stirred tanks are basically invariant of scale up to very large scales.

Table 6.2: Comparison of maximum stable drop sizes d_{max} and Sauter mean diameters d_{32} for all three scales at operating conditions with similar maximum stable drop sizes for the different scales. For gemetrical details see Table 2.2.

Reactor configuration	Agitation rate	Maximum stable drop size d_{max}	Sauter mean diameter d_{32}	d_{32}/d_{max}
	1/s	µm	µm	-
A-2	8.0	207	125	0.60
	5.2	305	183	0.60
	3.6	500	296	0.59
B-3	3.7	226	129	0.57
	2.3	350	196	0.56
	1.3	501	293	0.59
C-1	1.8	238	146	0.61
	1.3	355	215	0.61
	0.8	539	312	0.58

Maximum stable drop sizes calculated from these distributions are indicators for hydromechanical stress. To perform a scale-up or scale-down of hydromechanical stress it is necessary to correlate the maximum stable drop size with operating conditions. This is the focus of the following paragraphs.

6.4.3 Correlation of maximum stable drop size with impeller tip speed u_{tip}

Maximum stable drop sizes for the different scales and different impellers are compared in Figure 6.3 at an aeration rate of 0.7 vvm (volume gas/volume liquid/minute). The data for the different impellers within the 50 L and the 3 m^3 scale are in good agreement with each other. This shows that a correlation of hydromechanical stress with impeller tip speed gives reasonable results as long as the scale is not changed. However, a comparison of the results for the different scales shows that a scale-up with constant impeller tip speed will not result in comparable values of d_{max}. Therefore, the levels of hydromechanical stress in the different scales will be different if u_{tip} is kept constant. This is in accordance with the results of Jüsten et al. [16] who showed that the fragmentation of *Penicillium chrysogenum* mycelium can be correlated well with impeller tip speed for different impeller geometries within one scale but not for different scales.

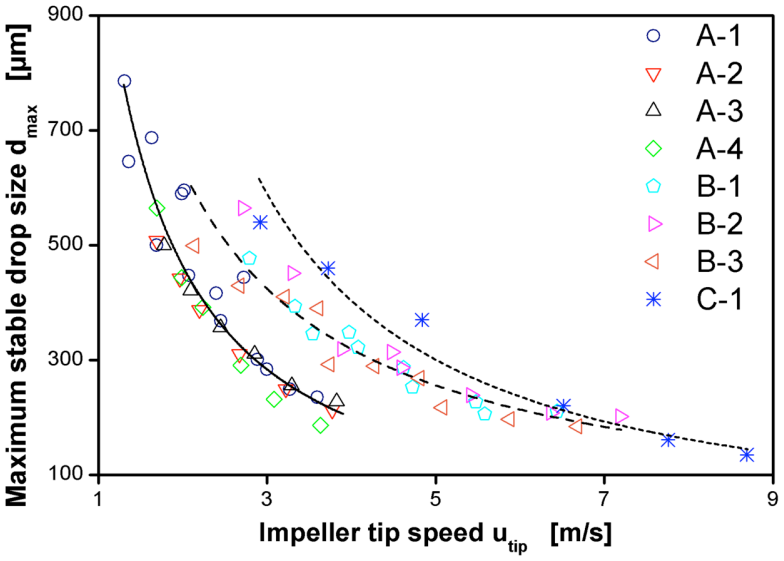

Figure 6.3: Maximum stable drop size as a function of impeller tip speed u_{tip} for all impellers as indicated in the legend (impeller geometries according to Table 2.2). Lines indicate power law fit for different scales: solid: 50 L scale, dashed: 3 m^3 scale, small dashed: 40 m^3 scale. Dispersion of paraffin oil in 1 mM PO_4-buffer at pH 7.3. Maximum stable drop size measured after 3 h agitation. Aeration rates in all measurements 0.7 vvm.

Figure 6.4 shows the maximum stable drop sizes versus impeller tip speed for reactor configuration B-3 operated with different aeration rates from 0.1 vvm to 0.7 vvm together with a power function correlation of the data. Most data for the highest aeration rate of 0.7 vvm lies at or above the fitted line while most data for the lowest aeration rate of 0.1 vvm lies below the fitted line. Generally, at the same impeller tip speed, higher aeration rates yield larger maximum stable drop sizes. This shows that there is an influence of aeration on maximum stable drop size that cannot be incorporated using u_{tip}.

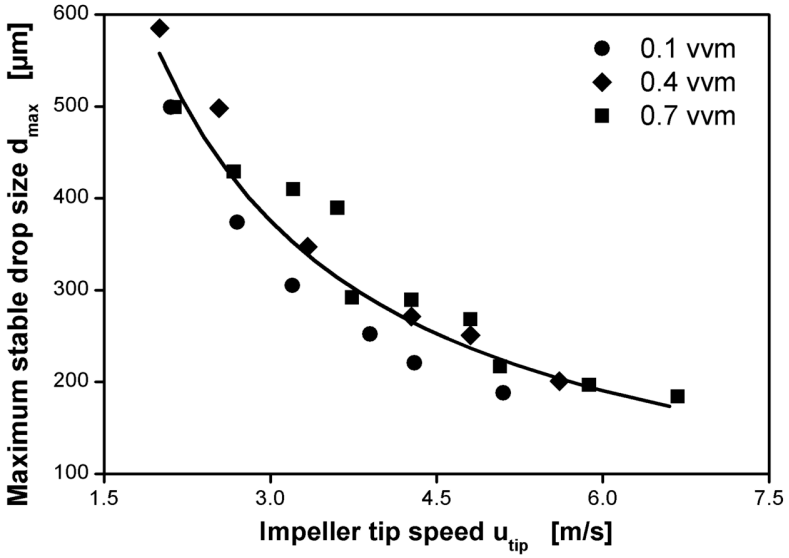

Figure 6.4: Correlation of maximum stable drop size with impeller tip speed for reactor configuration B-3 (3 m^3 scale, geometrical details: Table 2.2) for different aeration rates. Dispersion of paraffin oil in 1 mM PO_4-buffer at pH 7.3. Maximum stable drop size measured after 3 h agitation. Solid line indicates fitted power law curve.

Especially in industrial practice impeller tip speed $u_{tip} = \pi \cdot n \cdot d$ is frequently applied as a correlator for hydromechanical stress. Margaritis and Zajic [107] estimate that 20 % of the fermentation processes in industry are scaled up based on this rule. The results shown here, in accordance with earlier analyses on the value of impeller tip speed for scale-up of processes [16, 22, 23, 108], clearly show that impeller tip speed is not well suited to correlate hydromechanical stress in aerated stirred tanks.

6.4.4 Correlation of maximum stable drop size with volumetric power input

The theory on drop break-up suggests a correlation of maximum stable drop size for a given impeller with power per unit mass $\varepsilon_{Ø}$ or equivalently volumetric power input P/V_L. It was already reported in Chapter 5 for configurations B-1 and B-3 that if results are compared on the basis of aerated volumetric power input the aeration rate has no relevant influence on the maximum stable drop size in the investigated range. Hence, with aerated volumetric power input as the correlating parameter, the influence of aeration on energy dissipation is directly reflected. This is demonstrated in Figure 6.5 with the same data as in Figure 6.4. The solid line shows that the data is well in accordance with the theoretical prediction from Eqs. 6.1 and 6.2 ($\phi = 6.9$).

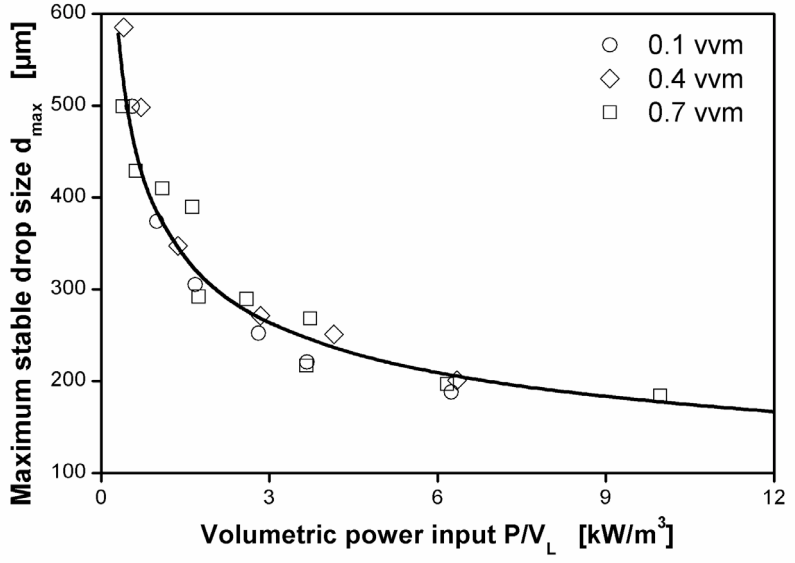

Figure 6.5: Correlation of maximum stable drop size with volumetric power input for reactor configuration B-3 (3 m^3, scale geometrical details: Table 2.2) for different aeration rates. Dispersion of paraffin oil in 1 mM PO_4-buffer at pH 7.3. Maximum stable drop size measured after 3 h agitation. Solid line represents theoretical prediction based on Eqs. 6.1 and 6.2 with $\phi = 6.9$.

Figure 6.6 shows the correlation of maximum stable drop sizes for all three reactor scales with volumetric power input. The results for configurations A-1 and A-4 in the 50 L reactor and for B-2 in the 3 m^3 reactor again demonstrate that the influence of aeration for each impeller type is well reflected by correlating the data with aerated volumetric power input.

Therefore, the data for the reactor configurations where aeration rate was not varied can be regarded as representative for these reactor configurations. The data for all scales and all impeller geometries follow generally the prediction of the theory for turbulent drop break-up. This is indicated by the lines in Figure 6.6. These were calculated on the basis of Eqs. 6.1 and 6.2 by fitting the value of ϕ to the whole data set of each impeller by means of the least squares method.

The measurements clearly discriminate between the different impeller configurations in the 50 L reactor. The larger the impeller, the larger the maximum stable drop size at a given volumetric power input. This is equivalent with a decrease in the ratio of maximum to specific energy dissipation rate with increasing impeller size and consistent with existing literature data for unaerated operating conditions [42].

The characteristics of the impellers used in the 3 m^3 reactor are relatively similar in relation to the measurement accuracy for the maximum stable drop size and the impellers can hardly be distinguished. Nevertheless, a sequence of the three impeller configurations is apparent that is in accordance with the results for the 50 L reactor. The smallest impeller B-1 produces the smallest maximum stable drop sizes at a given volumetric power input. The larger impeller B-2 with the same impeller blades as B-1 produces larger drops and the largest impeller with larger impeller blades B-3 results in the largest maximum stable drop sizes at a given volumetric power input.

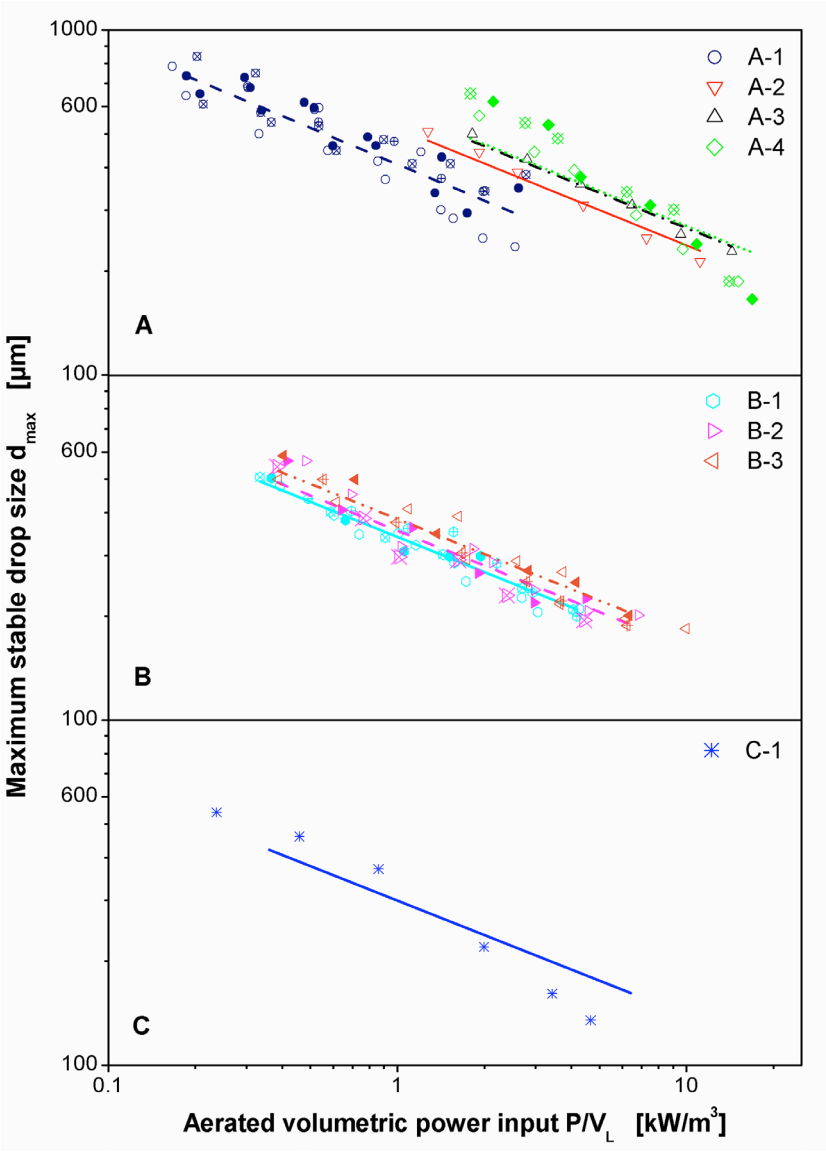

Figure 6.6: Maximum stable drop sizes measured in three different scales: A: 50 L, B: 3 m^3, C: 40 m^3. Dispersion of paraffin oil in 1 mM PO_4-buffer at pH 7.3. Maximum stable drop size measured after 3 h agitation. Symbols for different reactor configurations as indicated in legend of Figure 6.3 (geometries according to Table 2.1 and Table 2.2). Code for different aeration rates in A and B: +-center: 0.1 vvm, full symbol: 0.4 vvm, open symbol: 0.7 vvm, x-center: 1.0 vvm; 40 m^3 experiments C: 0.7 vvm.

For the 40 m^3 reactor, the data suggests a higher slope than predicted by the classic theory of drop dispersion that is represented by Eqs. 6.1 and 6.2. However, the data is relatively scarce because the reactor was only available for a short period of time. The quality of the fit of the data by the correlation is compared for all reactor configurations in Table 6.3. The quality of the fit is measured by the standard deviation of the relative difference between measured value and calculated value for d_{max}. For all reactor configurations, including the 40 m^3 reactor, the values are below the standard deviation of d_{max} for independent experiments which was determined to approx. 10 % (see Section 3.4.5). That means the deviation between measurement and model has a similar magnitude as the deviation between independent experiments. It is, therefore, not possible to clearly distinguish between a systematic deviation of the results from the classic theory of drop dispersion and measurement inaccuracy for a relatively small set of data as for the 40 m^3 reactor.

Table 6.3: Standard deviations of the relative difference between measured values for d_{max} and calculated values based on Eqs. 6.1 and 6.2 (values for ϕ see Table 6.4) as a measure for the quality of the fit.

Reactor configuration	A-1	A-2	A-3	A-4	B-1	B-2	B-3	C-1
Standard deviation [%]	6.1	2.0	1.7	9.0	3.9	5.1	4.0	6.7

Turbulence intermittency might explain an increased slope for d_{max}. This extension of the classic theory of drop dispersion takes into account the intermittent character of fine-scale turbulence as laid out by Baldyga and Podgorska [79] and Baldyga et al. [55]. In this concept, ε_{max} is not taken as a constant but as a stochastic variable that fluctuates about its mean value. The theory predicts that rare but strong bursts of high energy become more and more important for the evolution of the maximum stable drop size with increasing dispersion time. This results in a long-term drift of maximum stable drop sizes towards smaller drops and in a time-dependence of the exponent on energy dissipation rate with exponents up to -0.62 for very long dispersion times. Additionally, intermittency is stronger for higher Reynolds numbers [109] and, therefore, the effect becomes increasingly important with increasing scale.

All data presented in this study were measured between 100 and 180 min of dispersion time. The maximum stable drop sizes measured were essentially constant during this time span in all reactors. Examples for this were shown in Section 3.4.3 (Figure 3.5). Extending the experimental time to up to 9 h yielded a further decrease of the maximum stable drop size in the range of 10 % compared to the value at 3 h dispersion time in the 3 m^3 reactor (see Section 5.4.3, Figure 5.1). This is qualitatively in agreement with the prediction of the effect of intermittent turbulence, but the extend of the effect is relatively small and comparable to the reproducibility of the measured values in independent experiments. The data for the 3 m^3 reactor follows equally well the classic theory of drop dispersion as the data for the 50 L reactor. It must be assumed that the scale-effect on the slope cannot be resolved with the applied measurement method because it is below the reproducibilty of the experimental method. If the measurement accuracy in the 40 m^3 reactor is similar to that in the other scales and taking into account that the effect of turbulence intermittency on the slope was not strong enough to be detected for the other reactor configurations it seems justified to assume that the differences between measurement and model for the 40 m^3 reactor rather reflect measurement inaccuracy than the effect of intermittency on the slope. The analysis is, therefore, simplified by restricting the value of the slope to that of the classic theory of drop dispersion.

The data for the largest impeller in the 50 L reactor (A-4) exhibits a higher slope than expected for all aeration rates. This impeller has an extreme geometry with very large d/D_R-ratio of 0.65 and large impeller blades. The distance between the impeller tip and the baffles is only 0.02 m. This probably gives rise to a non-standard flow-field which may result in a modification of the turbulence characteristics. Additionally, the calculated values for power input based on Eq. 6.7 might possess a larger error than for the other impellers that are closer to standard geometry. The impellers for A-2, A-3 and A-4 have the same impeller blades but different impeller diameters. A-3 generates larger maximum stable drop sizes at the same power per unit volume than A-2. If this trend is extrapolated to A-4 than larger maximum stable drop sizes may be expected for A-4 than for A-3 at the same volumetric power input. The values for the lower range of power inputs for A-4 up to 4 kW/m^3 are in agreement with this expectation but the data for the higher power inputs tend towards smaller maximum stable drop sizes than expected. By interpreting the data on the basis of Eqs. 6.1 and 6.2 the value of ϕ for this impeller might be overestimated in comparison to the other impellers.

6.4.5 Estimation of maximum local energy dissipation rate ε_{max} and the ratio of maximum to specific energy dissipation rate ϕ

The literature correlations for ϕ from Table 6.1 can be used to calculate ε_{max} for different operating conditions and reactor geometries. It must be emphasized that these correlations were derived for single-phase, unaerated operating conditions and not for aerated operating conditions. However, up to now the only practical way to estimate ϕ for different reactor configurations for aerated operating conditions was to assume that these correlations can be applied also in the presence of aeration. This is supported by the data of Bourne [98] that is based on a chemical method to measure micromixing efficiency. Bourne [98] came to the conclusion that ϕ is not influenced by aeration. Fort et al. [97] report on a roughly 20 % reduction of turbulence intensity in the presence of aeration. However, their data is based on the measurement of pressure fluctuations at constant agitation rate. There is no clear conclusion with regard to the influence of aeration on ϕ. The data presented in Chapter 5 clearly shows that ϕ is reduced by aeration based on the measurement technique that is used in this work. The relation of these results to the findings of Bourne [98] and other literature data are discussed in Section 5.4.3. As an example for the value of the correlations from Table 6.1 for aerated operating conditions, Figure 6.7 compares all data obtained in this work with ε_{max} calculated with the correlation of McManamey [42]. This equation was used because it might be the most common correlation to estimate ε_{max} [49]. Given the simplicity of this type of correlation, the broad spectrum of impeller geometries used in the experiments and the broad range of scales applied, the results are in reasonable agreement. The prediction from this simple correlation is probably accurate enough for crude estimations in industrial practice.

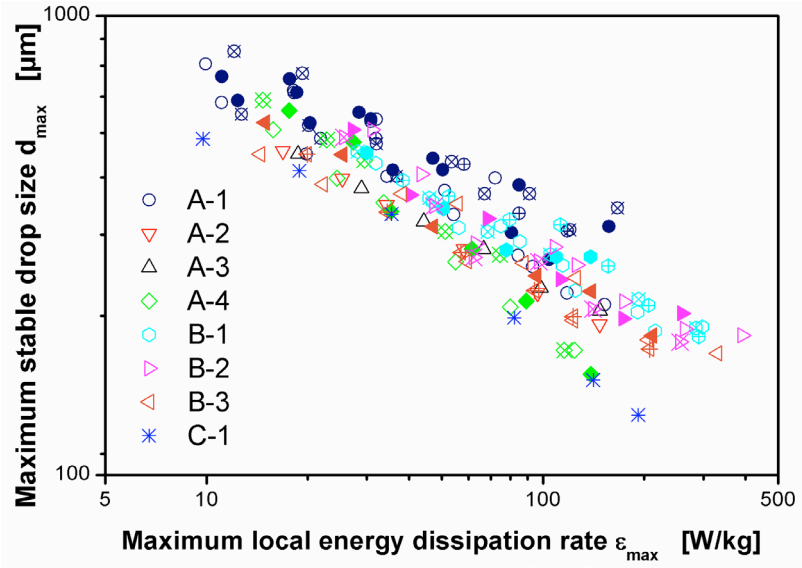

Figure 6.7: Maximum stable drop size as a function of maximum local energy dissipation rate ε_{max}. ε_{max} calculated from $\varepsilon_{\varnothing}$ with $\phi = \varepsilon_{max}/\varepsilon_{\varnothing}$ based on the equation of McManamey [42] for non-aerated conditions. Dispersion of paraffin oil in 1 mM PO_4-buffer at pH 7.3. Maximum stable drop size measured after 3 h agitation. Geometries for different reactor configurations according to Table 2.1 and Table 2.2. Code for different aeration rates for 50 L (A) and 3 m^3 (B) scale: +-center: 0.1 vvm, full symbol: 0.4 vvm, open symbol: 0.7 vvm, x-center: 1.0 vvm; ; 40 m^3 experiments (C-1): 0.7 vvm.

Figure 6.8 shows the data for all impeller configurations and all operating conditions for the three scales with the maximum local energy dissipation rate calculated with the values for ϕ based on the experimental data and Eqs. 6.1 and 6.2. Most of the data lies within ±20 % around the prediction as indicated by the solid and dashed lines in Figure 6.8. A very accurate correlation of the data is achieved. This emphasizes the importance of the experimental method developed in this work for scale-up and scale-down studies of hydromechanical stress in aerated stirred tanks.

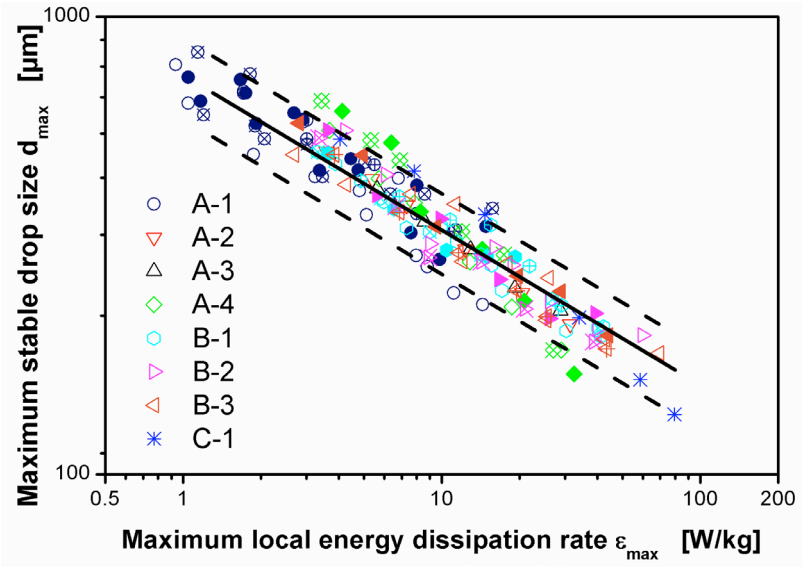

Figure 6.8: Maximum stable drop size as a function of maximum local energy dissipation rate ε_{max}. ε_{max} calculated on the basis of $\phi = \varepsilon_{max}/\varepsilon_{\varnothing}$ based on the measurements. Dispersion of paraffin oil in 1 mM PO_4-buffer at pH 7.3. Maximum stable drop size measured after 3 h agitation. Geometries for different reactor configurations according to Table 2.1 and Table 2.2. Code for different aeration rates for 50 L (A) and 3 m^3 (B) scale: +-center: 0.1 vvm, full symbol: 0.4 vvm, open symbol: 0.7 vvm, x-center: 1.0 vvm; 40 m^3 experiments (C-1): 0.7 vvm. Solid line: Theoretical prediction based on Eqs. 6.1 and 6.2, values for ϕ from Table 6.4. Dashed lines: ±20 % deviation from theoretical prediction.

Table 6.4 allows an analysis of the main factors that influence the value of ϕ. The table shows the values for ϕ that were derived from the aerated experiments and the values calculated with the different literature correlations from Table 6.1. The absolute values for ϕ for each impeller differ strongly for the different correlations and in comparison to the values that are based on the measurements. This was expected and already discussed in Chapter 5. Despite the differences in the absolute values, the relative order of the impeller configurations within the 50 L and the 3 m^3 scales is the same for the measurements as for all the different correlations. That means the influence of geometry within one scale is qualitatively well predicted by the correlations.

Table 6.4: Values for ϕ calculated for all 8 reactor configurations from the experimental data for maximum stable drop size from aerated experiments in comparison with results from literature correlations (Table 6.1) for single-phase, unaerated operation.

Reactor configuration	Results from experiments with aeration	Correlations for single-phase, unaerated operation			
		McManamey (1979) Eq. (6.3)	Okamoto (1981) Eq. (6.4)	Liepe (1988) Eq. (6.5)	Liepe (1988) Eq. (6.6)
	$\phi_{aerated}$ [−]	$\phi_{unaerated}$ [−]	$\phi_{unaerated}$ [−]	$\phi_{unaerated}$ [−]	$\phi_{unaerated}$ [−]
A-1	5.7	60	12	26	35
A-2	2.8	13	2.8	4.0	12
A-3	2.0	10	2.4	3.5	8.1
A-4	1.9	8.2	2.0	3.1	5.8
B-1	9.9	67	13	33	40
B-2	8.7	56	12	27	30
B-3	6.9	33	7.2	17	21
C-1	17	41	10	21	20

The absolute values for ϕ that were derived from the measurements are small compared to the values from literature correlations. It was shown in Chapter 5 that a comparison of maximum stable drop sizes under aerated and unaerated operating conditions for reactor configurations B-1 and B-3 reveals a much more uniform distribution of energy dissipation in aerated reactors than in unaerated reactors. ϕ was reduced by aeration by 64 % for B-1 and by 52 % for C-1 when compared with unaerated operating conditions on the basis of equal volumetric power input. The low values for ϕ found for the data presented here fit well into this pattern and support this finding.

If different scales are compared with each other the measured values for ϕ suggest a scale-effect with higher values for ϕ in larger scales. A-1 and B-1 for example are close to geometric similarity and the literature correlations predict similar values for ϕ for the two impeller configurations. McManamey's [42] correlation, e.g., predicts that the ratio of the values of ϕ for B-1 compared to A-1 should be 1.1. However, the ratio of the values of ϕ derived from the measurements is 1.7. That means that hydromechanical stress at equal volumetric power input is higher in the 3 m^3 reactor than in the 50 L reactor although the impeller geometries are close to geometric similarity. A comparison of the data for the 40 m^3 reactor with the 3 m^3 reactor also shows this scale-effect. C-1 has a larger diameter impeller than B-1 with similar sized impeller blades in relation to the reactor diameter.

Within one scale this combination results in a lower value for ϕ for the larger impeller (e.g. A-2 in comparison with A-1). This is also predicted by the correlation of McManamey [42] that predicts a ratio of the values of ϕ for C-1 compared to B-1 of 0.6. The experimental data however gives a ratio of 1.7 for C-1 compared to B-1, i.e. hydromechanical stress is higher at the same volumetric power input in C-1 than in B-1. The classic theory of drop dispersion as expressed in Eqs. 6.1 and 6.2 does not predict a scale-dependence of maximum stable drop size for geometrically similar reactor configurations for aerated operating conditions. However, Baldyga et al. [55] show for inviscid drops in unaerated dispersions that turbulence intermittency can explain a scale-dependence of d_{max} that leads to smaller drops in larger scales. The extend of the scale-dependence is related to dispersion time through the „multifractal scaling exponent“. A parameter that is not readily available for practical applications. For long dispersion times the theory predicts a dependence in the form $d_{max} \sim D_R^{-0.543}$ [55]. If this is the case and the data is still interpreted on the basis of the classic theory of drop dispersion this will result in an apparently higher value of ϕ for large reactors. If the case of inviscid drops is considered with $d_{max} \sim \varepsilon_{max}^{-0.4}$ then $\phi \sim D_R^{0.543}$ would result following the theory of Baldyga. The proportionality $\phi \sim D_R^{0.543}$ can be used to calculate the theoretical ratios of ϕ for the different reactor scales used in this study assuming geometric similarity: the ratio of ϕ for the 3 m^3 reactor compared to the 50 L reactor is 2.2. The calculated ratio of ϕ for the 40 m^3 reactor compared to the 50 L reactor is 3.4 and the ratio of ϕ for the 40 m^3 reactor compared to the 3 m^3 reactor is 1.6. These differences are in reasonable agreement with the differences seen in the experimental results. Although the effect of intermittency on the exponent on energy dissipation rate could not be resolved with the measurement method applied in the experiments, the effect of intermittency on ϕ is strong and must be incorporated in the analysis.

For practical applications it is desirable to estimate ϕ based on a simple engineering correlation instead of conducting time consuming and costly experiments (particularly in large scale). It is possible to get a first approximation by applying one of the correlations from Table 6.1. However, these only model the effect of geometry on ϕ for unaerated operating conditions. It would be favourable to generalize these correlations by additionally incorporating the effects of aeration and scale. It is clear that a correlation based on the limited set of data presented in this study can only be preliminary and approximate. Nevertheless, it might be helpful for practitioners and will hopefully inspire further work to elaborate the results presented in this work. The impeller geometry can be incorporated using, e.g. the equation of McManamey [42] for single-phase, unaerated operating conditions (Eq. 6.3, Table 6.1). The results presented in Chapter 5 indicated already that the

effect of aeration on ϕ is geometry-dependent, i.e. turbulence attenuation by aeration is stronger for impellers that exhibit larger values of ϕ under unaerated conditions. The data in this study strongly support the presence of this phenomenon. The results can only be correlated satisfactorily when the geometry-dependence of the effect of aeration on ϕ is considered. This can be done in the form $\phi \sim (\phi_{unaerated})^a$ where "a" is a constant. The effect of scale can be estimated by $\phi \sim D^{0.543}$ based on the work of Baldyga et al. [55]. This results in the following correlation:

$$\phi = 2.3 \cdot \phi_{unaerated}^{0.34} \cdot D_R^{0.543} \tag{6.11}$$

The proportionality constant and the exponent on $\phi_{unaerated}$ were found by means of least squares fitting to the values of calculated ϕ based on the measurements of maximum stable drop size (Table 6.4). Eq. 6.11 is valid for 3 impeller setups with H/D = 1.8. Figure 6.9 shows the excellent agreement of the results calculated with Eq. 6.11 with the values based on the measured data for maximum stable drop size for all impeller geometries and scales from 50 L to 40 m^3.

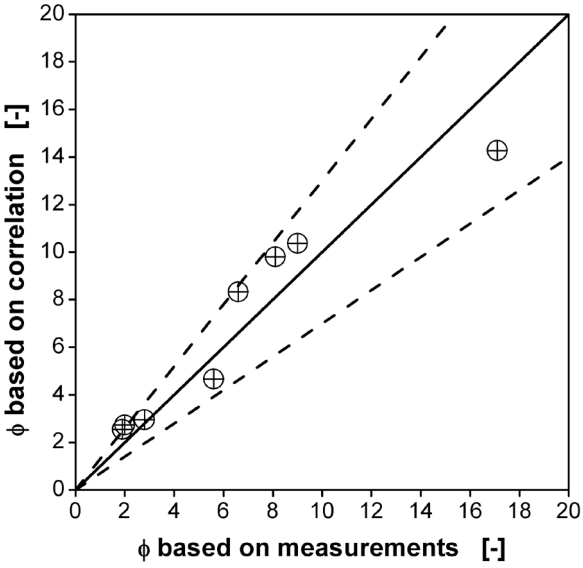

Figure 6.9: Parity plot of measured and calculated values of ϕ for all impeller configurations and scales. Measured values as given in Table 6.4, calculated values based on Eq. 6.11 with $\phi_{unaerated}$ calculated with Eq. 6.3. Dotted lines indicate ±30 %-lines.

6.5 Maximum energy dissipation of an Ekato Combijet/Phasejet impeller setup

The results in the previous sections of this chapter focused on Rushton type impellers. In this closing section, hydromechanical stress of impeller setup B-5 in the 3 m^3 reactor with an Ekato Combijet and four Ekato Phasejet impellers will be analyzed. These impellers are low power number impellers with Po = 1.6 for the Phasejet and Po = 0.8 for the Combijet. When Rushton type impellers are replaced by such low power number impellers, a larger impeller diameter can be chosen to conserve the level of agitation rate at a given impeller power input. This is important in large reactors where a change in the level of agitation rate typically necessitates further investments in the drive train in addition to the cost of the new impeller system. Two different impeller geometries are used in this setup. The volumetric power input of the whole impeller setup is the sum of the volumetric power inputs of the individual impellers. Maximum local energy dissipation of the impeller setup is governed by the impeller with the highest value of ε_{max} at a given agitation rate. It can be assumed that the bottom Phasejet impeller that is used for primary gas dispersion exhibits a higher hydromechanical stress than the upper Combijet impellers. It, therefore, governs the level of hydromechanical stress in impeller setup B-5. The effective value for ϕ for the whole impeller setup is determined by ε_{max} of the impeller with the highest value at a given agitation rate divided by $\varepsilon_{\emptyset}$ of the whole impeller setup. A correlation of maximum stable drop size from drop dispersion experiments with volumetric power input results in this effective value for ϕ. Maximum stable drop sizes vs. impeller power input of impeller setup B-5 are shown in Figure 6.10 together with the characteristic lines of the three other impeller setups B-1, B-2 and B-3 from the previous experiments (see Table 6.4 for values of ϕ for the Rushton setups). Maximum stable drop sizes at a given volumetric power input for the Ekato system B-5 is generally in the same range as for the Rushton setups. Although the diameter of the Ekato Phasejet is nearly as high (d/D_R = 0.42) as the diameter of the Rushton setup B-3 (d/D_R = 0.43) the characteristics of hydrodynamic stress is closer to the smaller Rushton setup B-2 (d/D_R = 0.38). The value of ϕ for the whole impeller setup that was calculated from these data is given in Table 6.5 together with further estimates for ϕ that are explained below.

The value for ϕ for the Phasejet impeller can be estimated by correlating the maximum stable drop sizes from Figure 6.10 with the volumetric power input of the Phasejet impeller. The volumetric power input of the Phasejet impeller can be calculated with Eq. 6.10. Based

on Eq. 6.10 the Phasejet impeller contributes 24% to the total power input and ϕ for the Phasejet impeller results in a value of 7.1.

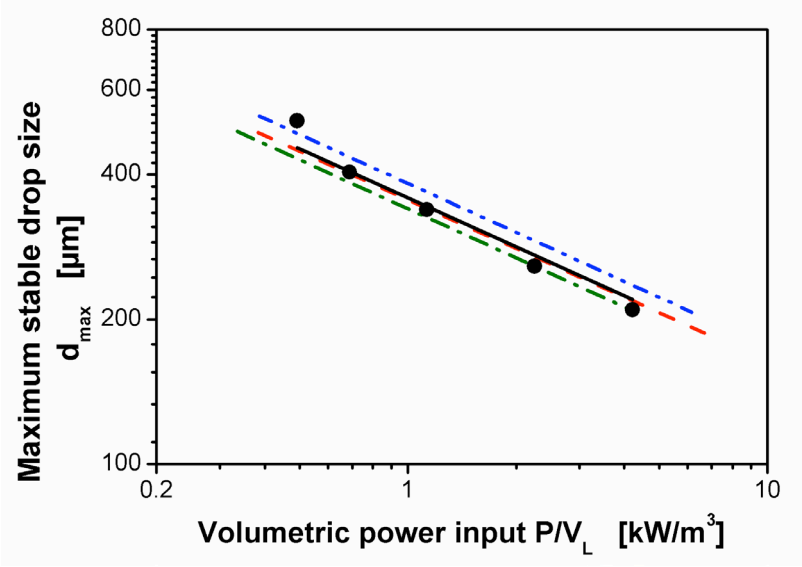

Figure 6.10: Maximum stable drop sizes for impeller setup B-5 (● and solid black line) in comparison with the characteristics of Rushton setups B-1 (green dotted-dashed line), B-2 (red dashed line) and B-3 (blue double dotted-dashed line). Geometries according to Table 2.1, Table 2.2 and Table 2.3. Dispersion of paraffin oil in 1 mM PO_4-buffer at pH 7.3. Maximum stable drop size measured after 3 h agitation.

Since the impeller is used in a 5 impeller setup with the same total liquid volume as the 3 impeller Rushton setups this value has to be corrected for the volume difference per impeller stage for comparison with the individual Rushton impellers. ϕ changes directly proportional to the volume per impeller stage (as explained in detail in Section 5.4.1). The resulting value for the Phasejet impeller in a hypothetical 3 impeller setup with H/D = 1.8 (equivalent with the other impeller setups used in this work) is 11.9. This value is 20 % higher than the value for the smallest Rushton impeller setup B-1 with d/D_R = 0.34 (ϕ = 9.9). Although the correlation Eq. 6.11 was developed based on data for Rushton type impeller setups only, it can be tested with the Ekato Phasejet impeller to see if it is possible to apply the correlation to non-Rushton impellers. $\phi_{unaerated}$ can be calculated with the equation of McManamey based on the impeller swept volume (Eq. 6.3). The distance between the impeller tips at the circumference of the impeller can be taken as the impeller

blade height which is 0.088 m. This results in calculated value for ϕ of 9.4. This is only 22 % lower than the measured value of 11.9.

Table 6.5 Values for ϕ for the Ekato Phasejet/Combijet setup B-5 with 1 Phasejet impeller and 4 Combijet impellers.

Parameter	ϕ [-]	Comment
Effective value for ϕ for the whole impeller system	8.4	Calculated from correlation of maximum stable drop size with volumetric power input for whole impeller system (Figure 6.10).
ϕ for Phasejet impeller in 5 impeller setup with H/D = 1.8	7.1	Calculated from correlation of maximum stable drop size with volumetric power input for Phasejet impeller based on Eq. 6.10.
ϕ for Phasejet impeller in 3 impeller setup with H/D = 1.8	11.9	Calculated from ϕ for Phasejet impeller with volume corrected to 3 impeller setup with H/D = 1.8.
ϕ for Phasejet impeller based on correlation	9.4	Calculated with Eq. 6.11. $\phi_{unaerated}$ calculated with Eq. 6.3 with distance of the impeller tips at the circumference as effective impeller blade height (0.088m).

6.6 Conclusions

For the first time, results from drop dispersion experiments in aerated stirred tanks were presented that cover an unprecedented broad range of operating conditions, impeller geometries and reactor scales of 50 L, 3 m^3 and 40 m^3 volume. A comparison of the volume density distributions in the three different scales show that the drop size distributions are self-similar and that d_{32}/d_{max} for the aerated dispersions are in the same range as reported by other groups for single-phase, unaerated dispersions [e.g. 54]. This is a strong indication that the basic mechanisms that shape drop size distributions in aerated stirred tanks are basically invariant of scale up to large scales. It was shown that the influence of aeration

and scale on hydromechanical stress is not considered correctly when using impeller tip speed as the correlator. The influence of aeration for each impeller type is well reflected by correlating the data with aerated volumetric power input. This is in accordance with the classic theory of break-up controlled drop dispersion if the ratio of maximum to volume averaged energy dissipation rate ϕ is independent of the operating conditions. Absolute values for ϕ that were calculated for each impeller based on literature correlations for unaerated operating conditions differ strongly for the different correlations and in comparison to the values derived from the measurements with aerated operating conditions. The relative order of the impellers within one scale is the same for all correlations for unaerated operating conditions as for the values that are based on the drop size measurements for aerated operating conditions. Hence, the behaviour of the impellers relative to each other within one scale is qualitatively well predicted by the correlations even though they are strictly valid only for unaerated operating conditions. The low values for ϕ found for the data presented in this study support the main finding from Chapter 5 that energy dissipation in the impeller region is much more uniformly distributed (ϕ is reduced by approx. 60 %) in aerated reactors than in unaerated reactors. Comparison of data in the different scales shows that there is a scale effect that results in higher values for ϕ in larger reactors. This behaviour is not covered by the classic theory of turbulent drop dispersion but is in good agreement with the theory of turbulence intermittency that predicts an up to 3.4 times larger value for ϕ in the 40 m^3 reactor than in the 50 L reactor. The data for all impeller configurations and all aeration rates for the three scales correlate very well when calculated values for ϕ based on the measured values for d_{max} are used to calculate the maximum local energy dissipation rate. Most of the data lies within 20 % around the theoretical prediction from the classic theory of drop dispersion when these values for ϕ are used. A correlation of the data for the Rushton impeller configurations for all scales in the form $\phi = 2.3 \cdot (\phi_{unaerated})^{0.34} \cdot (D_R)^{0.543}$ is suggested that successfully models the influence of impeller geometry, aeration and scale on ϕ for aerated operating conditions. Measurements for an Ekato impeller setup with one Phasejet and four Combijet impellers showed that this impeller setup has a similar characteristics than the Rushton impeller setup B-2 with d/D_R = 0.38 although the Ekato Phasejet impeller has $d/D_R = 0.42$. The effective value of ϕ for the Ekato setup was calculated to $\phi = 8.4$. Hydromechanical stress for the Phasejet impeller in a hypothetical 3 impeller setup with H/D = 1.8 (as for the Rushton setups used in this work) was estimated based on the measurements for the 5 impeller setup to a value of 11.9. Application of the new correlation for Rushton impellers to the Ekato Phasejet resulted in a predicted value for ϕ of 9.4 which is only 22 % lower than the value based on the

measurements. That means the correlation can be successfully applied to estimate hydromechanical stress for impeller geometries other than Rushton impellers.

7 Conclusions and Outlook

Turbulence intensity, or hydromechanical stress, is a controlling parameter in many industrially relevant processes. These processes are often characterized by intense aeration and agitation, particularly in the fermentation industries. Measurement of turbulence intensity is extremely difficult under such operating conditions and very few data on turbulence characteristics exists. Therefore, this thesis focused on three central topics related to hydromechanical stress in aerated stirred tanks in industrial application:

1. The development of a measurement technique for hydromechanical stress in aerated stirred tanks.

2. The investigation of the influence of aeration on hydromechanical stress.

3. The characterization of the influence of geometry and scale on hydromechanical stress in aerated stirred tanks.

Since the maximum stable drop diameter in a break-up controlled dispersion is directly correlated with turbulence intensity, the measurement of drop sizes can enable an indirect access to hydromechanical stress under aerated operating conditions. This principle was the basis for the measurement technique developed and applied in this work. Chapter 3 presented the constraints and the development of the experimental method. Continuous and dispersed phase properties were selected to achieve a break-up controlled dispersion with negligible coalescence. This was accomplished mainly by applying a dilute dispersion, a low ionic strength and by incorporating a dispersed phase, paraffin oil, with a negative spreading coefficient. The negative spreading coefficient prevents coalescence due to drop-bubble interactions for aerated operating conditions. It was demonstrated that the off-line

measured drop size distributions are representative for the conditions in the reactor and are not altered by sample handling. The sampling and measurement procedure was found to be highly reproducible with a standard deviation for the maximum stable drop size for independent experiments of approximately 10 %. Relevant constraints for the application of the method in large-scale experiments were discussed and accounted for during method development to allow a later application in production scale equipment.

Since hydromechanical stress is directly correlated with impeller power input, a reliable value for impeller power input is important for the interpretation of the experimental results from the drop dispersion experiments. Chapter 4 presented an analysis of the electrical power input measurement in a 3 m^3 reactor that was used for the drop dispersion experiments in the subsequent work. An instationary temperature method was applied to compare measurement values from electrical power draw of the engine with an independent measurement of power input. A correlation of power losses versus agitation rate was developed that allowed a correction of the fast and convenient electrical power measurement to measure the power input from agitation in the drop dispersion experiments.

Chapter 5 focused on the question of the influence of aeration on hydromechanical stress. Results from drop dispersion experiments with two different setups of 6-bladed Rushton turbine impellers with diameters of d = 0.41 m (d/D_R = 0.34, setup B-1) and d = 0.51 m (d/D_R = 0.43, setup B-3) in a 3 impeller configuration were presented. The results from experiments without aeration were well in agreement with the existing literature on drop dispersion. The results from experiments with aeration indicated a strong attenuation of turbulence intensity in stirred tank reactors by the presence of air. The ratio between maximum and volume-averaged energy dissipation rate was reduced by aeration by 64 % for the d/D_R = 0.34 impeller setup (B-1) and by 52 % for the d/D_R = 0.43 impeller setup (B-3) when compared with unaerated operating conditions on the basis of equal volumetric power input. The value of the aeration rate had no measurable effect in the range of aeration rates applied, which was between 0.1 vvm and 1 vvm.

Chapter 6 was dedicated to the questions of the influence of impeller geometry, operating conditions and scale on hydromechanical stress. Results from drop dispersion experiments in aerated stirred tanks were presented that cover a broad range of operating conditions, impeller geometries and reactor scales of 50 L, 3 m^3 and 40 m^3 volume. The results showed that impeller tip speed is not well suited to correlate hydromechanical stress despite its frequent use in industrial practice. Results from literature correlations for Rushton impellers

for unaerated operating conditions for the ratio of maximum to specific energy dissipation rate ϕ were qualitatively in agreement with each other. They were also qualitatively in agreement with the results for ϕ based on measured values for maximum stable drop size for aerated operating conditions for the impellers within each scale. Comparison of data between the different scales showed that there is a scale effect that results in higher values for ϕ in larger reactors. This behaviour is not covered by the classic theory of turbulent drop dispersion but is in good agreement with the theory of turbulence intermittency that predicts an up to 3.4 times larger value for ϕ in the 40 m^3 reactor than in the 50 L reactor. The data for all impeller configurations and all aeration rates for the three scales correlated very well when calculated values for ϕ based on the measured values for d_{max} were used to calculate the maximum local energy dissipation rate. Most of the data was within 20 % around the theoretical prediction from the classic theory of drop dispersion when these values for ϕ were used. A correlation of the data for all scales and all impeller configurations in the form $\phi = 2.3 \cdot (\phi_{unaerated})^{0.34} \cdot (D_R)^{0.543}$ was suggested that successfully models the influence of scale and impeller geometry on ϕ for aerated operating conditions. The results for an Ekato impeller setup with one Phasejet and four Combijet impellers were similar with the three impeller Rushton setup with $d/D_R = 0.38$. A comparison of the value for ϕ based on the measurement results with the value for ϕ based on the newly developed correlation for Rushton impellers resulted in a difference of only 22 % with $\phi = 11.9$ for the value based on the experimental data and $\phi = 9.4$ for the calculated value. It can be conclueded that the correlation can be successfully applied to estimate hydromechanical stress for impeller geometries other than Rushton impellers.

The measurement method and the data presented in this work represent an important step forward in the characterization of hydromechanical stress in stirred tanks under aerated operating conditions. For the first time a direct comparison of hydromechanical stress for a broad range of aerated and unaerated operating conditions showed strong turbulence attenuation in a 3 m^3 reactor. These results will hopefully trigger further research that aims at a sound theoretical understanding of the empirical findings gained in this work. Additionally, it would be interesting to explore the transitional range of operating conditions between 0.1 vvm and zero aeration which was not covered in the present work due to the technical limitations of the available equipment. The experiments were conducted with a continuous phase with water-like viscosity. An important extension of the results presented would be the application of a continuous phase with elevated viscosity to explore the influence of viscosity on hydromechanical stress under aerated and unaerated operating conditions.

The new measurement method and the data gained in this thesis also represent an important step forward in the characterization of hydromechanical stress in industrial scale processes. The method can be applied in the future to characterize further agitator and reactor designs under process relevant operating conditions which was frequently not possible in the past due to a lack of measurement techniques. The correlation for ϕ developed in this work can be beneficially used for approximate calculations of hydromechanical stress for geometries for which experimental data is not available. In combination with further important process parameters like mass transfer characteristics and mixing characteristics of impeller setups, characteristics of hydromechanical stress can be incorporated in reactor and process optimization in a more relevant manner than possible before.

Bibliography

1. Baldi S, Yianneskis M: On the quantification of energy dissipation in the impeller stream of a stirred vessel from fluctuating velocity gradient measurements. Chemical Engineering Science 2004, 59:2659-2671.

2. Hinze JO: Fundamentals of the hydrodynamic mechanism of splitting in dispersion processes. *AIChE Journal* 1955, 1(3):289-295.

3. Galindo E, Pacek AW, Nienow AW: Study of drop and bubble sizes in a simulated mycelial fermentation broth of up to four phases. *Biotechnology and Bioengineering* 2000, 69(2):213-221.

4. Fujasova M, Linek V, Moucha T: Mass transfer correlations for multiple-impeller gas-liquid contactors. Analysis of the effect of axial dispersion in gas and liquid phases on "local" k(L)a values measured by the dynamic pressure method in individual stages of the vessel. *Chemical Engineering Science* 2007, 62(6):1650-1669.

5. Kumar A, Hartland S: Unified correlations for the prediction of drop size in liquid-liquid extraction columns. *Industrial & Engineering Chemistry Research* 1996, 35(8):2682-2695.

6. Vivaldo-Lima E, Wood PE, Hamielec AE, Penlidis A: An updated review on suspension polymerization. *Industrial & Engineering Chemistry Research* 1997, 36(4):939-965.

7. Henzler H-J: Particle stress in bioreactors. *Advances in biochemical engineering/biotechnology* 2000, 67:35-82.

8. Fujita M, Iwahori K, Tatsuta S, Yamakawa K: Analysis of pellet formation of *Aspergillus niger* based on shear-stress. *Journal of Fermentation and Bioengineering* 1994, 78(5):368-373.

9. Peter CP, Suzuki Y, Büchs J: Hydromechanical stress in shake flasks: Correlation for the maximum local energy dissipation rate. *Biotechnology and Bioengineering* 2006, 93(6):1164-1176.

10. Büchs J, Zoels B: Evaluation of maximum to specific power consumption ratio in shaking bioreactors. *Journal of Chemical Engineering of Japan* 2001, 34(5):647-653.

11. Cui YQ, van der Lans RGJM, Luyben KCAM: Effects of dissolved oxygen tension and mechanical forces on fungal morphology in submerged fermentation. *Biotechnology and Bioengineering* 1998, 57(4):409-419.

12. Amanullah A, Christensen LH, Hansen K, Nienow AW, Thomas CR: Dependence of morphology on agitation intensity in fed-batch cultures of Aspergillus oryzae and its implications for recombinant protein production. *Biotechnology and Bioengineering* 2002, 77(7):815-826.

13. Rocha-Valadez JA, Hassan M, Corkidi G, Flores C, Galindo E, Serrano-Carreon L: 6-Pentyl-alpha-pyrone production by Trichoderma harzianum: The influence of energy dissipation rate and its implications on fungal physiology. *Biotechnology and Bioengineering* 2005, 91(1):54-61.

14. Jüsten P, Paul GC, Nienow AW, Thomas CR: Dependence of mycelial morphology on impeller type and agitation intensity. *Biotechnology and Bioengineering* 1996, 52(6):672-684.

15. Jüsten P, Paul GC, Nienow AW, Thomas CR: Dependence of *Penicillium chrysogenum* growth, morphology, vacuolation, and productivity in fed-batch fermentations on impeller type and agitation intensity. *Biotechnology and Bioengineering* 1998, 59(6):762-775.

16. Jüsten P, Paul GC, Nienow AW, Thomas CR: A mathematical model for agitation-induced fragmentation of *Penicillium chrysogenum*. *Bioprocess Engineering* 1998, 18(1):7-16.

17. Makagiansar HY, Shamlou PA, Thomas CR, Lilly MD: The influence of mechanical forces on the morphology and penicillin production of Penicillium chrysogenum. *Bioprocess Engineering* 1993, 9(2-3):83-90.

18. Smith JJ, Lilly MD, Fox RI: The effect of agitation on the morphology and penicillin production of Penicillium chrysogenum. *Biotechnology and Bioengineering* 1990, 35(10):1011-1023.

19. Van Suijdam JC, Metz B: Influence of engineering variables upon the morphology of filamentous molds. *Biotechnology and Bioengineering* 1981, 23(1):111-148.

20. Gregoriades N, Clay J, Ma N, Koelling K, Chalmers JJ: Cell damage of microcarrier cultures as a function of local energy dissipation created by a rapid extensional flow. *Biotechnology and Bioengineering* 2000, 69(2):171-182.

21. Einsele A: Scaling-up bioreactors. *Process Biochemistry* 1978, 7:13-14.

22. Junker BH: Scale-up methodologies for *Escherichia coli* and yeast fermentation processes. *Journal of Bioscience and Bioengineering* 2004, 97(6):347-364.

23. Humphrey A: Shake flask to fermentor: What have we learned? *Biotechnology Progress* 1998, 14(1):3-7.

24. Deen NG, Westerweel J, Delnoij E: Two-Phase PIV in bubbly flows: status and trends. *Chemical Engineering & Technology* 2002, 25(1):97 - 101.

25. Dudukovic MP: Opaque multiphase flows: experiments and modeling. *Experimental Thermal and Fluid Science* 2001, 26:747-761.

26. Joshi JB, Nere NK, Rane CV, Murthy BN, Mathpati CS, Patwardhan AW, Ranade VV: CFD simulation of stirred tanks: Comparison of turbulence models (Part II: Axial flow impellers, multiple impellers and multiphase dispersions). *The Canadian Journal of Chemical Engineering* 2011, 89(4):754-816.

27. Sungkorn R, Derksen JJ, Khinast JG: Euler–Lagrange modeling of a gas–liquid stirred reactor with consideration of bubble breakage and coalescence. *Aiche Journal* 2012, 58(5):1356-1370.

28. Olmos E, Mehmood N, Haj Husein L, Goergen JL, Fick M, Delaunay S: Effects of bioreactor hydrodynamics on the physiology of Streptomyces. *Bioprocess and Biosystems Engineering* 2013, 36(3):259-272.

29. Montante G, Horn D, Paglianti A: Gas-liquid flow and bubble size distribution in stirred tanks. *Chemical Engineering Science* 2008, 63(8):2107-2118.

30. Assirelli M, Wynn EJW, Bujalski W, Eaglesham A, Nienow A: An extension to the incorporation model of micromixing and its use in estimating local specific energy dissipation rates. *Industrial & Engineering Chemistry Research* 2008, 47(10):3460 - 3469.

31. Cutter LA: Flow and turbulence in a stirred tank. *AIChE Journal* 1966, 12(1):35-45.

32. Costes J, Couderc JP: Study by laser Doppler anemometry of the turbulent flow induced by a Rushton turbine in a stirred tank: Influence of the size of the units: Spectral analysis and scales of turbulence. *Chemical Engineering Science* 1988, 43(10):2765-2772.

33. Ducci A, Yianneskis M: Direct determination of energy dissipation in stirred vessels with two-point LDA. *AIChE Journal* 2005, 51:2133–2149.

34. Escudié R, Liné A: Experimental analysis of hydrodynamics in a radially agitated tank. *AIChE Journal* 2003, 49(3):585-603.

35. Micheletti M, Baldi S, Yeoh SL, Ducci A, Papadakis G, Lee KC, Yianneskis M: On spatial and temporal variations and estimates of energy dissipation in stirred reactors. *Chemical Engineering Research & Design* 2004, 82(A9):1188-1198.

36. Sharp KV, Adrian RJ: PIV study of small-scale flow structure around a Rushton turbine. *AIChE Journal* 2001, 47(4):766-778.

37. Wu H, Patterson GK: Laser-Doppler measurements of turbulent-flow parameters in a stirred mixer. *Chemical Engineering Science* 1989, 44(10):2207-2221.

38. Zhou GW, Kresta SM: Impact of tank geometry on the maximum turbulence energy dissipation rate for impellers. *AIChE Journal* 1996, 42(9):2476-2490.

39. Chen HT, Middleman S: Drop size distribution in agitated liquid-liquid systems. *AIChE Journal* 1967, 13(5):989-995.

40. Liepe F, Meusel W, Möckel HO, Platzer B, Weißgärber H: Stoffvereinigung in fluiden Phasen. In: *Verfahrenstechnische Berechnungsmethoden.* Edited by Weiß S, Berghoff W, Grahn E, Gruhn G, Güsewell G, Plötner W, Robel H, Schubert M, vol. 4. Weinheim: VCH Verlagsgesellschaft; 1988.

41. Okamoto Y, Nishikawa M, Hashimoto K: Energy dissipation rate distribution in mixing vessels and its effects on liquid-liquid dispersion and solid-liquid mass transfer. *International Chemical Engineering* 1981, 21(1):7.

42. McManamey WJ: Sauter mean and maximum drop diameters of liquid-liquid dispersions in turbulent agitated vessels at low dispersed phase hold-up. *Chemical Engineering Science* 1979, 34:432-434.

43. Davies JT: A physical interpretation of drop sizes in homogenizers and agitated tanks, including the dispersion of viscous oils. *Chemical Engineering Science* 1987, 42(7):1671-1676.

44. Kresta SM, Brodkey RS: Turbulence in mixing applications. In: *Handbook of industrial mixing: science and practice.* Edited by Paul EL, Atiemo-Obeng VA, Kresta SM. Hoboken, NJ, USA: John Wiley & Sons, Inc.; 2004.

45. Mudde RF: Advanced measurement techniques for GLS reactors. *Canadian Journal of Chemical Engineering* 2010, 88:638 - 647.

46. Khopkar AR, Rammohan AR, Ranade VV, Dudukovic MP: Gas-liquid flow generated by a Rushton turbine in stirred vessel: CARPT/CT measurements and CFD simulations. *Chemical Engineering Science* 2005, 60(8-9):2215-2229.

47. Büchs J: Introduction to advantages and problems of shaken cultures. *Biochemical Engineering Journal* 2001, 7(2):91-98.

48. Mollet M, Ma NN, Zhao Y, Brodkey R, Taticek R, Chalmers JJ: Bioprocess equipment: Characterization of energy dissipation rate and its potential to damage cells. *Biotechnology Progress* 2004, 20(5):1437-1448.

49. Leng DE, Calabrese RV: Immiscible liquid–liquid systems. In: *Handbook of industrial mixing: science and practice.* Edited by Paul EL, Atiemo-Obeng VA, Kresta SM. Hoboken, NJ, USA: John Wiley & Sons, Inc.; 2004.

50. Bauer R: Untersuchungen zur Dispergierung in flüssig-flüssig Systemen. PhD Thesis. *PhD Thesis*. Köthen, Germany: Engineering School of Köthen; 1985.

51. Hemrajani RR, Tatterson GB: Mechanically stirred vessels. In: *Handbook of industrial mixing: science and practice.* Edited by Paul EL, Atiemo-Obeng VA, Kresta SM. Hoboken, NJ, USA: John Wiley & Sons, Inc.; 2004.

52. Kolmogorov AN: The breakup of droplets in a turbulent stream. *Doklady Akademii Nauk* 1949, 66(5):825-828.

53. Arai K, Konno M, Matunaga Y, Saito S: Effect of dispersed-phase viscosity on maximum stable drop size for breakup in turbulent flow. *Journal of Chemical Engineering of Japan* 1977, 10(4):325-330.

54. Calabrese RV, Chang TPK, Dang PT: Drop breakup in turbulent stirred-tank contactors. 1. Effect of dispersed-phase viscosity. *AIChE Journal* 1986, 32(4):657-666.

55. Baldyga J, Bourne JR, Pacek AW, Amanullah A, Nienow AW: Effects of agitation and scale-up on drop size in turbulent dispersions: allowance for intermittency. *Chemical Engineering Science* 2001, 56(11):3377-3385.

56. Zhou GW, Kresta SM: Correlation of mean drop size and minimum drop size with the turbulence energy dissipation and the flow in an agitated tank. *Chemical Engineering Science* 1998, 53(11):2063-2079.

57. Atiemo-Obeng VA, Calabrese RV: Rotor-stator mixing devices. In: *Handbook of industrial mixing: science and practice.* Edited by Paul EL, Atiemo-Obeng VA, Kresta SM. Hoboken, NJ, USA: John Wiley & Sons, Inc.; 2004.

58. Ribeiro MMM, Guimaraes MML, Madureira CMN, Pinto JJCC: Non-invasive system and procedures for the characterization of liquid-liquid dispersions. *Chemical Engineering Journal* 2004, 97(2-3):173-182.

59. Cents AHG, Brilman DWF, Versteeg GF: Ultrasonic investigation of hydrodynamics and mass transfer in a gas-liquid(-liquid) stirred vessel. *International Journal of Chemical Reactor Engineering* 2005, 3(A19):1-32.

60. Laakkonen M, Honkanen M, Saarenrinne P, Aittamaa J: Local bubble size distributions, gas-liquid interfacial areas and gas holdups in a stirred vessel with particle image velocimetry. *Chemical Engineering Journal* 2005, 109(1-3):37-47.

61. Gaebler A, Wegener M, Paschedag AR, Kraume M: The effect of pH on experimental and simulation results of transient drop size distributions in stirred liquid-liquid dispersions. *Chemical Engineering Science* 2006, 61(9):3018-3024.

62. Tobin T, Ramkrishna D: Coalescence of charged droplets in agitated liquid-liquid dispersions. *AIChE Journal* 1992, 38(8):1199-1205.

63. Sathyagal AN, Ramkrishna D: Droplet breakage in stirred dispersions. Breakage functions from experimental drop-size distributions. *Chemical Engineering Science* 1996, 51(9):1377-1391.

64. O'Rourke AM, MacLoughlin PF: A comparison of measurement techniques used in the analysis of evolving liquid-liquid dispersions. *Chemical Engineering and Processing* 2005, 44(8):885-894.

65. ISO 13320-1:1999 Particle size analysis - laser diffraction methods - Part 1: General principles. In., vol. ISO 13320-1:1999.

66. Dalmau E, Sanchez A, Montesinos JL, Valero F, Lafuente FJ, Casas C: Study of the drop size frequencies in a microbial growth system with an aqueous-organic culture medium: lipase production from Candida rugosa. *Journal of Biotechnology* 1998, 59(3):183-192.

67. Rols JL, Goma G: Enhanced oxygen-transfer rates in fermentation using soybean oil-in-water dispersions. *Biotechnology Letters* 1991, 13(1):7-12.

68. Yoshida T, Yokoyama K, Chen KC, Sunouchi T, Taguchi H: Oxygen-Transfer in Hydrocarbon Fermentation by *Candida-Rugosa*. *Journal of Fermentation Technology* 1977, 55(1):76-83.

69. Pereira NE, Ni XW: Droplet size distribution in a continuous oscillatory baffled reactor. *Chemical Engineering Science* 2001, 56(3):735-739.

70. Brown DAR, Jones PN, Middleton JC, Papadopoulos G, Arik EB: Experimental Methods. In: *Handbook of industrial mixing: science and practice.* Edited by Paul EL, Atiemo-Obeng VA, Kresta SM. Hoboken, NJ, USA: John Wiley & Sons, Inc.; 2004.

71. Bae JH, Tavlarides LL: Laser capillary spectrophotometry for drop-size concentration measurements. *AIChE Journal* 1989, 35(7):1073-1084.

72. Calabrese RV, Wang CY, Bryner NP: Drop breakup in turbulent stirred-tank contactors. 3. Correlations for mean size and drop size distribution. *AIChE Journal* 1986, 32(4):677-681.

73. Baldi S, Yianneskis M: On the direct measurement of turbulence energy dissipation in stirred vessels with PIV. *Industrial & Engineering Chemistry Research* 2003, 42(26):7006-7016.

74. Ascanio G, Castro B, Galindo E: Measurement of power consumption in stirred vessels - a review. *Chemical Engineering Research and Design* 2004, 82(9):1282-1290.

75. Ascanio G, Castro B, Galindo E: Measurement of power consumption in stirred vessels - a review. In., vol. 82: Elsevier; 2004: 1282-1290.

76. Chisti Y, Moo-Young M: On the calculation of shear rate and apparent viscosity in airlift and bubble column bioreactors. 1989, 34(11):1391-1392.

77. Hardy B: ITS-90 formulations for Vapor Pressure, Frostpoint Temperature, Dewpoint Temperature, and Enhancement Factors in the Range of -100 to +100°C, Papers and Abstracts of the Third International Symposium on Humidity and Moisture, Vol. 1. In: *Papers and Abstracts of the Third International Symposium on Humidity and Moisture: 1998*; 1998.

78. Verein Deutscher Ingenieure: VDI-Gesellschaft Verfahrenstechnik und Chemieingenieurwesen, VDI-Wärmeatlas: Springer-Verlag; 2005.

79. Baldyga J, Podgórska W: Drop break-up in intermittent turbulence: maximum stable and transient sizes of drops. *Canadian Journal of Chemical Engineering* 1998, 76(3):456-470.

80. Davies JT: Drop sizes of emulsions related to turbulent energy dissipation rates. *Chemical Engineering Science* 1985, 40(5):839-842.

81. Henzler H-J, Biedermann A: Modelluntersuchungen zur Partikelbeanspruchung in Reaktoren. *Chemie Ingenieur Technik* 1996, 68(12):1546-1561.

82. Baldyga J, Bourne JR: Drop breakup and intermittent turbulence. *Journal of Chemical Engineering of Japan* 1993, 26(6):738-741.

83. Middleton JC, Smith JM: Gas-liquid mixing in turbulent systems. In: *Handbook of industrial mixing: science and practice.* Edited by Paul EL, Atiemo-Obeng VA, Kresta SM. Hoboken, NJ, USA: John Wiley & Sons, Inc.; 2004.

84. Alves SS, Maia CI, Vasconcelos JMT, Serralheiro AJ: Bubble size in aerated stirred tanks. *Chemical Engineering Journal* 2002, 89(103):109-117.

85. Bluestein M, Mockros LF: Hemolytic effects of energy dissipation in flowing blood. *Medical and Biological Engineering* 1969, 7(1):1-16.

86. Li F, Hashimura Y, Pendleton R, Harms J, Collins E, Lee B: A Systematic Approach for Scale Down Model Development and Characterization of Commercial Cell Culture Processes. *Biotechnology Progress* 2006, 22(3):696-703.

87. Liu Y, Li F, Hu W, Wiltberger K, Ryll T: Effects of bubble–liquid two-phase turbulent hydrodynamics on cell damage in sparged bioreactor. *Biotechnology Progress*, 30(1):48-58.

88. Hu W, Berdugo C, Chalmers JJ: The potential of hydrodynamic damage to animal cells of industrial relevance: current understanding. *Cytotechnology*, 63(5):445-460.

89. Oh SKW, Nienow AW, Al-Rubeai M, Emery AN: The effects of agitation intensity with and without continuous sparging on the growth and antibody production of hybridoma cells. *Journal of Biotechnology* 1989, 12(1):45-61.

90. Meier SJ, Hatton TA, Wang DIC: Cell death from bursting bubbles: Role of cell attachment to rising bubbles in sparged reactors. *Biotechnology and Bioengineering* 2001, 74(6):544-546.

91. Dey D, Emery AN: Problems in predicting cell damage from bubble bursting. *Biotechnology and Bioengineering* 1999, 65(2):240-245.

92. Dhotre MT, Nere NK, Vedantam S, Tabib M: Advances in computational fluid dynamics. *International Journal of Chemical Engineering* 2013, 2013:2.

93. Gore RA, Crowe CT: Effect of particle size on modulating turbulent intensity. *International Journal of Multiphase Flow* 1989, 15(2):279-285.

94. Rensen J, Luther S, Lohse D: The effect of bubbles on developed turbulence. *Journal of Fluid Mechanics* 2005, 538:153-187.

95. Balachandar S, Eaton JK: Turbulent dispersed multiphase flow. *Annual Review of Fluid Mechanics* 2010, 42:111-133.

96. Kerdouss F, Bannari A, Proulx P: CFD modeling of gas dispersion and bubble size in a double turbine stirred tank. *Chemical Engineering Science* 2006, 61(10):3313-3322.

97. Fort I, Machon V, Kadlec P: Distribution of energy dissipation rate in an agitated gas-liquid system. *Chemical Engineering & Technology* 1993, 16:389 - 394.

98. Bourne JR: Distribution of energy-dissipation rate in an agitated gas-liquid system. *Chemical Engineering & Technology* 1994, 17(5):323-324.

99. Hofinger J, Sharpe RW, Bujalski W, Bakalis S, Assirelli M, Eaglesham A, Nienow AW: Micromixing in two-phase (G-L and S-L) systems in a stirred vessel. *The Canadian Journal of Chemical Engineering* 2011, 89(5):1029-1039.

100. Brilman DWF, Antink R, van Swaaij WPM, Versteeg GF: Experimental study of the effect of bubbles, drops and particles on the product distribution for a mixing sensitive, parallel-consecutive reaction system. *Chemical Engineering Science* 1999, 54(13-14):2325-2337.

101. Hilber CP: Untersuchungen zur Mikrovermischung in der flüssigen Phase eines begasten Rührkessels. Dissertation No. 8254. *Dissertation.* ETH Zürich; 1987.

102. Deen NG, Solberg T, Hjertager BH: Flow generated by an aerated Rushton impeller: Two-phase PIV experiments and numerical simulations. *Canadian Journal of Chemical Engineering* 2002, 80(4):638-652.

103. Montante G, Laurenzi F, Paglianti A, Magelli F: Two-phase flow and bubble size distribution in air-sparged and surface-aerated vessels stirred by a dual impeller. *Industrial & Engineering Chemistry Research* 2010, 49:2613-2623.

104. Brown DE, Pitt K: Drop size distribution of stirred non-coalescing liquid-liquid system. *Chemical Engineering Science* 1972, 27(3):577-583.

105. Konno M, Kosaka N, Saito S: Correlation of transient drop sizes in breakup process in liquid-liquid agitation. *Journal of Chemical Engineering of Japan* 1993, 26(1):37-40.

106. Pacek AW, Man CC, Nienow AW: On the Sauter mean diameter and size distributions in turbulent liquid/liquid dispersions in a stirred vessels. *Chemical Engineering Science* 1998, 53(11):2005-2011.

107. Margaritis A, Zajic JE: Mixing, mass transfer, and scale-up of polysaccharide fermentations. 1978, 20(7):939-1001.

108. Märkl H, Bronnenmeier R, Wittek B: Hydrodynamische Belastbarkeit von Mikroorganismen. *Chemie Ingenieur Technik* 1987, 59(12):907-917.

109. Baldyga J, Bourne JR: Interpretation of turbulent mixing using fractals and multifractals. *Chemical Engineering Science* 1995, 50(3):381-400.

Hydromechanische Belastung in begasten Rührreaktoren

Die Turbulenzintensität bzw. die hydromechanische Belastung ist in vielen industriell relevanten Prozessen, die in begasten Rührreaktoren betrieben werden, ein bestimmender Parameter. Diese Prozesse sind häufig charakterisiert durch intensive Begasung und Rührung. Dies gilt insbesondere für großtechnische Fermentationsprozesse. Die Messung der hydromechanischen Belastung unter Bedingungen hoher Begasungs- und Rührintensität ist überaus schwierig. Auf Grund fehlender Messmethoden gibt es nur wenige Untersuchungen zur Turbulenzcharakteristik unter diesen Bedingungen. Daher konzentrierte sich die vorliegende Arbeit auf die folgenden drei Themenschwerpunkte: (1) die Entwicklung einer Messmethode zur Charakterisierung der hydromechanischen Belastung in begasten Rührreaktoren, (2) die Untersuchung des Einflusses der Begasung auf die hydromechanische Belastung und (3) die Charakterisierung des Einflusses der Geometrie und des Maßstabs auf die hydromechanische Belastung in begasten Rührreaktoren.

Eine neue Messmethode wurde etabliert, die auf der bekannten Korrelation des maximalen stabilen Tropfendurchmessers einer koaleszenzgehemmten Dispersion mit der hydromechanischen Belastung beruht. Die spezifischen Eigenschaften der kontinuierlichen und der dispersen Phase wurden so gewählt, dass es zum ersten Mal möglich wurde, dieses Prinzip auf begaste Rührreaktoren anzuwenden. Dies wurde hauptsächlich erreicht durch die geringe Konzentration der dispersen Phase, einer geringen Ionenstärke der kontinuierlichen Phase und der Wahl einer dispersen Phase – Paraffinöl – mit negativem Spreitungskoeffizienten. Der negative Spreitungskoeffizient führt zur Vermeidung von Koaleszenz auf Grund von Tropfen-Blasen-Interaktionen bei begasten Betriebsbedingungen.

Diese neue Methode wurde eingesetzt um den Einfluss der Begasung auf die hydromechanische Belastung in einem breiten Bereich von begasten und unbegasten Betriebsbedingungen in einem 3 m^3 Reaktor zu untersuchen. Es wurden Ergebnisse von Dispergierexperimenten mit zwei unterschiedlichen Konfigurationen 6-blättriger Scheibenrührer mit Durchmessern d = 0.41 m (d/D_R = 0.34, Konfiguration B-1) und d = 0.51 m (d/D_R = 0.43, Konfiguration B-3) gezeigt. Die Ergebnisse von Experimenten ohne Begasung waren in guter Übereinstimmung mit Daten aus der Literatur. Die Ergebnisse von Experimenten mit Begasung zeigten eine ausgeprägte Dämpfung der Turbulenzintensität in Rührreaktoren durch die Gegenwart von Gasblasen. Das Verhältnis zwischen maximaler und durchschnittlicher Energiedissipationsrate, ϕ, wurde durch die Begasung bei gleichem spezifischen Leistungseintrag im Vergleich zu unbegasten Bedingungen für die Rührerkonfiguration mit d/D_R = 0.34 (B-1) um 64% verringert und für die Rührerkonfiguration mit d/D_R = 0.43 (B-3) um 52%. Im Bereich der untersuchten Begasungsraten (0.1 vvm bis 1 vvm) hatte der Wert der Begasungsrate keinen Einfluss auf das Ergebnis.

Die Methode wurde weiterhin in einem breiten Bereich von Reaktormaßstäben (50 L, 3 m^3 und 40 m^3 Nennvolumen), Rührergeometrien (Scheibenrührer und eine Ekato Phasejet/Combijet Kombination) und Betriebsbedingungen eingesetzt um den Einfluss der Geometrie und des Maßstabs auf die hydromechanische Belastung zu untersuchen. Der Vergleich von Daten aus unterschiedlichen Maßstäben zeigte einen Maßstabseffekt, der zu höheren Werten für ϕ mit steigender Reaktorgröße führt. Dieses Verhalten wird durch die klassische Theorie des turbulenten Tropfenaufbruchs nicht beschrieben, ist aber in guter Übereinstimmung mit dem Phänomen der intermittierenden Turbulenz. Die Daten für alle Rührerkonfigurationen und Begasungsraten für die drei untersuchten Maßstäbe korrelierten sehr gut, wenn für die Berechnung der maximalen lokalen Energiedissipation aus den gemessenen Werten für d_{max} abgeleitete Werte für ϕ verwendet wurden. Bei Verwendung dieser Werte für ϕ fiel der größte Teil der Daten auf einen Bereich von 20% um die theoretische Vorhersage aus der klassischen Theorie des turbulenten Tropfenaufbruchs. Eine Korrelation der Daten für alle Maßstäbe und Rührerkonfigurationen in der Form $\phi = 2.3 \cdot (\phi_{unbegast})^{0.34} \cdot (D_R)^{0.543}$ wurde vorgeschlagen, die den Einfluss des Maßstabs und der Rührergeometrie auf ϕ für begaste Betriebsbedingungen mit guter Genauigkeit beschreibt. Die Ergebnisse für eine Ekato Phasejet/Kombijet Rührerkonfiguration zeigen, dass diese Korrelation auch eingesetzt werden kann, um die hydromechanische Belastung für andere Rührergeometrien als für Scheibenrührer abzuschätzen.